DEVELOPMENT OF LOW COST POLYSULFONE BASED ANION EXCHANGE MEMBRANES AND NON-PLATINUM OXYGEN REDUCTION CATALYSTS FOR FUEL CELL APPLICATIONS

A Thesis Submitted By

XU WANG

For the Degree of Doctor of Philosophy

School of Chemical Engineering & Advanced Materials
Newcastle University

June 2012

Abstract

Proton exchange membrane fuel cells (PEMFCs) are currently based on high cost materials such as Nafion® membrane and Pt based catalysts. The high cost and limited abundance of noble metal hinder the commercialization of such fuel cells. For the future hydrogen economy, alkaline anion exchange membrane fuel cells (AAEMFCs) offer advantages of the potential use of non-Pt group metal catalysts, low-cost membranes (e.g. polysulfone based membranes) and cheaper bipolar plate (e.g. stainless steel). The research described in this thesis focused on the research and development of alternative anion conducting membranes and catalyst materials for fuel cells.

Quaternary 1,4-diazabicyclo-[2.2.2]-octane (DABCO) polysulfone (QDPSU) was synthesized with different degree of substitution (DS) and characterized. The higher DS showed the better ionic conductivity; 0.015 S cm^{-1} for DS 58, 0.027 S cm^{-1} for DS 80 and 0.039 S cm^{-1} for DS 106 at 50 $^{\circ}$C and 100 % relative humidity (RH). Based on the QDPSU, a thin PTFE-QDPSU composite membrane was prepared. Compared to the pristine QDPSU membrane, the composite membrane exhibited a better mechanical strength (32 MPa, maximum strength), less swelling and lower water uptake. The ionic conductivity of the composite membrane was 0.051 S cm^{-1} at 55 $^{\circ}$C and 100 % RH. In fuel cell tests, power densities of 146 mW cm^{-2} and 103 mW cm^{-2} were achieved using oxygen and air, respectively.

Severe degradation was found during preliminary experimental investigation on the KOH loaded polybenzimidazole (PBI) membrane including an ammonia smell came out the bottle and anode methanol solution turns yellow brown color in fuel cell tests.

The QDPSU membrane was absorbed with phosphoric acid and tested in an intermediate temperature fuel cell. It was found that the higher DS, the higher membrane conductivity. When the DS reached 180 %, the QDPSU polymer cannot form

a film with a suitable mechanical strength for the fuel cell application. A high power density of 400 mW cm^{-2} was achieved using DS106 of PA/QDPSU membrane at 150 ^{o}C and atmospheric pressure.

Pd supported on carbons pre-treated in 5 % nitric acid, 0.07 M phosphoric acid, 0.2 M potassium hydroxide or 10 % hydrogen peroxide and evaluated in a half-cell. All Pd/C catalysts gave Tafel slopes close to 60 mV dec^{-1}. Mass activities, measured at 0.025 V, for the 0.07 M H_3PO_4 and 0.2 M KOH treated carbon deposited with Pd were 6 mA mg^{-1}_{Pd}. Pre-treatments using 5 % HNO_3 and 10 % H_2O_2 lead to an unfavorable effect on the morphology of Pd/C (metal particle agglomeration).

Metal macrocycle based catalysts were examined for the ORR in alkaline media. FePc/KJB was found more active catalyst than the other metal macrocycles (CoPc, CoTMPP). The stability study in half-cell tests suggests that the FePc/KJB catalyst showed no degradation. The FePc/KJB was heat-treated under N_2 atmosphere and 800 ^{o}C. The electrochemical behavior for ORR was characterized in half cell and single cell tests. The electron transfer number (n) of FePc/KJB-H8 was calculated to be 3.9 for ORR at -0.4 V. In AAEMFC, the peak power densities were 13.5 and 9.2 mW cm^{-2} for Pt/C and FePc/KJB-H8 under the same operating conditions, respectively.

A direct methanol carbonate fuel cell using anion exchange materials and non-noble catalyst was demonstrated. The MEA performance using non-noble catalyst Acta 4020 was superior to the Pt/C based MEA. A maximum power density of 4.5 mW cm^{-2} was achieved at 50 ^{o}C using 6.0 M methanol and 2.0 M K_2CO_3. For the fuel cell stability study, the MEA exhibited a degradation rate of 2.52 $\mu A\ cm^{-2}\ min^{-1}$.

ACKNOWLEDGEMENTS

Over the last three years I have been blessed with the opportunity to work with people in the fuel cell group who supported me unconditionally. I would like to take this occasion to thank and acknowledge some individuals who made contribution to this thesis.

Prof. Keith Scott, my supervisor and mentor, who offered me with a lot of opportunities. Your patience, guidance and generosity truly brightened my research life and daily life. What I have learned from you is invaluable for my future. I am truly grateful for all these.

Dr. Eileen Hao Yu, my second supervisor, who also played an important role in my life during the last three years. I appreciate a lot for the support both technical and moral and your encouragement.

I would like to thank the UK EPSRC and DSTL for their financial support.

I am very thankful for Prof. Bernard T. Golding and Mr. Mashi Sadeghi from School of Chemistry who were assisting with the polymer synthesis through which we had fruitful discussions and lab works. Dr. Senthil Kumar, I am thanking you for providing Pd catalysts sample and I do admire your great knowledge on electrochemistry. Mr. Chenxi Xu was assisting with the fuel cell test on intermediate temperature fuel cells and I am thankful for that. Moodie, Yuancheng, Xu Wu and the other colleagues are also acknowledged for sharing ideas.

My gratitude to UDEL and SGL, they provided free samples of polysulfone and carbon papers used in this work.

Thanks to my mother, uncle and others. I will always remember that blood is thicker than water.

Finally, thanks to my beloved wife Dan Li for your love and caring.

TABLE OF CONTENTS

LIST OF FIGURES

CHAPTER 4

CHAPTER 5

CHAPTER 6

CHAPTER 7

CHAPTER 8

LIST OF TABLES

LIST OF ABBREVIATIONS

AFCs	Alkaline fuel cells
AAEMFCs	Alkaline anion exchange membrane fuel cells
PEMFCs	Proton exchange membrane fuel cells
DOAFCs	Direct oxidation alkaline fuel cells
ORR	Oxygen reduction reaction
MEA	Membrane electrode assembly
RRDE	Rotating ring disk electrode
FRA	Frequency response analyse
CV	Cyclic voltammetry
FePc	Iron phthalocyanine
CoPc	Cobalt phthalocyanine
CM-PSU	Choloromethylated polysulfone
DABCO	1,4-diazabicyclo-[2.2.2]-octane
QDPSU	Quaternary DABCO polysulfone
NMR	Nuclear magnetic resonance
FT-IR	Fourier transform infrared spectroscopy
SEM	Scanning electron microscopy
EDX	Energy-dispersive X-ray spectroscopy
TGA	Thermogravimetric analysis
DSC	Differential scanning calorimetry
CoTMPP	Co-tetramethoxyphenylporphirine
PBI	Polybenzimidazole
CHP	Combined heat power (system)
KJB	Ketjenblack EC-300J carbon powder
VC	Vulcan XC-72R carbon powder
SP	SuperP carbon powder

CHAPTER 1. INTRODUCTION AND OBJECTIVES

1.1   Introduction

Fuel cells using aqueous KOH electrolyte were first patented by Reid in 1902 and Noel in 1904, 63 years after Grove's acid fuel cells in 1839. Dr. Francis Bacon commenced his research on alkaline fuel cell (AFC) in 1932 and completed the construction of a 5 kW hydrogen-oxygen fuel cell power plant in 1952. One of the main reasons Bacon chose an alkaline electrolyte was to use non-noble metal catalysts. In his fuel cell, nickel was the catalyst for the anode and lithiated nickel oxide was the catalyst for the cathode. In NASA's Apollo missions, fuel cells using 80-85 % KOH (molten KOH), operated at 250 ^{o}C and close to atmospheric pressure, were developed by the Pratt and Whitney Division of United Technologies Corporation [1]. These fuel cells could last for two to four weeks. Siemens and Exxon also developed highly efficient alkaline fuel cells and a current density of 420 mA cm^{-2} at a cell potential of 0.77 V was achieved with their systems [1, 2]. Although the alkaline fuel cell system is the most efficient of all fuel cells, the major problem is carbonation of the electrolyte due to CO_2 present in the fuel and from air [1]:

$$2OH^- + CO_2 \rightarrow CO_3^{2-} + H_2O \qquad (1)$$
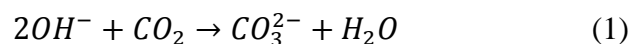
This can cause solid precipitation of carbonate salts on the porous electrode and a decrease of pH in the alkaline electrolyte solution [1]. Complete removal of CO_2 from the anodic and cathodic gas stream is a great challenge and leads to high costs.

Since the development of perfluorinated proton exchange membranes (PEMs), such as Nafion$^®$ (DuPont), PEMs have dominated as the electrolyte for fuel cells for decades. However, several obstacles have restrained more rapid development and applications of

PEM fuel cells:

- High cost of membrane and noble metal catalysts

- The relatively low activity and complex reaction mechanism of most organic fuels

- Limitations in operating temperature, typically less than 100 $^{\circ}$C

- Fuel crossover when using organic based fuels

Direct alcohol fuel cells (DAFCs), which oxidize fuel directly on the anode in alkaline media, have attracted attention again in recent years because of the potential solutions to overcome the problems in PEMFCs. The application of anion exchange membranes (AEMs) as the solid polymer electrolyte can reduce formation of carbonate from carbon dioxide, compared to aqueous electrolyte [3]. It was also discovered that the electro-oxidation of fuels, such as methanol, in alkaline electrolyte is structure insensitive [4] which opens up the opportunity for use of non-precious metals, such as Pd, Ag, Ni and perovskite-type oxides in such fuel cells [5-7], which can significantly reduce the catalyst cost compared to Pt based catalysts. Furthermore, the ionic current in the alkaline fuel cell is due to conduction of hydroxide ions. This ionic flow is in the reverse direction to that in proton conducting systems and as such, the direction of the electro-osmotic drag is reversed, reducing fuel crossover [8].

1.2 Objectives and thesis structure

This work was funded by EPSRC and DSTL. The aims of this work focus on developing new solid polymer electrolytes, non-noble metal catalysts and their electrochemical behaviour. This thesis consists of eight chapters which are listed as below:

Chapter 1- An introduction to the subject of the research and objectives.

2

Chapter 2- A literature review that covers an introduction of different types of fuel cell, anion exchange membrane materials, catalysts (ORR and alcohol oxidation) and anode oxidation reaction.

Chapter 3- In this chapter, basic electrochemical methods {cyclic voltammetry (CV), rotating ring disk electrode (RRDE) and frequency response analysis (FRA)} and experimental procedures for catalyst and membrane characterizations will be introduced. All the chemicals and supplied samples will be listed.

Chapter 4- Anion exchange membranes were prepared for the low temperature fuel cell application. A quaternary 1,4-diazabicyclo-[2.2.2]-octane (DABCO) polysulfone (QDPSU) polymer was synthesised through a typical two steps reaction: chloromethylation reaction and quaternization reaction. For the chloromethylation reaction, chloromethylether is a well-known carcinogen, however, in-situ generation of chloromethylether avoids human exposure to toxic chemicals [9]. The conventional amination agent (trimethylamine-TMA) is corrosive, toxic and bad smell. In this work, DABCO (solid powder) was used instead of TMA which is easier to handle, odour-less and less toxic [10]. The obtained product was confirmed using Nuclear Magnetic Resonance (NMR) and Fourier Transform Infared spectroscopy (FTIR). A thin (30 μm) polytetrafluoroethylene-quaternary 1,4-diazabicyclo-[2.2.2]-octane polysulfone (PTFE-QDPSU) composite membrane for AAEMFC was also prepared. The thermal stability and morphology of prepared membranes were examined using thermogravimetric analysis (TGA) and scanning electron microscopy (SEM). The ionic conductivity of membranes was measured using the four-point method. The properties of obtained membranes with different degree of substitution (DS) were compared. A maximum power density of 146 mW cm^{-2} was achieved using the PTFE-QDPSU composite membrane.

The KOH loaded polybenzimidazole (PBI) was investigated for AAEMFCs. Previous

reports suggested that it has a reasonable ionic conductivity (0.0185 S cm^{-1} at room temperature) and stability in KOH solution [11-13]. Surprisingly, the PBI membrane was unstable during the KOH treatment and fuel cell operation especially at elevated temperatures (> 30 ^{o}C).

Chapter 5- Phosphoric acid loaded quaternary 1,4-diazabicyclo-[2.2.2]-octane (DABCO) polysulfone (PA/QDPSU) membranes were prepared and characterized. The effect of DS on ionic conductivity and fuel cell performance are described. Conductivities of 0.12 and 0.064 S cm^{-1} were achieved for the high degree of substitution membrane (DS106) and low degree of substitution membrane (DS58), respectively. Fuel cell tests gave a high power output of 400 mW cm^{-2} using H_2 and O_2 at 150 ^{o}C and atmospheric pressure.

Chapters 6-The electrochemical activity of oxygen reduction reaction (ORR) on different pre-treated carbon supported Pd/C catalysts in alkaline media was compared and discussed. Electrochemical characterization was performed using cyclic voltammetry in 1.0 M KOH solution. A rotating ring disk electrode (RRDE) was used to quantify the hydrogen peroxide yield from ORR on all samples. The Tafel plot and electron transfer number (n) of the ORR on all catalysts were derived from polarization curves. Comparison with the commercial Pt/C (20 wt %) was made to help interpret the reaction mechanism of the ORR on Pd/C catalysts.

Chapter 7-In this chapter, carbon supported metal macrocycles were prepared for the ORR in alkaline media using the impregnation method. Metal macrocycle catalysts were characterized and compared to the commercial Pt/C (BASF) in both half-cell and single fuel cell tests. Electrochemical characterizations were conducted on a RRDE electrode using CV technique. The Tafel slope, electron transfer number (n) and hydrogen peroxide production of catalysts for the ORR were established in alkaline media. Furthermore, the stability of the selected metal macrocycle catalyst was examined using cyclic voltammetry in a half cell and potentiostatic method in single

cell test.

Chapter 8- Direct methanol fuel cells performance using anion exchange materials and non-noble catalysts were reported. The chapter focused on electrode optimization as well as the operating conditions. A direct methanol fuel cell was evaluated in carbonate form. Compared to the literature, a thin AAEM, anion conducting ionomer and non-noble metal catalyst were used for the direct methanol carbonate fuel cell [14]. The effect of QDPSU ionomer loading and operating conditions on the fuel cell performance were compared and discussed.

Chapter 9- Conclusions were given which form the basis for perspectives of anion exchange membrane fuel cells.

CHAPTER 2. LITERATURE REVIEW

Most countries depend heavily upon fossil fuels as the primary energy source and the demand is predicted to increase rapidly (Figure 2-1) [15], due to population growth and industrialization of developing countries. Unfortunately, the distribution of fossil fuels is limited by geographic boundaries, eight countries have 81 % of all world crude oil reserves, six countries have 70 % of all natural gas reserves and eight countries have 89 % of all coal reserves. The supply of fossil fuels is finite and is predicted to be unable to match demand within 50 years. Meanwhile, reliance on fossil fuels produces a huge amount of greenhouse gases and other harmful substances into the environment. Additionally combustion of fossil fuels makes a major contribution to global warming. The pressure from the oil crisis and environment pollution provides the motivation for the development of new energy and related technologies.
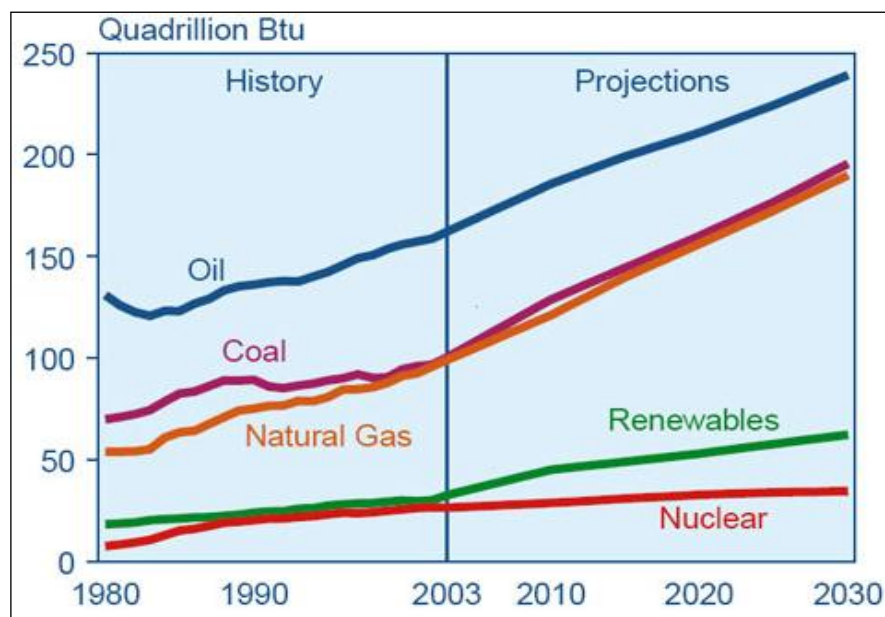
Figure 2-1 Prediction of Word Energy Consumption [15]

Hydrogen is a high energy density, carbon-emission-free fuel and abundant in the form of water. An energy network system based on hydrogen and hydrogen generation provides renewable and sustainable energy. The hydrogen network involves production, storage and utilization, as a part of the so-called "hydrogen economy" which offers a

6

reasonable alternative to the current energy supply system.

2.1 Introduction to fuel cells

Fuel cells are electrochemical energy devices that convert the chemical energy of fuels (e.g. hydrogen, alcohols or short-chain carbon containing compounds (in Table 2-1) and oxidant (mostly air or oxygen) into direct current (DC), water and heat under certain conditions [16].

Table 2-1 The standard thermodynamic voltage (E^0), energy density (W_e), number of electrons (n) and maximum reversible efficiency (η_{rev}) of hydrogen and alcohols in fuel cells under standard conditions [3, 17].

Fuel	E_0 /V	We/kWh kg^{-1}	Number of Electron transfer per mole/n	Reversible efficiency(η_{rev})/ %
Hydrogen	1.23	39.0 (2.6 for liquid H_2)	4	83
Methanol	1.21	6.1	6	97
Ethanol	1.17	8.0	12	97
Iso-propanol	1.07	8.6	6	93
Ethylene glycol	1.22	5.3	6	99
Sodium borohydride	1.64	9.0	8	91

Taking the well-known proton exchange membrane fuel cell (PEMFC) using hydrogen and pure oxygen as example, the principle of fuel cell can be illustrated as shown in Figure 2–2. In order to study each reaction separately, a reference electrode (RE) is introduced (e.g. normal hydrogen electrode − NHE which is defined as 0.0 V) into fuel cell system. Hydrogen and oxygen are fed into the anode and the cathode respectively. Reactions take place accordingly as follows:
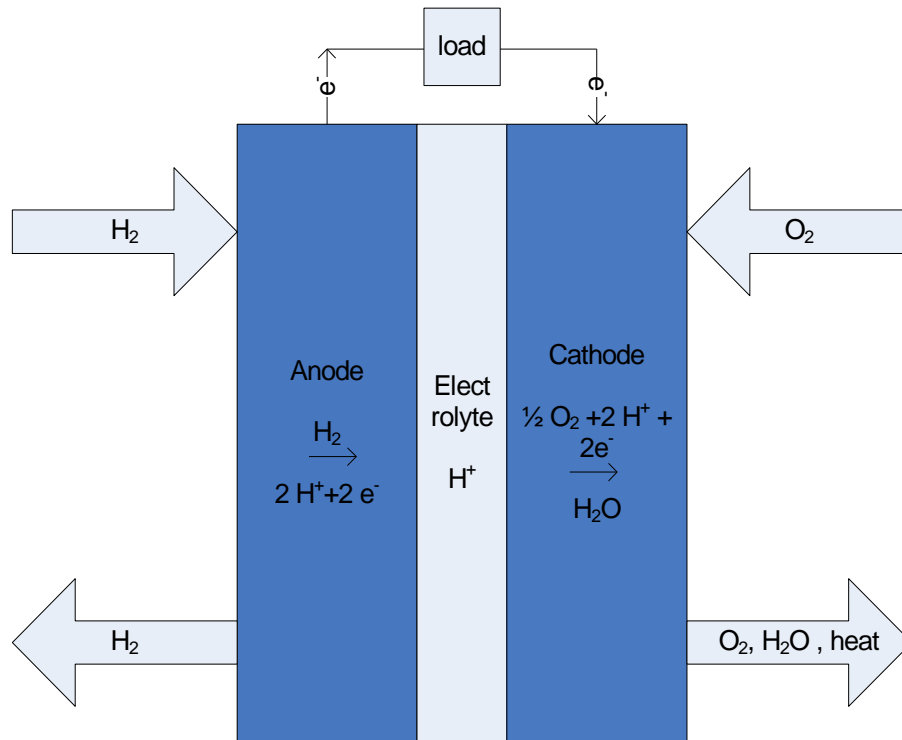
Figure 2-2 Schematic diagram of Proton Exchange Membrane Fuel Cell

Anode	$H_2 \rightarrow 2H^+ + 2e^-$	$E_0=0$ V (vs. NHE)	(1)
Cathode	$O_2 + 4H^+ + 4e^- \rightarrow 2H_2O$	$E_0=1.23$ V (vs. NHE)	(2)
Overall	$2H_2 + O_2 \rightarrow 2H_2O$	$E_0=1.23$ V (vs. NHE)	(3)
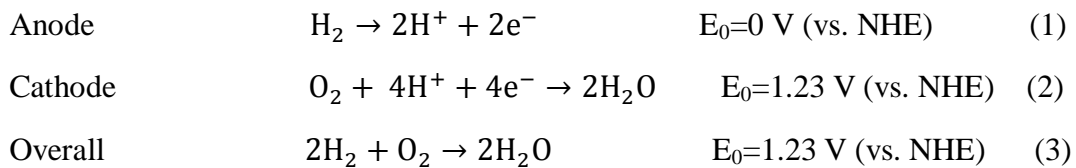
At anode, hydrogen splits into two protons and electrons. They travel through the electrolyte (proton exchange membrane) and external circuit (electrical load) to the cathode. While oxygen is electrochemically reduced to water by reacting with the protons and electrons produced from the anode reaction.

In general, there are five types of fuel cell as shown in Table 2-2 which are normally named after the ionic conducting electrolytes in use - alkaline fuel cell (AFC), proton exchange membrane fuel cell or polymer electrolyte membrane fuel cell (PEMFC), phosphoric acid fuel cell (PAFC), molten carbonate fuel cell (MCFC) and solid oxides fuel cell (SOFC) [18, 19].

Table 2-2 Types of Fuel Cells [18]

	AFC	PEMFC	PAFC	MCFC	SOFC
Electrolyte	Aqueous alkaline solution (e.g. KOH)	Polymer membrane (e.g. Nafion® or PBI)	Molten phosphoric acid	Combination of alkali (e.g. Li, Na)	Nonporous metal oxide (e.g. ZrO_2)
Mobile ion	OH^-	H^+	H^+	CO_3^{2-}	O^{2-}
Operating temperature (°C)	50-200 °C	Nafion®30-100 °C or PBI[a] 125-220 °C	220 °C	600-650 °C	500-1000 °C
Efficiency (%)	50-70	40-50	40-45	50-60	50-60
Power (W)	Up to 10kW	Up to 500kW	10MW	10MW	10MW
Note	Used in spacecraft (Apollo)	Vehicles and portable application	200kW CHP[b] system in use	MW capacity CHP system	2kW to multi-MW CHP system

a- Combined Heating power (CHP) system

b-Polybenzimidazole (PBI)

William Grove produced the first fuel cell in 1839. Although he attempted to make it a practical device, no significant improvement was made for almost a century. Francis T. Bacon worked on the alkaline fuel cell (AFC) for over 25 years and made a great contribution to the high power density operation with hydrogen and oxygen at around 200 °C and high pressures (up to 28 bar). Based on Bacon's work, united technology corporation (UTC) manufactured the AFC for the first application in the Apollo space program (1961-1975). Just few years before Apollo space program commenced, Willard

T. Grubb invented the proton exchange membrane fuel cell (PEMFC) and General Electrical proposed its use for the Gemini manned space project. In the middle of 1960s, Dupont developed a novel membrane based on sulfonated tetrafluorethylene copolymer, which is called "Nafion[®]", boosted the development of PEMFC and it is the most widely used and investigated fuel cell system. Nafion[®] has excellent conductivity (0.1 Scm^{-1} at 80 ^oC and 100 % RH), thermal and mechanical stability. A lot of manufacturers made a great effort on PEMFC powered vehicles.

The initial development of PAFC was in the 1960s which was designed to achieve high conductivity at temperatures of around 200 ^oC. PAFC simplifies the water and heat management, it also improves the tolerance to carbon monoxide because of the high operating temperature range. The state of the art PAFC system can generate up to 10 MW power with high efficiency [16, 18]. Compared with the other types of fuel cells, MCFC and SOFC operate at high temperature range (> 600 ^oC). The main motivation of high temperature fuel cells development was due to oil crisis in the 1970s. The advantages of high temperature fuel cells are their ability to run on natural gas instead of hydrogen and their high efficiency [18].

The estimated significant commercialization of fuel cells is approximately the time of 2010s, with the PEMFC leading the way due to its wide application and environmental benefits (reduced carbon emission by using hydrogen and air). However, a major issue for commercialization of PEMFCs is the cost of noble metal (e.g. platinum and platinum alloys) catalysts and PEMs (e.g. Nafion[®]) [18].

2.2 Introduction to anion exchange membrane fuel cells

2.2.1 Alkaline anion exchange membrane fuel cells

The principle of AAEMFCs is no different to the traditional alkaline fuel cell as shown in Figure 2-3. From equation 4 to 6, oxygen reduction reaction takes place at the

cathode and generates hydroxide ion. It transports from the cathode to the anode with water which oppose to the water transport in PEMFC (from the anode to the cathode). Hydrogen is oxidized by hydroxide and produce water at the anode.
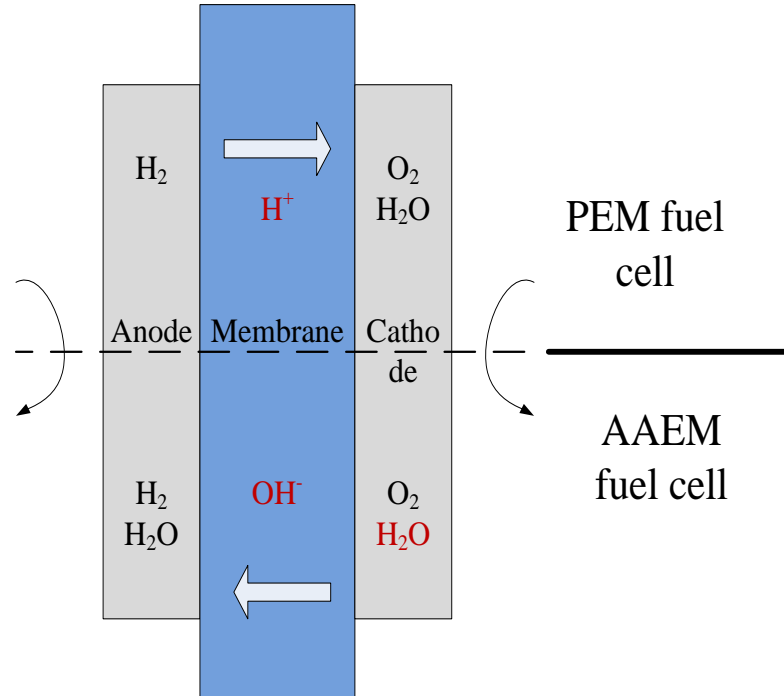
Figure 2-3 Comparison of alkaline anion exchange membrane fuel cells and proton exchange membrane fuel cells

Anode reaction:

$$H_2 + 2OH^- \rightarrow 2H_2O + 2e^- \quad E_0 = -0.83 \text{ V (vs. NHE)} \quad (4)$$

Cathode reaction:

$$O_2 + 2H_2O + 4e^- \rightarrow 4OH^- \quad E_0 = 0.4 \text{ V (vs. NHE)} \quad (5)$$

Overall reaction:

$$2H_2 + O_2 \rightarrow 2H_2O \quad E_0 = 1.23 \text{ V (vs. NHE)} \quad (6)$$

Traditional alkaline fuel cells utilise aqueous KOH as cheap electrolyte and non-noble catalysts (e.g. nickel for the anode and silver nanoparticle for the cathode) are much cheaper and relatively abundant [3, 20]. Compared to the aqueous KOH electrolyte for the conventional AFC, a solid state electrolyte based AAEMFC offers no leakage of electrolyte, less corrosive environment and most importantly zero carbonation. The

carbonation issue is because of the aqueous KOH electrolyte which caused by salt accumulation on catalyst layer of cathode. It is not only just reducing the ionic conductivity of electrolyte, but also block the pores of the electrode which lead to the oxygen starvation [3].

2.2.2 Direct methanol carbonate fuel cells

Recently, direct oxidation alkaline fuel cells (DOAFCs) have attracted interest due to the possible use of low-cost and more abundant materials for catalysts and membranes[3, 21-25]. Progress has been also made on achieving high power output. An et al reported that direct alcohol alkaline fuel cell consisted of non-noble metal cathode catalyst (Acta 4020), PdNi/C for ethanol oxidation, PTFE as binder in catalyst layers and commercial Tokuyama A201 anion exchange membrane [25]. The fuel cell produced a power density of as much as 100 mW cm^{-2} using 3.0 M methanol and 5.0 M KOH at anode [25]. However, there has been a great concern on the CO_2 production from alcohols oxidation and ambient air which can cause carbonation of fuel cell especially with KOH or NaOH circulating at anode [3, 26]. An example is a methanol fuel cell operating with 6.0 M KOH by Murray [18]. Performances at 0.3 V decreased steadily over 70 h at 60 ^{o}C and 94 h at 30 ^{o}C, mainly due to anode degradation [18]. Furthermore, a comprehensive review by Antonlini summarised that the stability of DOAFCs is reasonable with either no alkaline solution presence in the fuel cell or no CO_2 from the anode oxidation of alcohols [20]. The other challenge is that DOAFCs still feed on pure oxygen or CO_2 free air at the cathode side. In a hydrogen fuelled alkaline anion exchange membrane fuel cell, Piania et al reported that the power density of fuel cell with CO_2 free air dropped from around 350 mW cm^{-2} to less than 100 mW cm^{-2} after switch to atmospheric air for the cathode [27]. The main disadvantage of using pure oxygen in DOAFCs is the oxygen storage especially for portable device applications. Thus, it is highly desirable to develop a direct alcohol fuel cell system can handle CO_2 from both alcohol oxidation and atmospheric air.

Lang et al proposed a low temperature carbonate fuel cells (LTCFCs) what is shown in Figure 2-4 [14]. Carbon dioxide and oxygen are fed to the cathode and produce carbonate ions by electrochemical reduction (equation 1), which transport through the electrolyte to reach the anode. At the anode, methanol is oxidized to carbon oxide and water (equation 8). The CO_2 from the anode could potentially be reused in the cathode reaction as indicated by the dash arrows in Figure 2-4. Furthermore, they established that CO_2 is crucial to maintain the cell reaction, the cell potential dropped continuously without CO_2 supply due to the insufficient carbonate ions for anode oxidation reaction [14].
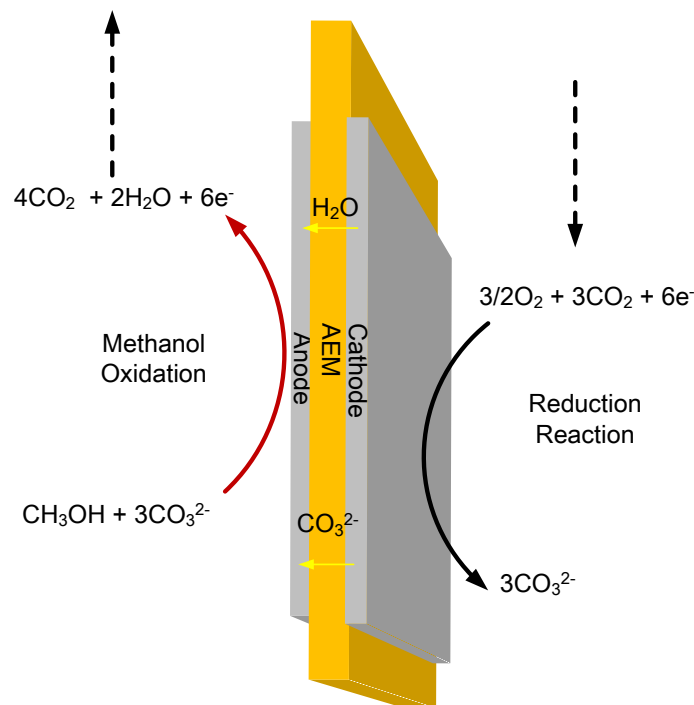
Figure 2-4 Schematic diagram of direct methanol carbonate fuel cell

The direct alcohol carbonate fuel cell system allows using ambient air and its own recycled CO_2 at the cathode to increase the fuel capacity compared to direct alcohol alkaline fuel cells.

Cathode reaction: $$3CO_2 + 3/2\,O_2 + 6e^- \rightarrow 3CO_3^{2-} \qquad (7)$$

Anode reaction: $$CH_3OH + 3CO_3^{2-} \rightarrow 2H_2O + 4CO_2 + 6e^- \qquad (8)$$

Overall reaction: $$CH_3OH + 3/2\,O_2 \rightarrow 2H_2O + CO_2 \qquad (9)$$
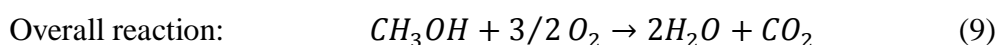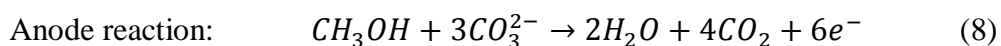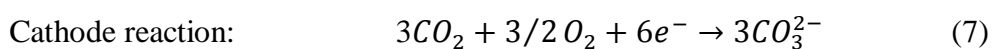
2.3 Introduction to intermediate temperature fuel cells

Fuel cells are a key enabling technology for the future hydrogen economy. Nafion based proton exchange membrane fuel cells (PEMFCs) play an important role for the fuel cell development. However, the high cost of Nafion membrane and Pt group catalysts hinders the commercialization and further development of PEMFC. In addition, Pt catalyst is sensitive to carbon monoxide which can lead to an irreversible adsorption on the catalyst and the complex PEMFC system experiences reduced efficiency due to water management requirements. To overcome shortcomings of low temperature PEMFC, operation at elevated temperatures (> 120 ^{o}C) offers a number of potential advantages: a) high CO tolerance, b) faster kinetics, c) avoidance of cathode flooding, d) increased system efficiency by removing water management units [28].

Compared to aqueous phosphoric acid fuel cells (PAFCs) operate at higher temperatures (150-200 ^{o}C) than PEMFCs, solid state electrolytes provide advantages such as a less corrosive environment for catalysts and lower internal resistance losses. The phosphoric acid loaded polybenzimidazole (PBI) is the best known example which has produced reasonably successful membranes for fuel cells with excellent thermal, chemical stability and good conductivity [28-30]. A number of insoluble heteropolyacids (e.g. $Cs_{2.5}H_{0.5}PMo_{12}O_{40}$ and Cs-HPAs) were used for PBI composite membrane to improve the ionic conductivity of PBI membrane for high and low phosphoric acid doping level [31, 32]. Recently, a TiO_2 /PBI composite membrane was prepared by Lobato and co-workers, they found the water retention and acid loading level were improved compared to pristine PBI giving a high conductivity of 0.18 S cm^{-1} at 125 ^{o}C [33]. Such composite membrane gave a peak power density of 800 mW cm^{-1} using hydrogen and oxygen at 150 ^{o}C.

The sulfonated poly (ether ether ketone) (SPEEK) was characterized and the increase in degree of sulfonation resulted in increased glassy transition temperature (T_g) and enhanced membrane hydrophilicity which lead to a improved proton conductivity [34]. Xing et al synthesised a sulfonated poly (biphenyl ether sulfone) membranes exhibited a

good conductivity (0.18 S cm^{-1} at 25 $^{\circ}$C) and high thermal stability (up to 280 $^{\circ}$C) [35]. Lately, they reported a montmorillonite/sulfonated poly (phenylether sulfone)/PTFE composite membrane with low swelling ratio and good stability at high temperature and high strength conditions [36].

As an alternative method of preparing PEM for ITFCs, Li et al reported quaternized polymers as matrices for H_3PO_4 and they added that the quaternary ammonium group is stable in the operating condition of ITFCs and it has a good bonding with phosphoric acid [37, 38]. Our previous works on quaternary ammonium polysulfone (QAPSU) loaded with H_3PO_4 exhibited a promising fuel cell performance (700 mW cm^{-1} at 150 $^{\circ}$C and 1 bar pressure) [38, 39]. There are few reports on quaternary ammonium polymers for ITFCs compared to reports on PBI based composite membranes and sulfonated polymer membranes.

2.4 Preparation of anion exchange membranes and their stability

Owing to the successful development of Nafion$^{\circledR}$ membranes, PEMFCs have made a great advance in the last two decades. In contrast, the development of alkaline anion exchange membrane is still in its infancy [3]. AAEMs are solid polymer electrolyte membranes that contain positive ionic groups (e.g. quaternary ammonium (QA) functional groups such as poly-N^+Me_3) and mobile negatively charged anions (e.g. usually OH$^-$). Basic requirements of AAEM to meet fuel cell application demands are:

1) High conductivity of hydroxide – in order to obtain good power output, the internal resistance   contributed by the membrane should be minimized.

2) Durable mechanical property, thermal and chemical stability (especially in high pH working environment) – to meet commercial standard fuel cell, the membrane should be stable at working condition for thousands of hours

3) Low permeability of hydrogen and other fuels (e.g. alcohols, hydrazine and soudium borohydride) – Fuel crossover from anode to cathode will lead to a lower

open-circuit voltage (OCV) and causes performance loss

In this section, several types of AAEMs will be reviewed and categorized based on their material and synthesis technology employed.

2.4.1 Radiation grafted AAEMs

Scott et al reported a series of radiation-grafted AAEMs for direct alcohol fuel cell (DAFC) and achieved a superior fuel cell power density (70 mW cm^{-2} at 90 ^{o}C and 2 bar air pressure) than Nafion$^{®}$ based DAFC under the same operating conditions [8, 40-44]. The advantages of using AAEM instead of Nafion$^{®}$ for DAFC are due to the reversed osmosis drag which can ease the cross-over effect of alcohols from the anode to the cathode, enhanced kinetics (both anode and cathode) and applying non-noble metal catalyst for the cathode which is insensitive to alcohols [8, 40-44]. Varcoe and co-workers reported polyvinylidene fluoride (PVDF, $-[CH_2CF_2]_n-$) and polytetrafluoroetheneco-hexafluoropropylene (FEP, $-[CF_2CF_2]_n[CF(CF_3)CF_2]_m-$) films grafted with vinylbenzyl chloride (VBC) using radiation-grafting technique are compared [45, 46]. However, the cost of FEP is relatively high which limits its further application. The later reports from the same group synthesised AAEM using commercial available ETFE thin film as subtract grafting with VBC (Figure 2-5), such AAEM delivers a good ionic conductivity (up to 0.034 S cm^{-1}) and mechanical strength (maximum strength 25 MPa) [47, 48].
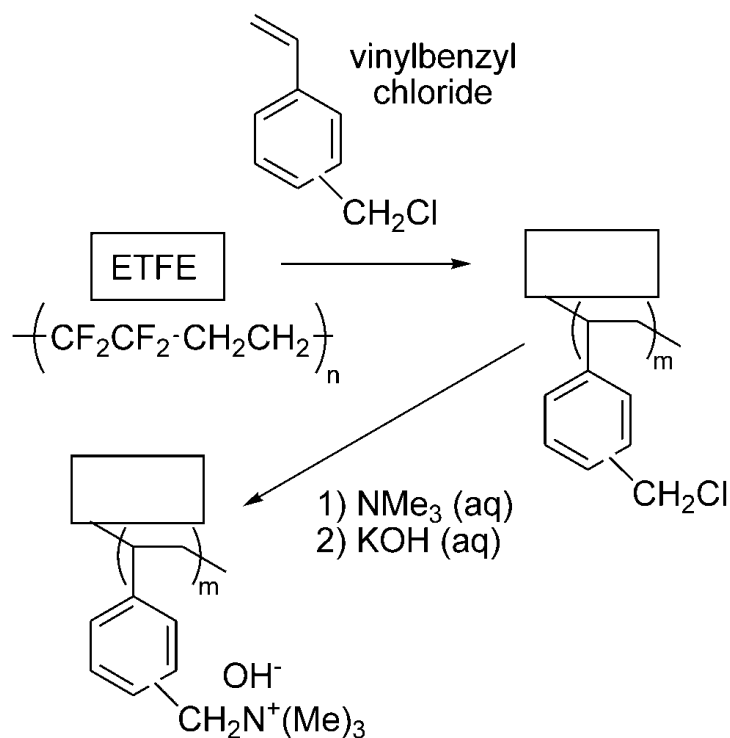
Figure 2-5 Synthesis procedures of PVBC radiation-grafted ETFE membrane [47]

A power density of 130 mW cm^{-2} was achieved using high loading of catalyst (4 mg cm^{-2} unsupported PtRu for the anode and 4 mg cm^{-2} unsupported Pt black for the cathode) using hydrogen and pure oxygen. The major issues of radiation-grafted AAEMs are insoluble to any solvent which cannot make ionomer solution that apply in catalyst layer, unevenly distributed function group through the cross section of membrane, high cost and limited yield of material [21, 46, 49].

2.4.2 Non-radiation grafted AAEMs

Poly (2,6-dimethyl-1,4-phenylene oxide) (PPO) is an unique material with strong hydrophobicity, high glass transition temperature (T_g = 212 °C) and hydrolytic stability which was investigated for direct methanol alkaline fuel cell (DMAFC) applications [50]. Chloroacetylated poly(2,6-dimethyl-1,4-phenylene oxide) (CPPO) blended with bromomethylated poly(2,6-dimethyl-1,4-phenylene oxide) (BPPO) membranes (in Figure 2-6) were characterized. These AAEMs exhibited a highest ionic conductivity of 0.032 S cm^{-1} at 25 °C [51]. A silica hybrid membrane was developed by the same group

using PVBC and γ-methacryloxypropyl trimethoxy silane (γ-MPS) copolymer which exhibited excellent mechanical strength (up to 65 MPa of maximum strengthing), however, the ionic conductivities of such hybrid membranes were relatively low (4.0 $\times 10^{-4}$ S cm^{-1}) [52]. Later, an improved silica/PPO hybrid membrane was reported with a ionic conductivity of up to 0.035 S cm^{-1} and 32 mW cm^{-2} single cell peak power density using hydrogen and pure oxygen at 50 ^{o}C [53].
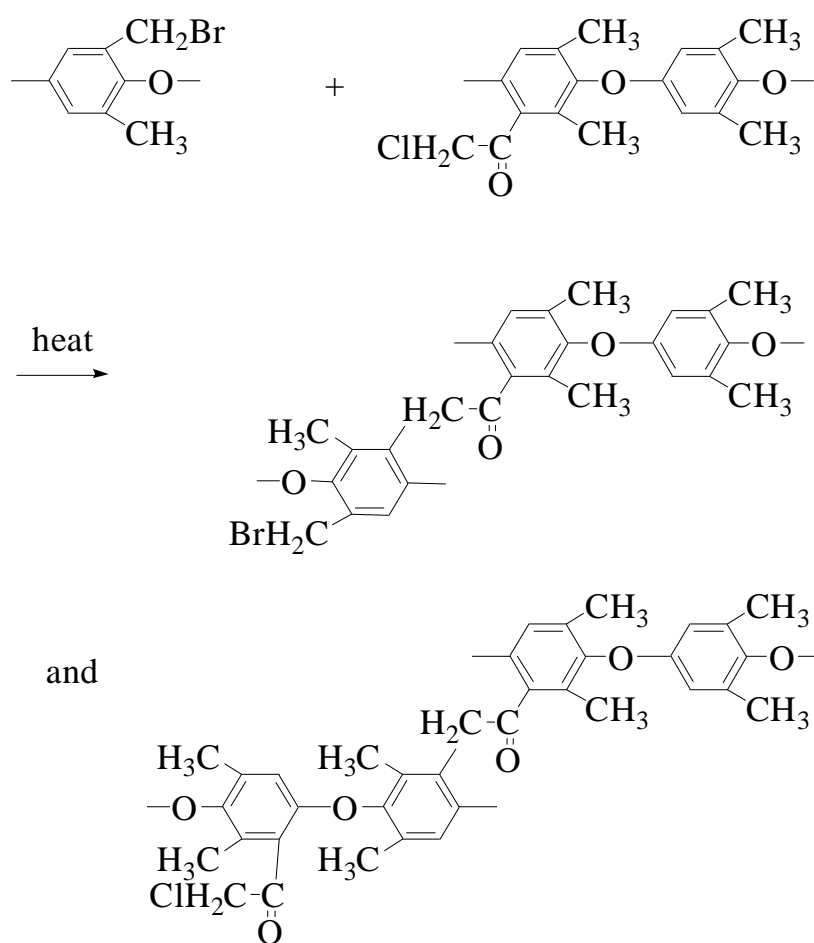
Figure 2-6 Formation of BPPO and CPPO blend membrane

Polysulfone based materials were investigated by a number of groups due to its high glassy transition temperature and chemical stability [21, 22, 54-61]. Pan et al synthesised a quaternized ammonium polysulfone (QAPSU) through a choloromethylation procedure following by aminating with trimethylamine (TMA) as shown in Figure 2-7. The effect of ion exchange capacity on membrane properties (e.g.

18

conductivity, water uptake, mechanical strength) was discussed. A power density of over 100 mW cm^{-2} was achieved using high catalyst loading ($4mg_{Pt}$ cm^{-2}) in the single cell test using hydrogen and pure oxygen. Fang et al used poly (phthalazinon ether sulfone ketone) as backbone and quaternized with TMA for direct alkaline alcohol fuel cells. The ionic conductivity of such membrane was as high as 0.14 Scm^{-1} in 2.0 M KOH at room temperature [55].
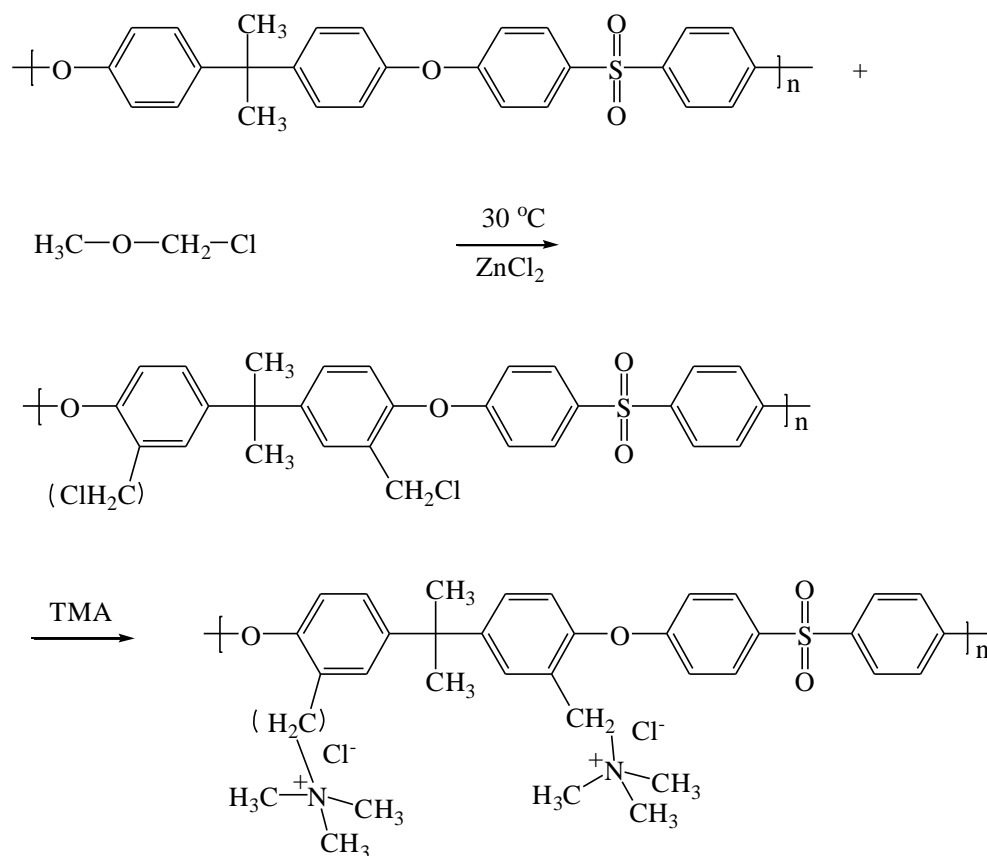
Figure 2-7 Synthesis procedure of QAPSU

Different pendant groups were quaternized with polysulfone and the ionic conductivities of these AAEMs were in an order of TMA > Dimethylethylamine (DMEA) > Dimethylisopropylamine (DMIPA) > Dimethylethylenediamine (TMEDA) > Triethylamine (TEA) [56]. After an optimized procedure of quaternization, the ionic conductivity was as high as 0.073 S cm^{-1} at 90 ^{o}C in deionised water. Hickner et al identified a non-cluster structure of such QAPSU using small-angle x-ray scattering (SAXS) and later they developed a new route for QAPSU synthesis with cluster

structure (similar to the structure of Nafion®) which benefits the ionic conductivity and mechanical strength [57, 60]. Later, Gu and co-workers synthesised a water-soluble ionomer for AAEMFC using tris(2,4,6-trimethoxyphenyl) polysulfone-methylene quaternary phosphonium hydroxide (TPQPOH in Figure 2-8) [61]. The ionomer is not soluble to water or any alcohols when it is crystallized and the fuel cell peak power density of 196 mW cm^{-2} was achieved using the ionomer in catalyst layer at 80 $^{\circ}$C, 100 % RH and 250 kPa backpressure on both sides.
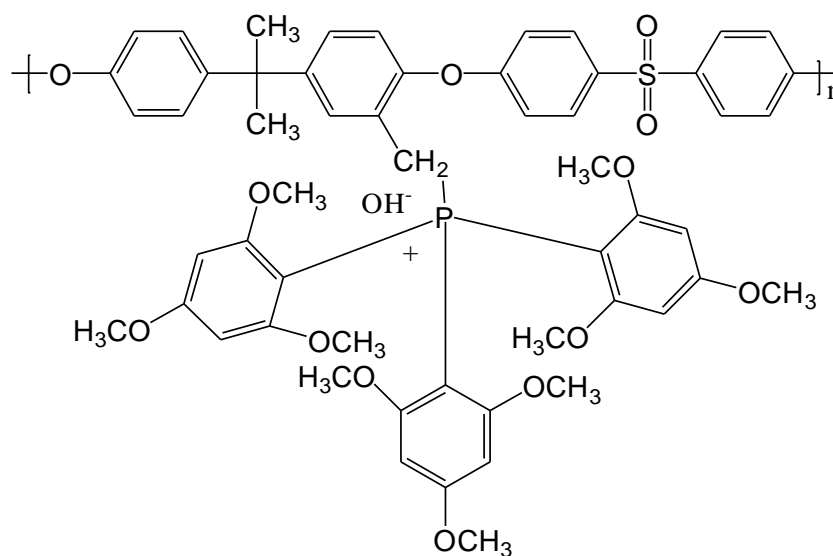
Figure 2-8 Chemical structure of TPQPOH ionomer

Copolymerization is a promising route of producing AAEMs due to a vast number of monomers. Guo et al synthesised an ionic liquid based copolymers via free-radical polymerization using methyl methacrylate (MMA) or butyl methacrylate (BMA) and 1-allyl-3-methylimidazolium chloride (AmimCl) as monomers (in Figure 2-9) [62]. These AAEMs were stable in 6.0 M NaOH solution at 60 $^{\circ}$C for 120 h and the highest ionic conductivity was 0.033 S cm^{-1} at 30 $^{\circ}$C and 100 % RH. Poly (methyl methacrylate-co-butyl acrylate-co-vinylbenzyl chloride) copolymers were synthesised and characterized using free-radical polymerization. The peak power density of 59 mW cm^{-2} was achieved using hydrogen and pure oxygen at 80 $^{\circ}$C and 60 % relative humidity (RH) [63, 64]. A cross-linked AAEM using tetraalkylammonium-functionalized cross-linker and cyclooctene (COE) exhibited a high hydroxide conductivity of 0.11 S

cm^{-1} at 50 ^{o}C which is similar to Nafion$^{®}$ 112 [65]. The high cost of these cross-linkers can be replaced with cheaper compounds. Block copolymers are considered as ideal materials for membranes for PEMFC due to the benefit of clustered structure [66]. However, there are few reports on these materials. Zeng et al prepared a quaternized polystyrene-block-poly (ethylene-ran-butylene)-block-polystyrene (QSEBS) through chloromethylation and quarterisation reaction [67]. The ionic conductivity of QSEBS block polymer AAEM is relatively low and no morphology or confirmation of clustered structure of quaternary ammonium group was reported.
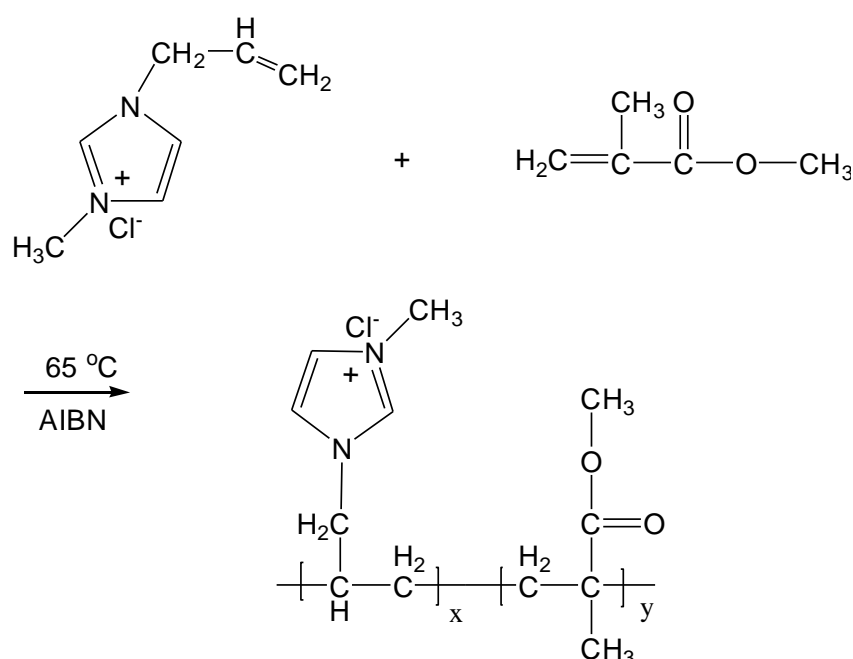
Figure 2-9 Synthesis of poly (AmimCl-MMA) copolymer

PTFE has an excellent chemical stability and studies showed the PTFE support reinforces the membrane mechanical strength which allows synthesis thinner membrane with less ionic resistance [68-70]. Lately, Zhang et al used polytetrafluoroethylene (PTFE) as a substrate thermally induced with PVBC and divinylbenzene (DVB, as cross-linker of PVBC) composite membrane (in Figure 2-10) for direct hydrazine fuel cells (DHFCs) [71]. The peak power density reached 110 mW cm^{-2} using non-noble metal catalysts for both anode (Co) and cathode (CoN$_x$/C) in the aqueous DHFCs.
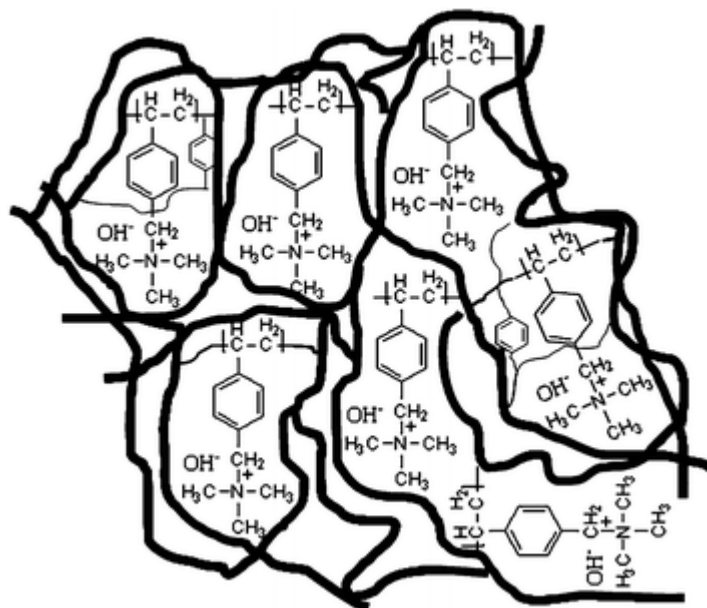
Figure 2-10 Schematic of PTFE-PVBC composite membrane (The bold black line represents PTFE chain).

Commercial AAEMs such as Tokuyama A201 (Polyolefin based AAEM) was investigated in aqueous fuel cells system [72-74]. Li et al applied commercial non-noble metal catalysts in the anode (Acta 3020 for ethanol oxidation) and the cathode (Acta 4020 for oxygen reduction), and a power density reached 60 mW cm^{-2} at 40 ^{o}C. Recently, Asazawa et al achieved a high power density of DHFC (617 mW cm^{-2}) using the same A201 AAEM and non-noble catalysts for both anode and cathode at a cell temperature of 80 ^{o}C [75].

Other materials were also investigated. For example, Fauvarque and co-workers prepared quaternized 1, 4-diazabicyclo-[2.2.2]-octane (DABCO) AAEMs with various commercial chlorine group ended polymer [76-78]. PVA/hydroxyapatite (HAP) composite membrane and cross-linked PVA composite membrane were investigated in DAFCs [79, 80]. However, the conductivity of these membranes is relatively poor (less than 0.01 S cm^{-1} at 60 ^{o}C and 100 % RH).

An alternative approach to the production of AAEMs is the use of suitable doping/reaction of polymer films with KOH. One example is an alkaline-doped polybenzimidazole (PBI) membrane for DAFCs which the ionic conductivity was 0.018

S cm^{-1} at room temperature and a power density of 60 mW cm^{-2} was achieved [11, 12]. In my later experiment, the results suggest that it has a questionable stability in the presence of KOH.

2.4.3   The stability of alkaline anion exchange membranes

The AAEMs stability was also a great concern, especially under the temperatures higher than 60 $^{\circ}$C. Varcoe and Slade suggested that the degradation pathways of AAEMs mainly go through two different mechanisms [3, 78]:

a) Direct nucleophillic displacement;
b) Hoffmann elimination;

In the first mechanism, a hydroxide ion performs an S_N2 attack on the methyl group and forms ethanol. In the second mechanism, an ylide (trimethylammonium methylide) and a water molecule are formed by the abstraction of a proton from a methyl group. The ylide subsequently reacts with water to form methanol [81]. The reactions are listed as below [81]:

$$[N(CH_3)_4]^+ + OH^- \rightarrow N(CH_3)_3 + CH_3OH \qquad (10)$$

$$[N(CH_3)_4]^+ + OH^- \rightarrow CH_2 = N(CH_3)_3 + H_2O \qquad (11)$$

$$CH_2 = N(CH_3)_3 + H_2O \rightarrow N(CH_3)_3 + CH_3OH \qquad (12)$$
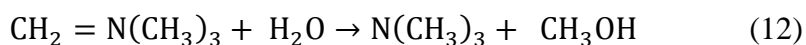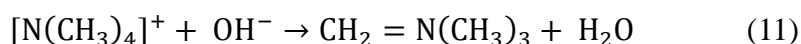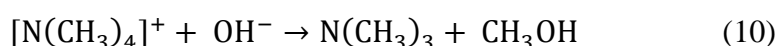
They further added that the tetraalkylammonium based cations are stable at higher temperatures (> 60 $^{\circ}$C) as long as these groups are not in water/solvent hydration environment. Macomber et al also came to the same conclusion using thermogravimetric analysis (TGA), differential scanning calorimetry (DSC) and evolved gas analysis [82].

2.5 Oxygen reduction reaction and its catalysts

The oxygen reduction reaction (ORR) is one of most basic reactions in nature (e.g. corrosion, metabolism) [55]. As the most abundant material on the planet earth, it exists in atmosphere and almost unlimited supply. In human industry, there are massive interests for chlori-alkali, metal-air cells and fuel cells [83].

In fuel cells, ORR is the rate determination reaction (e.g. PEMFCs). Thus, it is important to understand reaction mechanisms first and develop an effective catalyst for ORR.

2.5.1 *Pt based catalysts for ORR and their mechanism*

Pt based catalysts are most successful catalysts developed in either research or commercial scale. The ORR on Pt has been most extensively studied which makes it important to understand the mechanism, kinetic parameters of ORR and technologies for characterization.

The ORR mechanism on Pt is very complex due to a large number of intermediate species during the reaction. Damijanovic and co-workers conducted a detailed study of ORR on Pt, they reported that there are 14 pathways and over 50 mechanisms for ORR in acidic and alkali media [19]. However, these mechanisms can be further simplified under certain conditions. In alkaline media, mechanisms of ORR include direct four-electron transfer reaction to hydroxide (OH^-), two-electron transfer reaction to peroxide (HO_2^-) and possibly peroxide further reduce to hydroxide [19, 83].

In other cases, such as carbon or gold material electrode, the two electrons transfer reaction is the predominate reaction which means less current generation form the redox reaction and more hydrogen peroxide generation which is corrosive to the MEA and leads to a significant performance drop. It can be detected and quantified using RRDE

(details in section 2.6.6.2).

2.5.1.1 Derivation of Tafel equation from Bulter-Volmer equation

The kinetics of fuel cell reactions is described by the Butler-Volmer equation under the condition of one-electron transfer process, a mathematical expression explains how the rate of reaction depends on the potential:

$$i = i_0 \left\{ (\frac{Cs}{C_B})^n \exp\left[\frac{-\alpha_{Rd}F(E-Er)}{RT}\right] - (\frac{C_{Rs}}{C_{Rb}})^m \exp\left[\frac{\alpha_{Ox}F(E-Er)}{RT}\right] \right\} \quad (13)$$

Where Cs is the surface concentration of oxidant, C_B is the bulk concentration of oxidant, C_{Rs} is the surface concentration of reductant, C_{Rb} is the bulk concentration of reductant. α_{Rd} is the transfer coefficient of the reduction reaction and α_{Ox} is the transfer coefficient of the oxidation reaction, T is temperature (K), R is universal gas constant which is 8.314 J K^{-1} mol^{-1}, F is Faraday constant which is 96485, i is the current density of overall reaction (A cm^{-2}), i_0 is the exchange current density (A cm^{-2}), n and m are the reaction orders, E_r is the reversible potential (V) and E_r is 1.229 V (vs. NHE) at the fuel cell cathode (at 25 °C and atmospheric pressure).

At large overpotentials, such as those at the fuel cell cathode, when there are no mass transport limitations the first term in the Bulter-Volmer Equation becomes dominant [84]:

$$\eta = E - Er = \frac{RT}{\alpha_c F} \ln\left(\frac{i}{i_0}\right) \quad (14)$$

Where η is overpotential (V), This equation can be simplified as

$$\eta = a + b \log(i) \quad (15)$$

25

where

$$a = -2.3\frac{RT}{\alpha F}\log(i_0), \text{ and } b = 2.3\frac{RT}{\alpha F}$$

Equation 15 is the so-called Tafel equation, and term b is the Tafel Slope. By plotting the overpotential versus logarithm of the current density (Tafel Plot, Figure 2-11) is possible to obtain useful information regarding the reaction kinetics.
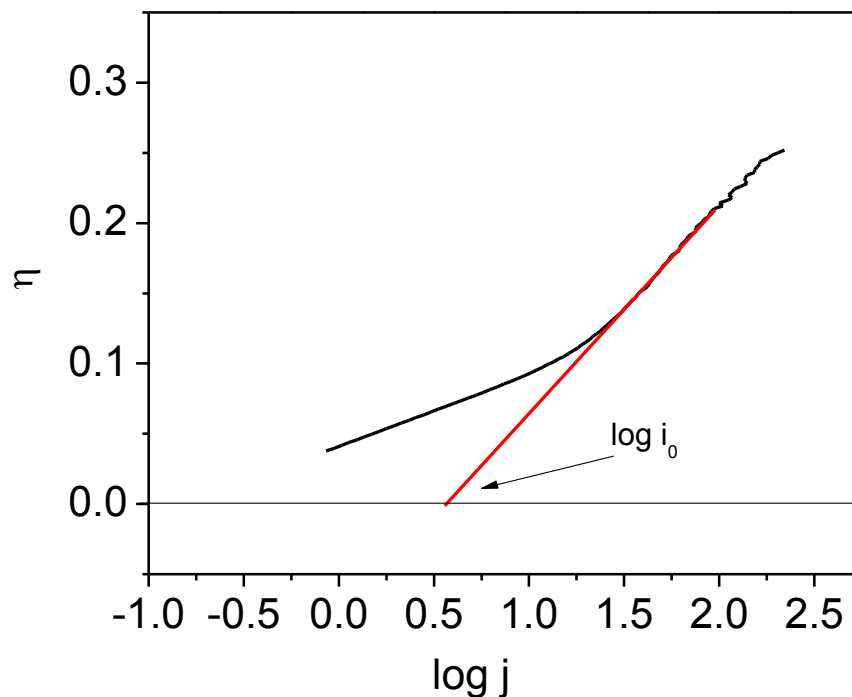
Figure 2-11 Plot of Tafel Equation

1. The point at which the curve intersect the potential axis gives the value of the reversible potential or OCP (overpotential equal to zero)

2. If we extrapolate the linear parts of the curve to the current axes, the point where both lines interject gives the value of i_0

3. The slope of the linear part of the graph gives the value of the b term. The transfer coefficient can thus be calculated from this term.

2.5.1.2 <u>Tafel slopes of ORR</u>

The kinetics of ORR on Pt in both acid and alkaline media has been well-defined over decades. According to Damjanovic et al [85, 86], the expression of the Tafel slope of ORR at the low current density region (under Temkin condition-high coverage of oxygen species) in both acid and alkaline media can be written in a form of $b = -2.3 \times RT/F$. The calculated value is -0.060 V dec^{-1}. At high current density region, the coverage of oxygen species is low which is so-called "Langmuirian condition" and the Tafel slope is $b = -2.3 \times 2 \times RT/F$ (-0.012 V dec^{-1}).

2.5.2   Pd based catalysts for ORR

Pd based catalysts have been studied extensively for ORR in acid media and alcohol oxidation in alkaline media [20, 26, 87-91]. There are only few reports on the catalytic activity of ORR on Pd/C catalyst [92, 93]. Recently, Jiang et al reported the ORR activity on Pd catalysts and suggested that it promotes a four-electron transfer reaction of ORR similar to ORR on Pt/C catalyst [92, 94]. In addition, the study on the relationship between the ORR activity and the metal d-band centre in alkaline solutions showed that Pd (111) single crystal and nano-Pd/C both had a d-band centre value close to Pt (111) or Pt/C suggesting that Pd may be a viable alternative to Pt in fuel cells [95].

The carbon support modified by certain chemicals (e.g. KOH, H_3PO_4 and etc) can have a significant impact on catalyst activity [95-97]. Figureueiredo et al explained that the carbon surface can be functionalized with different groups (carboxylic, anhydride, phenolic and carbonyl) after oxidative treatment using for example H_2O_2, HNO_3 or 5 % O_2 in N_2 [98]. It has been well established in the literature that surface oxygen groups can form anchoring sites for metallic precursors as well as for metals which determine the properties of pre-treated carbon as a catalyst support material [97]. However, to the best of my knowledge, no previous work has attempted to uncover the effect of carbon pre-treatment on the Pd/C morphology and its ORR activity in alkaline media.

Understanding the effects of carbon pre-treatment on the ORR activity of Pd catalyst will help to design and optimize cathode catalysts for alkaline anion exchange membrane fuel cells.

2.5.3 Non-noble metal catalysts for ORR

The motivation of developing non-noble metal catalysts was driven by the pressure of oil crisis in the 1970's, high cost of Pt based catalysts and perfluorosulfonic acid (PFSA) membranes [18] [24, 99]. In Figure 2-12, the Pt price obtained from Johnson Matthey (JM) shows an increase trend and it is predicted to be a dramatic increase after the fuel cell commercialization.
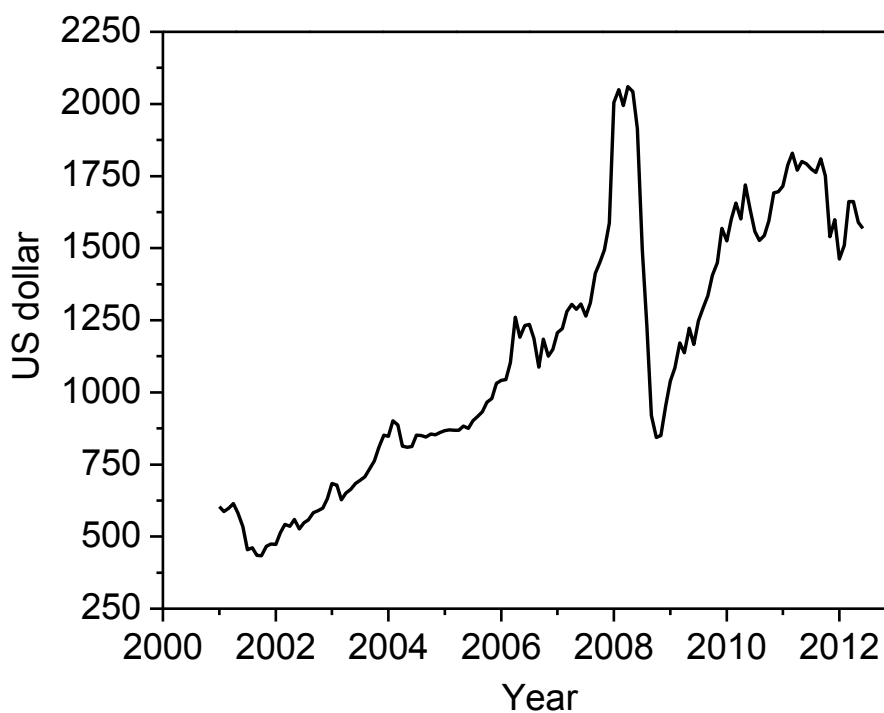
Figure 2-12 Pt price in the latest decade from Johnson Matthey (JM)

A number of materials were recommended as ORR catalysts which are listed in Table 2-3 including low cost and more abundant materials.

Table 2-3 Catalyst materials for oxygen reduction reaction in low-temperature fuel cells

Material	Catalysts	Fuel cell type	References
Metal oxides	MnO_x, $NiCoO_x$, Perovskites and Spinels type	PEMFCs, AAEMFCs or water electrolysers	[100-105]
Non-noble metals	Ag based, Au	AFCs, AAEMFCs, PEMFCs	[106-108]
Metal macro-cycles	CoPc, FePc, FeTMPP, CoTMPP, CoPPy	PEMFCs, AAEMFCs, Microbial fuel cells (MFCs)	[99, 109-113]
Carbons	N-doped carbon nanotube, Activated carbon	PEMFCs, AAEMFCs	[114-119]

Non-noble metal oxides have been using for evolution/reduction reaction in alkaline media. Chang et al reported a $La_{0.6}Ca_{0.4}Co_{0.8}Ir_{0.2}O_3$ perovskite for both oxygen evolution and reduction reaction in alkaline media [100]. The presence of IrO_2 only improved the oxygen evolution activity of $La_{0.6}Ca_{0.4}Co_{0.8}Ir_{0.2}O_3$ perovskite, but also an unexpected significant improvement on ORR was observed. No further explanation on this matter was given. High surface area spinel-type oxides $LiMn_{2-x}M_xO_4$ [M=Co, Fe, (CoFe)] were synthesised using an improved amorphous citric precursor method (IACP). A zinc-air cell will be more efficient (up to 10 %) using such catalysts [103].

Since the first report of ORR activity of Co phthalocyanine (CoPc) for fuel cell applications [110], metal macro-cycles catalysts has been investigated extensively. Metal macrocylces have been shown to be effective ORR catalysts in acid, neutral and alkaline solution [99, 109, 110, 120-122]. Active sites of these compounds are the four-nitrogen ring coupled with transition metal, normally iron or cobalt based for the ORR. The main motivation for developing metal macrocycle catalysts for the ORR in AAEMFCs include high catalytic activity, low cost and alcohol tolerance [123]. However, the stability of these metal macrocycle catalysts is a concern [111, 124, 125].

For example, iron phthalocyanine (FePc) is unstable in a low pH (< 3) environment due to the de-metalisation process (equation 16), with protons replacing the central metal ion and the catalyst eventually losing its activity [125].

$$FePc + 2H^+ \rightarrow H_2Pc + Fe^{2+} \qquad (16)$$
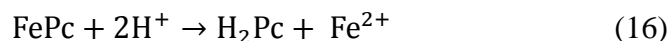
It was found that the stability and activity of metal macrocycles in acid electrolytes can be significantly improved after heat treatment at up to 1000 ^{o}C [111, 112, 124].

Behret and co-workers reported a series of polymeric metal Pc for both acid and alkaline media. They further added FePc showed better activity than other metal Pc in alkaline media, however, an instability for polymeric and monomeric metal Pc was found in acid media [126]. Zagal et al also investigated the electrochemical behaviour of different metal Pc (in Figure 2-13) in acid and alkaline media [127]. Based on molecular orbit theory, they identified Fe shows higher activity (among Co, Mn, Ni) for ORR which match the energy of the corresponding π* orbit of dioxygen.
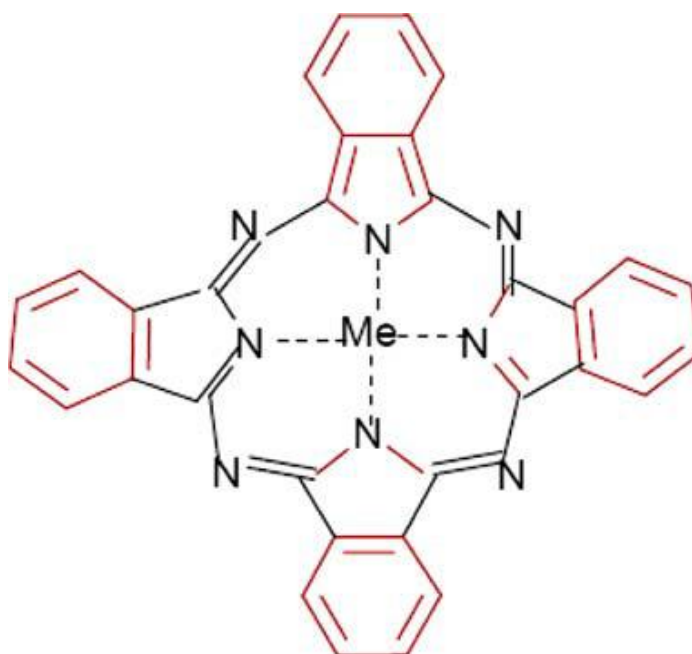
Figure 2-13 Molecular structure of metal phthalocyanines

Dodelet and co-workers prepared heat-treated iron, cobalt phthalocyanine and

tetracarboxylic iron phthalocyanine supported on carbon black catalysts and characterized in PEMFC [128, 129]. The heat-treated catalysts under 900 ^{o}C showed a reasonable stability and activity of ORR (40 % of current) compared to the same metal loading commercial catalyst (2 wt %, Pt/C). Further report from the same group pointed out the Fe and N were equally important for generation of the catalytic site for ORR [130]. However, nitrogen atoms incorporated in the carbon structure (C-N) during heat-treatment is not active for ORR [131]. The formation of metal core and carbon shell was observed by heat-treatment which stabilized the catalytic site [111, 128].

A novel cobalt polypyrrole (PPy) catalysts which are physically bonded to carbon surface (in Figure 2-14) were prepared and it showed a four-electron transfer reaction towards ORR in half cell test in acid media [132]. Bashyam et al evaluated similar catalysts in PEMFC and the short-term stability test (100 h) showed minimal degradation at 0.4 V and 80 ^{o}C [109].
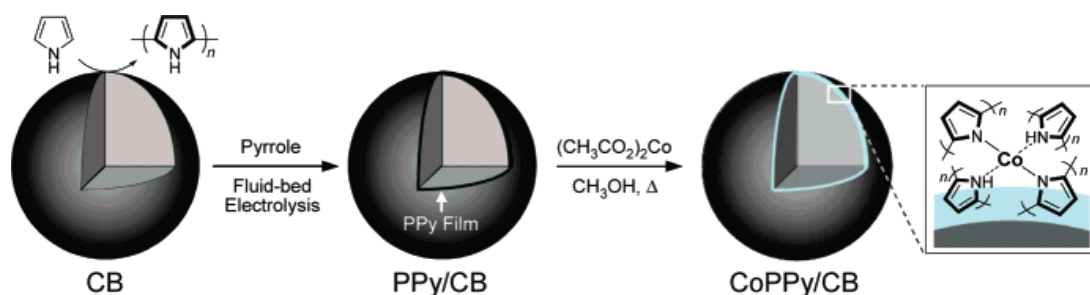
Figure 2-14 Schematic synthesis procedures of CoPPy/C [132].

Recently, Gong et al synthesised a vertically-aligned nitrogen-containing carbon nanotubes (VA-NCNTs) for ORR in alkaline media [24]. The catalytic activity of ORR, stability and co-poisoning tests showed a similar activity to commercial Pt/C, but with higher electrochemical stability (10,000 cycles in O_2-saturated 1.0 M KOH solution) and inert to co-poisoning. Non-aligned nitrogen-doped CNTs were also prepared using a new approach - CNT oxidation and followed by heat-treatment in NH_3 atmosphere at high temperatures [133]. The X-ray photoelectron spectroscopy (XPS) and half-cell results suggested that pyridine-N-oxide groups (N_4) on the CNT surface make the major

contribution to its ORR activity in alkaline media.

2.6 Anode oxidation reactions in alkaline media

2.6.1   Catalysts for the alcohol oxidation reaction in alkaline media

Pd based catalysts for alcohols oxidation have been studying extensively. Oxides (CeO_2, NiO, Co_3O_4, and Mn_3O_4) promoted Pt and Pd catalysts for alcohols oxidation were examined by Shen et al [134-138]. Results suggested that the addition of NiO into Pt/C or Pd/C catalysts showed the best activity and it significantly improve electrode performance for methanol and ethanol oxidation in terms of reaction activity and poisoning resistance [134, 139]. Recently, Zhao et al reported that carbon supported PdNi alloy with atomic ratio of 2 to 3 exhibits the best activity towards ethanol oxidation and direct ethanol fuel cell performance reached 90 mW cm^{-2} at 60 ^{o}C using Pd_2Ni_3/C catalyst at anode [140]. With different supports, the activity of Pd towards the alcohol oxidation was investigated as well. Shen et al prepared Pd catalyst and used carbonizaed TiO_2 nanotube as support [136]. Such support material oxidizes CO on Pd surface effectively which makes Pd more stable. The tungsten carbide (WC) single nanocrystal support was also reported by the same group [141]. Compared to the exchange current densities (j_0) of ethanol oxidation on Pd/C, the j_0 of Pd-WC/C is two orders of magnitude higher. They further added that the significant improvement was contributed by the lower activation energy of ethanol oxidation on Pd-WC/C (10.59 J mol^{-1}) than Pd/C (26.96 J mol^{-1}). An Italian company, Acta, has recently reported good activity for the alcohol oxidation, with complete oxidation to CO_2 or carbonate, on anodes consisting of small nanoparticles or clusters of Ni–Fe–Co alloys in a matrix of hydrazone-based polymer, with the trade name HYPERMEC^{TM} [20].

2.6.2   Hydrogen oxidation in AAEMFCs

There are still few reports on the hydrogen oxidation reaction in alkaline media

especially in an AAEMFC. It is well-known that the kinetic of hydrogen oxidation reaction (HOR) is much faster than the ORR at the cathode in PEMFC. However, Varcoe et al reported otherwise that the HOR causes greater performance loss than the ORR at cathode in solid state electrolyte single cell system using a novel hydrogen riched Pd coated Pt wire as reference electrode [142]. They added that the anode flooding caused by the water production may be responsible for the higher impedance at the anode than the cathode (as shown in Figure 2-15). Lately, the kinetics of HOR in acid and alkaline media was compared using RDE in half cell [143]. Their measurements and analysis also confirm that the HOR/HER kinetics on Pt/C are several orders of magnitude slower in alkaline compared to acid electrolyte.
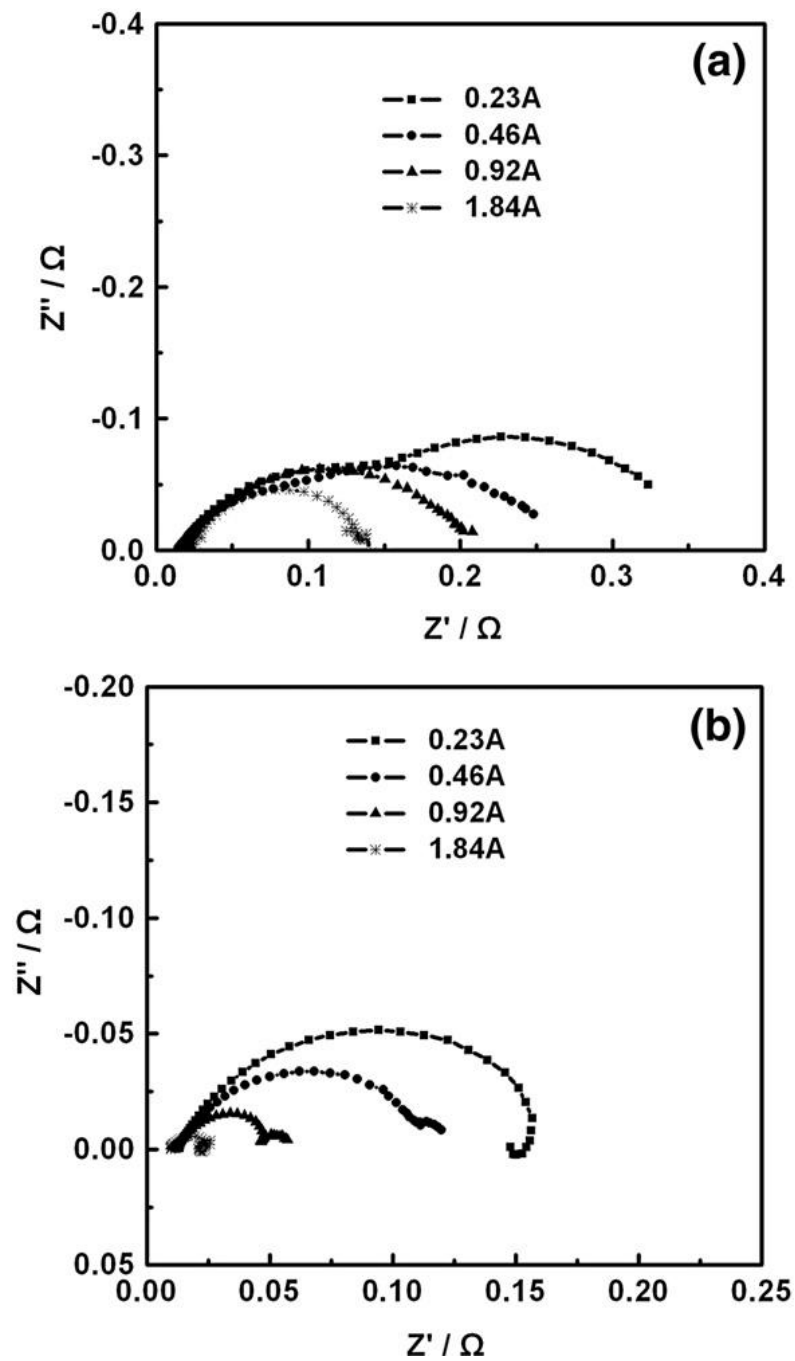
Figure 2-15 The impedance of an AAEMFC, a) anode and b) cathode at 50 ^{o}C, 100% RH and atmospheric pressure [142]

2.7 Conclusions and Perspectives

Rapid development in solid polymer membranes suggests that AEM based AFCs will be the dominant type of fuel cell for various applications. Anion exchange membrane fuel cells (AEMFCs) have special advantages over PEM fuel cells providing the possibility of developing versatile power source systems with low cost membrane and catalyst materials. Following suggestions can be considered:

- Developing high ionic conductivity and electrochemical stability ionomer- Radiation-grafted and cross-linked AEMs exhibited promising performance [65, 144]. Due to the insolubility of such materials, it cannot be applied in the catalyst layer and lack of suitable ionomer in the catalyst layer will result in a significant fuel cell performance loss

- Non-noble metal catalysts for both anode and cathode- As the price of gold and platinum hit the record high on the market, the catalyst development for AFCs will be more and more focused on non-noble metal catalysts

It can be envisaged that AEMFCs will play a major role in energy research and applications in the near future.

CHAPTER 3. EXPERIMENTAL METHODS

3.1 Electrochemical methods

3.1.1 Cyclic voltammetry

The most used electrochemical method for catalysts characterization is cyclic voltammetry. In Figure 3-1, the typical three electrodes system for CVs consists of a working electrode– target of investigation, a reference electrode– a known couple potential which is used to measure against the potential of working electrode, and a counter electrode – forms a complete electronic circuit with working electrode in aqueous electrolyte [145].
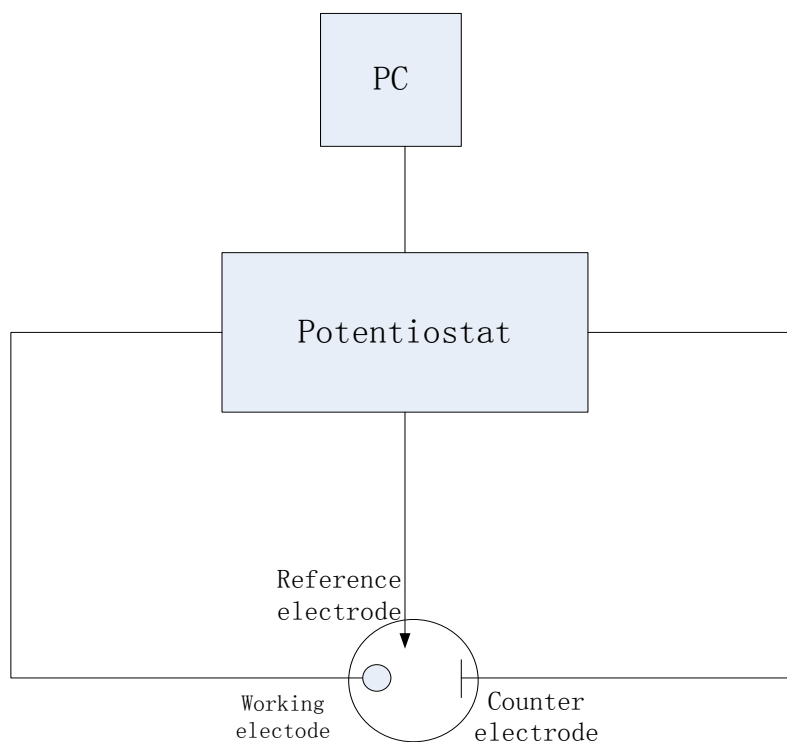
Figure 3-1 Typical three electrodes configuration: working electrode, reference electrode and counter electrode.

CV technique can be described as follow (in Figure 3-2). Potential is sweeping in a positive direction, and in the electrode's vicinity there is a large concentration of the oxidizable anion radical of anthracene. As the potential approaches, then passes, E_0', the electrochemical balance at the surface grows more and more favorable toward the

36

neutral anthracene species. Thus the anion radical becomes reoxidized and an anodic current flows. This reversal current has a shape much like that of the forward peak for essentially the same reasons. For a reversible reaction, is a reversal technique and is the potential-scan equivalent of double potential step chronoamperometry. Cyclic voltammetry is a very popular technique for electrochemical studies and has proven very useful in obtaining information about fairly complicated electrode reactions (such as ORR) [84].
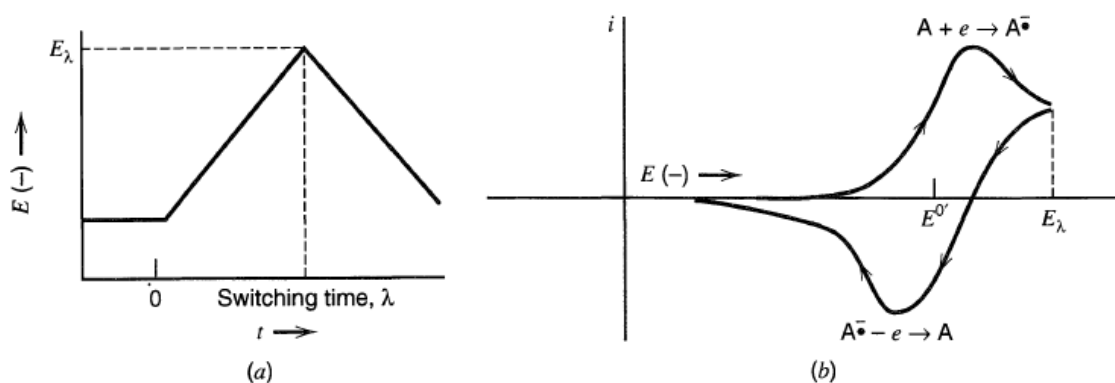
Figure 3-2 a) Cyclic potential scan, b) Resulting cyclic voltammogram [84]

3.1.2   Rotating ring disk electrode

In order to investigate intermediate species during the ORR, one of commonly used techniques is so-called rotating ring disk electrode (RRDE). Typical RRDE is shown in Figure 3–4, it consists of a disk electrode, insulation gap (between disk and ring electrode), ring electrode (e.g. Pt or Au) and insulator outer layer [19]. Taking ORR as example (as shown in Figure 3–3), the inert glassy carbon disk electrode is normally coated with carbon supported catalyst as the working electrode (e.g. Pt/C) and Pt ring can partially oxidizes (or reduces) hydrogen peroxide at certain potential (access the ring electrode – some of them can also diffuse to solution and the rest of them is undetectable after disproportionation reaction).

$$O_{2\ bulk} \xrightarrow{\text{diff}} O_{2\ \text{adp}} \xrightarrow{2e^-} HO_2^- \xrightarrow{2e^-} 4OH^-$$

$$4e^-$$
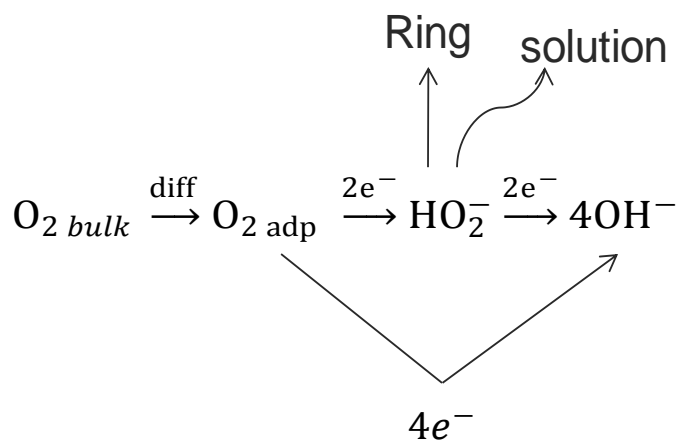
Figure 3-3 Schematic of ORR on Pt in alkaline media and detection of H_2O_2
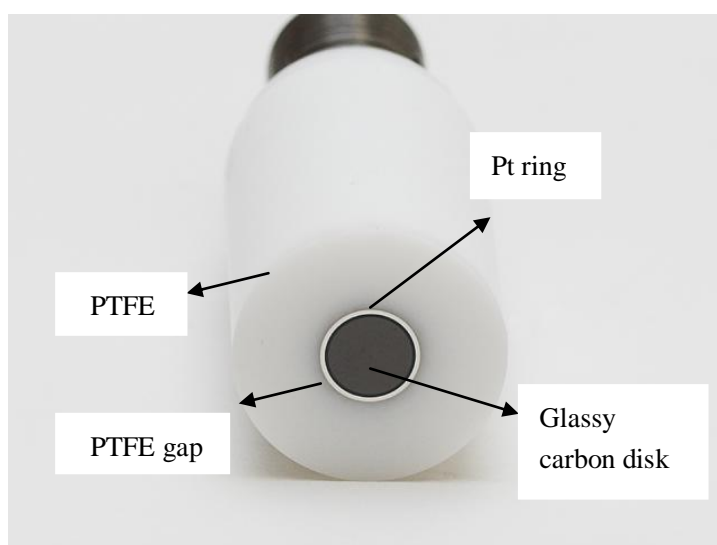
Figure 3-4 The image of a commercial RRDE from pine instrument

The fraction of hydrogen peroxide yield can be calculated from RRDE polarization curves using following equation [106]:

$$X = (2I_r/N)/(I_r + I_d/N) \times 100\ \% \qquad (1)$$

Where X is the fraction of hydrogen peroxide, I_r is the ring current, I_d is the disk current, and N is the collection efficiency of Pt ring

3.1.3 Frequency response analyser

The ionic conductivity of membranes was measured using frequency response analysis (FRA) technique. The complete electrical circuit of FRA is drawn in Figure 3–5 which consists of a frequency response analyser, a home-made conductivity cell (four Pt foil with 0.5 cm width and locates in parallel with an equal distance of 0.5 cm), an ampermeter and a voltammeter. In this thesis, The measurement of samples was conducted using four-point probe method [52, 69].
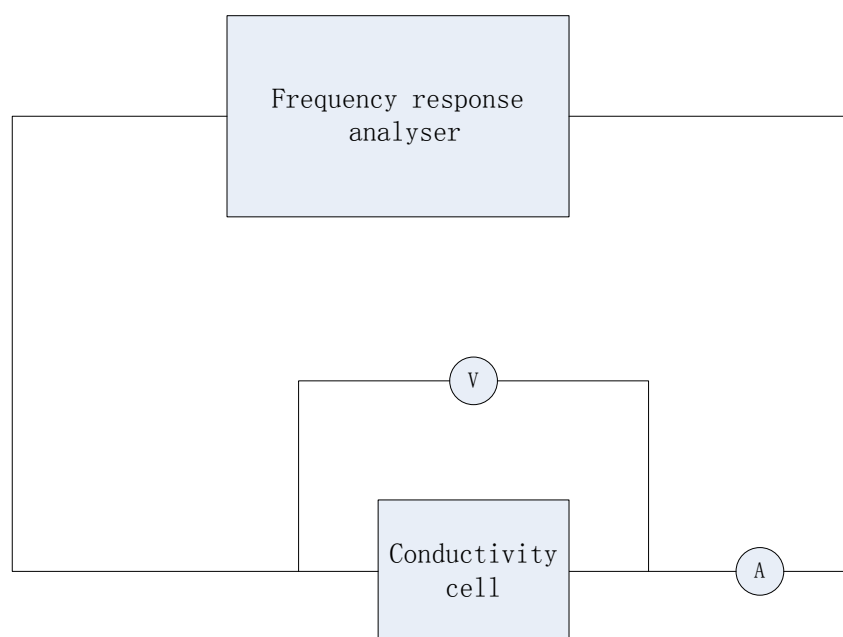
Figure 3-5 Electric circuit of frequency response analysis

The final results were calculated using following equation (2):

$$\sigma = i\delta/vA \qquad\qquad (2)$$

where σ is the membrane conductivity (S cm^{-1}), i is the response current (A), v is the response voltage (V), δ is the distance between platinum foils (cm) and A is the membrane area of cross-section (cm^{-2})

3.2 Membrane preparation and characterizations

3.2.1 Synthesis of quaternary DABCO polysulfone

The synthesis of QDPSU was achieved by two steps as shown in Figure 3-1. First, the method for synthesis of choloromethylated polysulfone (CM-PSU) by a Friedel-Crafts like reaction was used, as developed by Avram and co-workers [146]. 10 g (2.26 mmol) polysulfone (P-1700, Udel) was dissolved in 400 cm^3 (mL) of 1,2-dichloroethane. 6.78 g (22.6 mmol) paraformaldehyde and 24.6 g (22.6 mmol) trimethylchlorosilane were added to the solution with magnetic stirring. Stannic chloride 1.178 (0.452 mmol) was added dropwise and the reaction proceeded for 12 to 48 hours at 50 ^{o}C, to 5 produce different degrees of substitution of CM-PSU. The white CM-PSU was precipitated in high purity ethanol (99.9 %) to remove the excess of reactants. The product was purified by dissolving in dimethylacetamide (DMAc), filtering and precipitating with distilled water several times. After that treatment, the product was dried in high vacuum to remove any residual solvent and kept in a vacuum before further use.

In order to avoid producing cross-linked QDPSU (Figure3-1b) which is not soluble in DMAc, the quaternization at a different degree of substitution (DS) was completed by adding CM-PSU and DABCO in DMAc in a molar ratio of 1 (-CH_2Cl): 5 (DABCO). The mixture was stirred at 80 ^{o}C for 14 hours, whereupon the product was precipitated using diethyl ether and dried at 60 ^{o}C in vacuum.
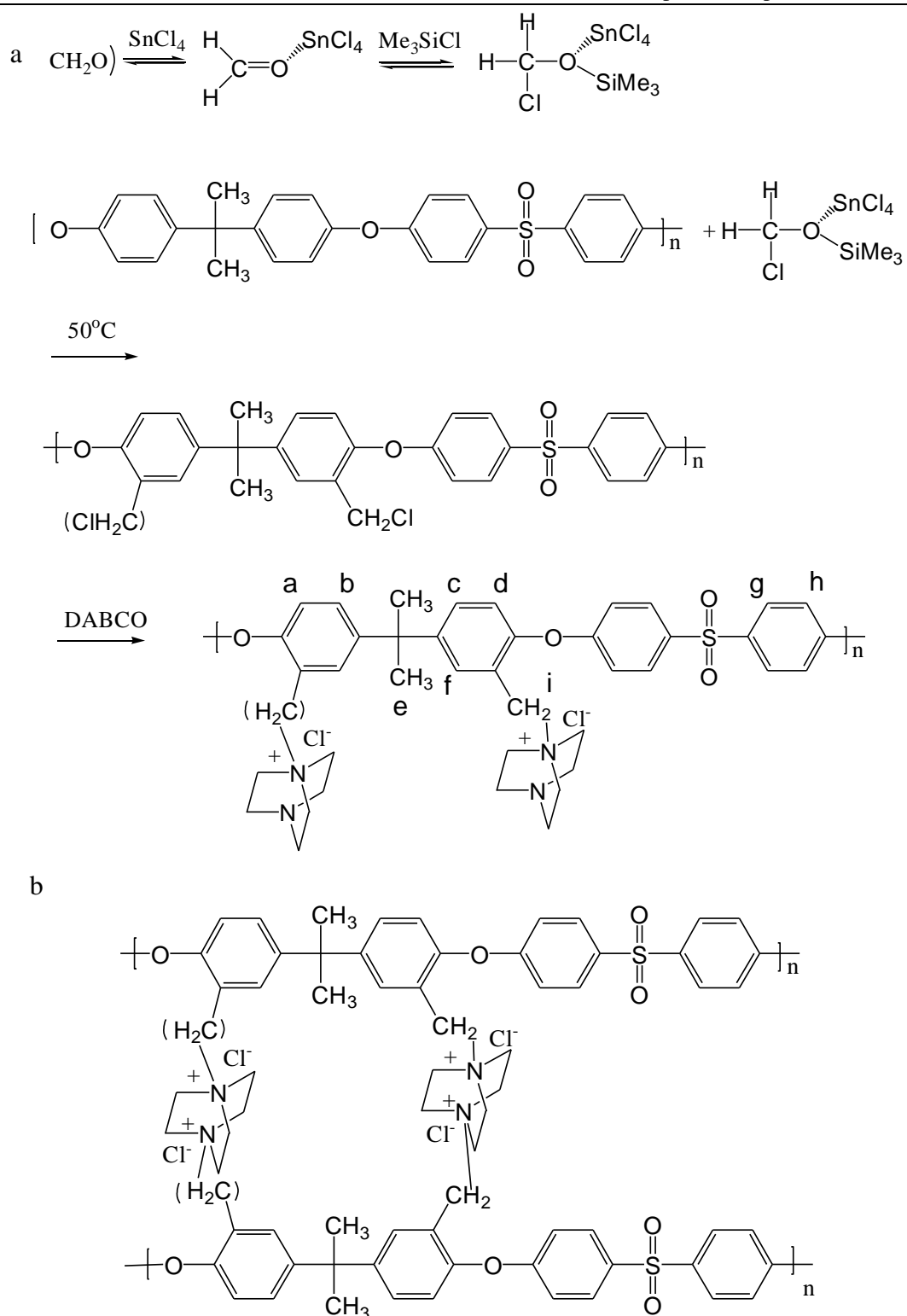
Figure 3-6 a) Synthesis scheme of quaternary DABCO polysulfone, b) cross-linked QDPSU

3.2.2 *Preparation of PTFE-QDPSU composite membrane*

The preparation of PTFE-QDPSU composite membrane was carried out according to the procedure in Figure 3-5. Microporous PTFE with 82 % porosity was obtained from membrane solution (US) and used as support. First, the hydrophobic PTFE sheet was pre-treated using the method developed by Li et al [69, 70], namely the PTFE membrane was treated with seven parts H_2SO_4 (98 wt% aqueous solution) and three parts H_2O_2 (30 wt% aqueous solution) at 80 ^{o}C for 1 h. Then, the porous PTFE was rinsed with copious amounts of de-ionised (DI) water and further treated by immersion in a solution containing one part aqueous NaOH (1.0 mol dm^{-3}) solution, one part H_2O_2 (30 wt% aqueous solution), and five parts DI water at 70 ^{o}C for 30 min, followed by rinsing with copious amounts of DI water .

The pre-treated PTFE sheet was boiled in DMAc for 10 min, then the PTFE sheet was immersed in a low-concentration quaternary 1,4-diazabicyclo-[2.2.2]-octane polysulfone (3 wt % QDPSU in DMAc) for 10 min. QDPSU solution was casting with or without pre-treat PTFE on an optical glass and left at 60 ^{o}C for 14 h to form a membrane and remove any residual solvent. The conversion from Cl$^-$ form to OH$^-$ or CO_3^{2-} form was achieved by leaving membranes in 1.0 M KOH or K_2CO_3 for 14 h at room temperature.
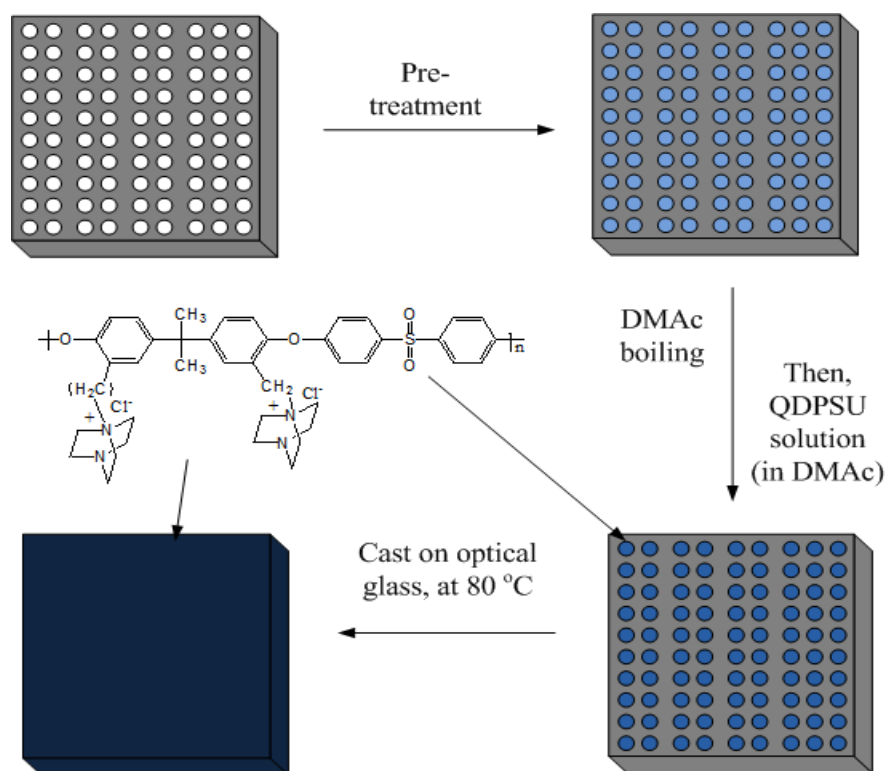
Figure 3-7 Preparation procedures of PTFE-QDPSU composite membrane

3.2.3   PBI-KOH membrane preparation

PBI solution (8 wt %) was casted on an optical glass and the thickness was adjusted using a doctor blade (Sheen instrument). Then, it was left at 80 $^{\circ}$C overnight to form a membrane and remove any residual solvent. The conversion from Cl^{-} form to OH^{-} form was achieved by leaving membranes in different concentration of KOH for different time at room temperature.

3.2.4   Preparation of phosphoric acid loaded quaternary DABCO polysulfone membrane

QDPSU membrane was immersed in 11.0 M phosphoric acid at room temperature for three days to obtain the PA/QDPSU membrane.

3.2.4   *^{1}H NMR analysis*

^{1}H NMR (400 MHz) was performed on JEOL-ECS 400 using deuterochloroform and dimethyl sulfoxide (DMSO) as the solvent and tetramethylsilane (TMS) as the internal reference.

3.2.5   *Thermo-gravimetric analysis*

Thermo-gravimetric analysis (TGA) was performed on a TGA Q500 (TA instrument) using samples (20 mg) placed in a ceramic crucible. The samples were heated from room temperature to 600 ^{o}C at a rate of 5 ^{o}C min^{-1} under flowing nitrogen (30mL min^{-1}).

3.2.6   *SEM and EDX analysis*

A low vacuum environmental scanning electron microscopy (ESEM, JSM-5300LV, Japan) incorporated with energy dispersive X-ray (EDX) spectroscopy was used to investigate the morphology and microstructure of membrane. The membrane was immersed in liquid N_2 for 10 min and was then broken off to investigate the morphology of membrane cross-section.

3.2.7   *FT-IR analysis*

Fourier transform infrared spectroscopy (FT-IR) of samples was measured on a Varian 800 FT-IR spectrometer system between 4000 and 400 cm^{-1}.

3.2.8   *Swelling behaviour and water uptake*

Swelling degree and water uptake were calculated using following equations:

$$Water\ uptake = (m_{wet} - m_{dry})/m_{dry} \times 100\ \% \qquad (3)$$

$$Swelling\ degree = (\delta_{wet} - \delta_{dry})/\delta_{dry} \times 100\ \% \qquad (4)$$

where m_{wet} and δ_{wet} are the weight and cross-sectional thickness of fully hydrated membrane respectively and m_{dry} and δ_{dry} are the weight and cross-sectional thickness of fully dehydrated membrane respectively. The weight and thickness of samples were taken in the OH⁻ form when they were fully hydrated and dried, respectively. The drying of samples was carried out by placing them in a container fully filled with nitrogen gas for 1 h at 55 °C.

3.2.9   *Ionic conductivity measurement*

A four-point probe technique was used in a home-made cell for membrane conductivity measurement. The membrane was contacted with platinum foils and connected to a frequency response analyser (FRA, Voltech TF2000, UK). All samples were cut into 1.0 cm wide, 5.0 cm long strips and placed on the platinum foil with 0.5 cm gap between them. For the KOH loaded PBI membrane, the excessive KOH at the surface of membrane was carefully removed using filter paper. AC impedance measurements were carried out at frequencies between 1 and 20 kHz with an oscillating amplitude of 10 mV. The polymer membranes were held at the desired temperature for 30 min to reach steady state under N_2 or CO_2 atmosphere. The final results were calculated the data using equation (2).

3.3 **Catalysts preparation and characterizations**

3.3.1   *Preparation of metal macrocycle catalysts*

Carbon supported metal macrocycle catalysts were prepared using the impregnation method which is reported elsewhere [147, 148]. Specifically, iron phthalocyanine

(FePc), cobalt phthalocyanine (CoPc) (as shown in Chapter 2) or Co-tetramethoxyphenylporphirine (CoTMPP in Figure 3-8) and Vulcan XC-72R (Cabot) with a surface area of 213 m^2 g^{-1} were mixed in concentrated H_2SO_4 (98 %) and magnetic stirred for 30 minutes in open air. Then, the mixture was poured into a large amount of cold DI water to obtain the precipitate and stirred continuously for another 20 h. The precipitate was collected by centrifuge and washed repeatedly until pH 7 was achieved. The obtained precipitate was then fully dried in an oven at 100 ^{o}C for 10 h. Alternative carbon supports; Ketjenblack EC-300J (Akzol Noble) and SuperP (Timcal) with different surface area (795 and 62 m^2 g^{-1}) were also used as support for catalysts preparation in order to investigate the effect of different carbon support on the ORR activity of catalysts. All the chemicals were used as received.
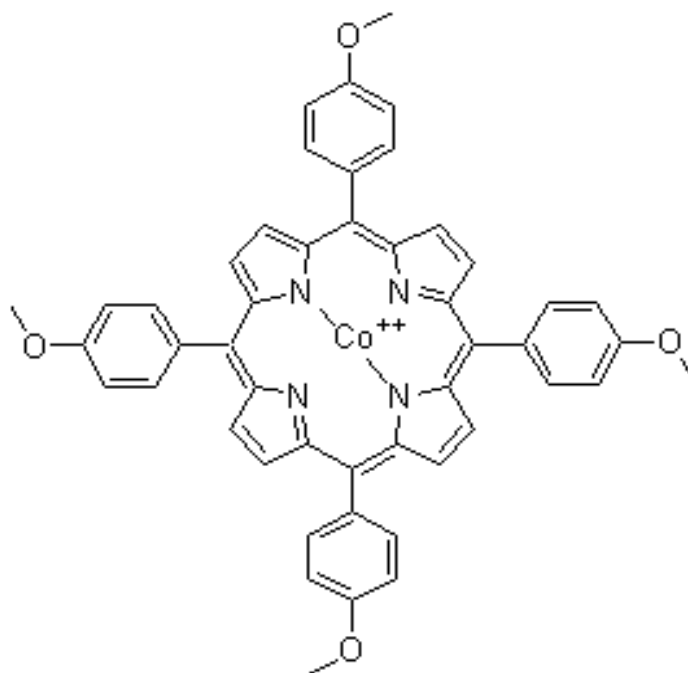
Figure 3-8 Molecular structure of CoTMPP

For the heat treatment procedure, the KJB supported FePc (FePc/KJB) was pyrolyzed at 800 ^{o}C and N_2 atmosphere for 6 h which is the reported optimized condition [124, 149]. Then it was cooled down naturally to room temperature. The obtained catalyst will be referred to FePc/KJB-H8. Commercial K-14 non-noble catalyst (Fe and Ni based catalyst supplied from Acta, Italy) and 20 wt % Pt/C (BASF) were evaluated as benchmark.

3.3.2   Electrochemical characterizations

For half-cell test, the catalyst inks were prepared by dispersing 21.2 mg of catalysts in 3.0 mL Nafion®/ethanol solution (0.5 wt % Nafion). The mixture was ultrasonicated for 40 min in an ice bath [148]. Then, 15 µL of the catalyst ink (catalyst loading of 0.43 mg cm^{-2}) was pipetted onto a glassy carbon disk electrode (0.2475 cm^2) and dried under an infra-red lamp for 1 h.
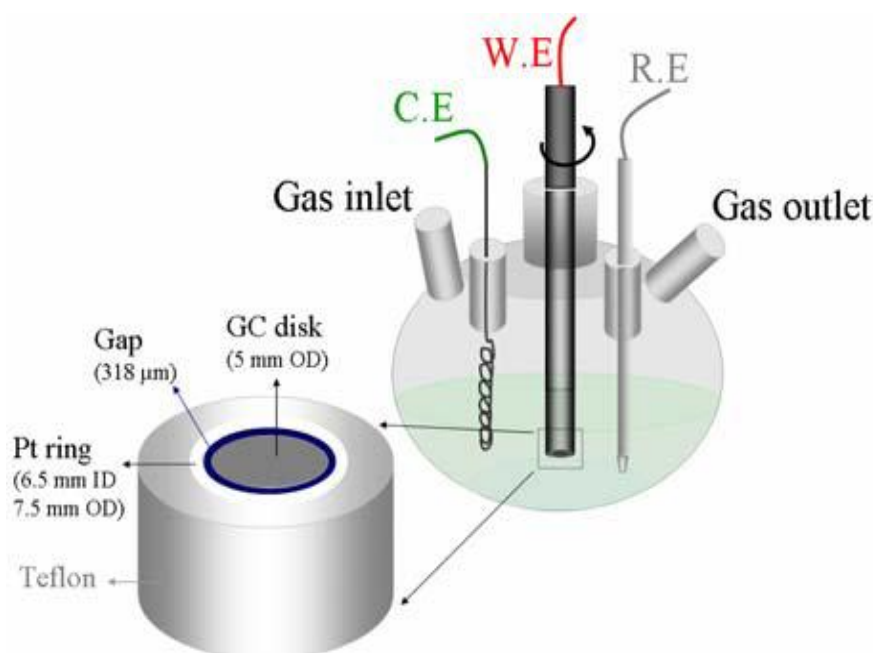
Figure 3-9 Schematic diagram of three-electrode cell [24]

Electrochemical characterization was carried out in a typical three-electrode cell system (as shown in Figure 3-9) in N_2 or O_2 saturated 1.0 M KOH solution at room temperature. A Pt coil with a large surface area was used as the counter electrode and a mercury/mercury oxide (Thermo®, 0.140V vs. NHE) in 1.0 M KOH was used as the reference electrode. The working electrode was an RRDE electrode (Pine Instrument, US) with a geometric area of 0.2475 cm^2 glassy carbon disk and a Pt ring electrode (collection efficiency is 37 % - manufacture data). The Pt ring potential was maintained at 0.27 V (vs. Hg/HgO). RRDE measurements were conducted using an Autolab

PGSTAT 303 bipotentiostat. The working electrode was conditioned by running 20 cycles of CV at a 0.1 V s^{-1} scan rate, prior to any test. CVs of all catalysts were extracted from the negative-going scan for metal macrocycle catalysts and the positive-going scan for Pt/C as explained in the earlier chapter. This is due to the Pt-O formation at high potential, and therefore Pt-site for ORR on the negative scan as Pt-O is reduced to Pt.

For making Tafel plots, the mass-transport corrected ORR currents at the disk electrode were calculated using the following equation [93]:

$$j_k = (j_L \times j)/(j_L - j) \qquad (5)$$

where j_L is the limiting current density (A cm^{-2}), j_k is the kinetic current density (A cm^{-2}) and j is the current density (A cm^{-2}). j_L was taken as the ORR limiting current at −0.4 V (vs. Hg/HgO).

3.4 MEA fabrication and fuel cell tests

3.4.1 MEA fabrication

For preparing the electrode, catalyst inks for both anode and cathode were prepared by dispersing catalyst (e.g. 40 wt % Pt/C electrocatalyst from Johnson Matthey) with various amount of QDPSU solution (6 wt %) in DMAc. Then, the mixture was ultra-sonicated for 40 minutes. The ink was sprayed onto SGL 25BA carbon paper with a specific loading of catalyst.

For the electrodes in DMFC tests, catalyst inks for both anode and cathode were prepared by dispersing catalyst PtRu/C (Pt:Ru atomic ratio 1:1, 60 wt %, JM) and Pt/C (60 wt %, JM) in PBI (3 wt %) and DMAc solution, repectively. Then, it was ultra-sonicated for 40 minutes. The ink was sprayed onto SGL 25BA carbon paper with

48

a specific loading of catalyst.

A radiation-grafted low density polyethylene AAEM provided by Cranfield University was used in this study for preparation of MEAs. After converting the AAEM to a desired form (OH^- or CO_3^{2-}) as described in the previous section, it was rinsed with large amount of distilled and deionized water to remove any KOH. Finally, electrodes and membrane were cold-pressed at 120 kg cm^{-2} for 5 minutes to make a membrane electrode assembly (MEA) [23].

3.4.2   Fuel cell design and test

AAEMFC measurements were conducted using a single cell (as shown in Figure 3- 10) with 1.0 cm^2 stainless steel serpentine flow field surrounded by the O-ring seal and it is contact to the copper current collector. The temperature of the cell was controlled by thermostatically controlled cartridge heaters inserted into the cell body (three round holes in Figure 3-10c). A PTFE sheet (for each side) was placed between cell body which prevent from short circuit. Fuel cell tests were carried out using H_2 and O_2 or CO_2 free air with flow rates of 80 cm^3 min^{-1} for the anode and 100 cm^3 min^{-1} for the cathode, respectively.

e)

f)
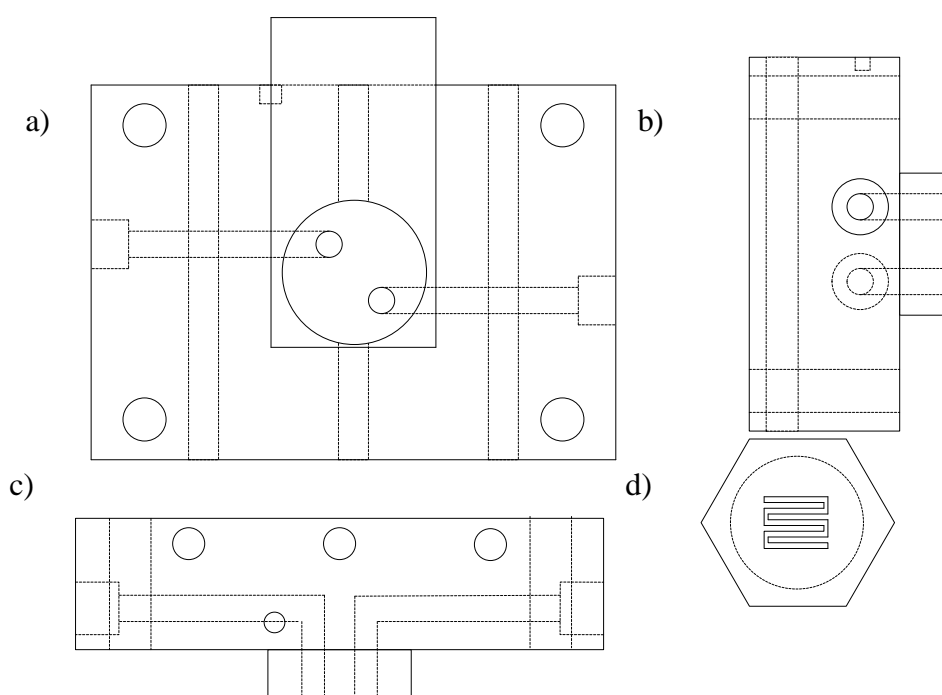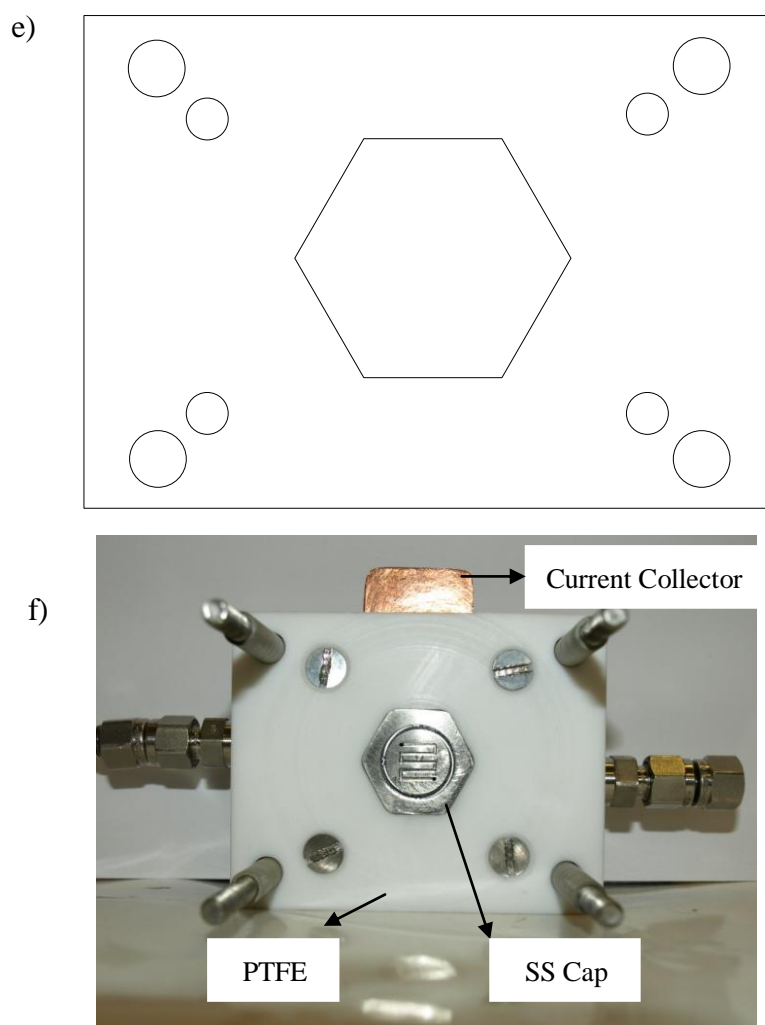
Figure 3-10 Single cell design for AAEMFC test using hydrogen and oxygen/air, a) front view of cell body, b) side view, c) top view, d) stainless steel cap, e) PTFE insulator and f) an image of complete cell

Direct methanol fuel cell (DMFC) tests were performed in a phenolic resin-impregnated graphite cell with a 1.0 cm^2 serpentine flow fields (as shown in Figure 3-11). The active electrode area was 1 cm^2. Electric cartridge heaters were mounted at the rear of the graphite blocks to maintain the desired temperature, which was monitored by imbedded thermocouples and controlled with a temperature controller. Gold-plated steel bolts were screwed into the blocks to allow electrical contact. The anode was fed with a solution containing 1.0 M methanol and 1.0 M KOH at a flow rate of 1 mL min^{-1}, while the cathode was supplied with O$_2$ (100 cm^3 min^{-1}).

For the direct methanol carbonate fuel cell, tests were carried out using 2.0 M or 6.0 M methanol in 2.0 M K_2CO_3 solution and O_2/CO_2 mixutre with flow rates of 10 cm^3 min^{-1} for the anode which was controlled by an electrical pump (Watson-Marlow, England) and 40/20 cm^3 min^{-1} for the cathode, respectively.

Humidifiers at the cathode side were maintained at 10 ^{o}C higher than cell temperature to ensure 100 % relative humidity (RH) to keep the membrane fully hydrated. All polarisation curves were recorded using a sweep at a scan rate of 5 mV s^{-1}, employing an Autolab 302N potentiostat until stable performance was reached.
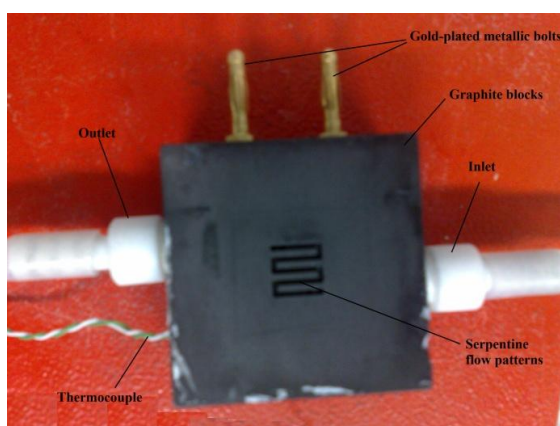
(A)
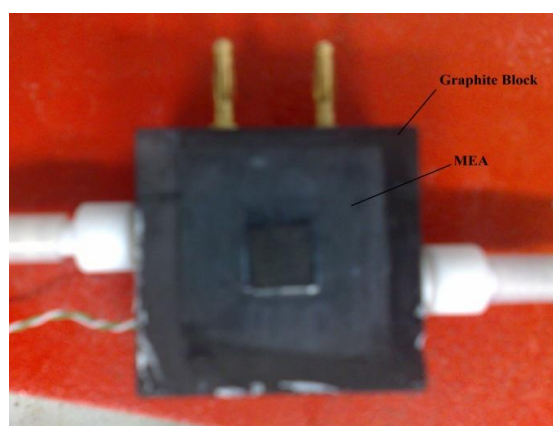
(B)

(C)
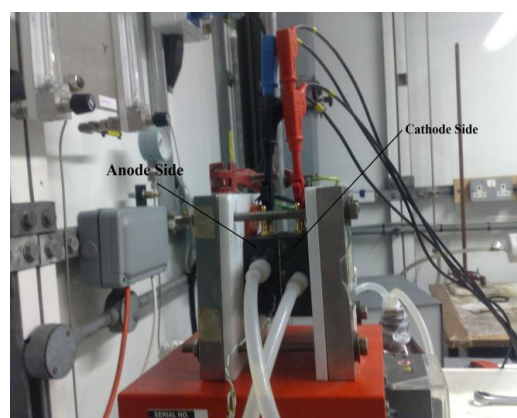
(D)

Figure 3-11 Images of graphite current collectors and fuel cell test experimental setup (A) Graphite current collector blocks, (B) MEA placed over the graphite block, (C) Front view of the fuel cell test experimental setup, (D) Side view of the experimental setup

For the intermediate temperature fuel cell tests, catalyst inks were prepared by blending carbon-supported catalysts (50 wt. % Pt/C, Alfa Aesar) and polytetrafluoroethylene (PTFE) solution (60 wt % Aldrich) in a water–ethanol mixture under ultrasonic vibration for 10 min [31, 150]. Gas diffusion electrodes (carbon paper) incorporated with wet proofed micro-porous layer (H2315 T10AC1), obtained from Freudenburg (FFCCT, Germany), were used as substrates to deposit the catalyst layer for both anode and cathode. The catalyst inks were sprayed onto the micro-porous gas diffusion layer, at 100 °C, and the electrodes were held at a temperature of 150 °C for 2 h. The Pt loading was 0.7 mg cm^{-2}. The required amount of phosphoric acid, which was diluted with a water/ethanol mixture, was added to the surface of the electrodes by means of a micropipette and electrodes were kept in an oven, at 80 °C, for 1 h to dry the residue of water/ethanol mixture [150]. The MEA was finally obtained by hot pressing the electrodes on 4.5 mole% phosphoric acid loaded membranes at 150 °C for 10 min at a pressure of 40 kg cm^{-2}. H_2 and O_2 were fed to the cell at flow rates of 0.4 and 0.7 dm^3 min^{-1}, respectively. These flow rates were some 4 times more than stoichiometric requirements corresponding to the maximum current obtained from the cell tests. The humidifiers were kept at room temperature.

3.5 List of chemicals and samples

All chemicals and samples are listed below and they were used as received without further purification.

Table 3-1 List of chemicals and samples

Chemicals	Purity	Manufacturer
Polysulfone P-1700	N/A	UDEL[®], Germany
Stannic chloride	99 %	Sigma Aldrich, UK
Paraformaldehyde	95 %	Sigma Aldrich, UK
trimethylchlorosilane	≥98 %	Sigma Aldrich, UK
Iron phthalocyanine	96 %	Alfa asear, UK
Cobalt phthalocyanine	97 %	Alfa asear, UK
Co-tetramethoxyphenylporphirine	96 %	Alfa asear, UK
Ethanol	99 %	Sigma Aldrich, UK
Methanol	99 %	Sigma Aldrich, UK
Nafion ionomer solution	5 %	Dupont, US
Sulphuric acid	98 %	Sigma Aldrich, UK
Hydrogen peroxide	30 %	Sigma Aldrich, UK
Potassium hydroxide	≥85%	Sigma Aldrich, UK
Phosphoric acid	85 %	Sigma Aldrich, UK
Potassium carbonate	99 %	Sigma Aldrich, UK
dimethylacetamide (DMAc)	99.5%	Sigma Aldrich, UK
1,2-dichloroethane	99.8	Sigma Aldrich, UK
1,4-diazabicyclo-[2.2.2]-octane (DABCO)	99 %	Sigma Aldrich, UK
Radiation-grafted low density polyethylene	N/A	Provided by Cranfeild University
Microporous PTFE film[a]	N/A	Membrane solution, US
Pd/C on different pre-treated carbon supports[b]	N/A	Provided by Dr. Senthil Kumar in Newcastle University

Note: a-82 % porosity, b-Details of physical properties are listed in the tables (3-2 to 3-4)

Table 3-2 Physical parameters of Pd/C catalysts [97]

Sample	Percentage of metal[a], wt %	Particle size[b], nm	Electrochemical active surface area[c], m^2g^{-1}
Pd/C	21.50	8.0	9.26
Pd/C-5 % HNO$_3$	21.27	5.7	26.78

Pd/C-0.07 M H$_3$PO$_4$	23.79	7.8	12.71
Pd/C-0.2 M KOH	22.48	6.9	18.38
Pd/C-10 % H$_2$O$_2$	22.23	6.9	18.28
Pt/C	-	-	40.96

a and b were provided by Dr. Kumar, c-Using the charge for O$_{upd}$ (upd, under-potential deposition) of 420 μC cm^{-2}.

Table 3-3 Surface elemental composition of Vulcan XC-72R (at.%) after different type of chemical treatments (obtained from XPS analysis) [97]

Treatment method	C (at. %)	N (at. %)	O (at. %)	S (at. %)
Un-treated Carbon	93.62	0.38	6.00	0.49
5 % HNO$_3$	90.85	0.92	8.23	0.15
0.07 M H$_3$PO$_4$	94.40	0.32	5.28	0.26
0.2 M KOH	91.24	0.54	8.22	0.21
10 % H$_2$O$_2$	93.63	0.39	5.98	0.16

Table 3-4 Textural properties of Vulcan XC-72R carbon support after different treatments obtained from nitrogen adsorption isotherms at 77 K [97]

	Un-treated Carbon	5 % HNO$_3$	0.07 M H$_3$PO$_4$	0.2 M KOH	10 % H$_2$O$_2$
BET surface area (m^2/g)	222	158	223	229	103
t-Plot micropore area (m^2/g)	68	41	65	70	7
t-Plot external surface area (m^2/g)	154	117	158	159	96
t-Plot micropore volume (m^2/g)	0.031	0.019	0.030	0.032	0.003
Adsorption average pore width (4 V/A by BET) (nm)	6.02	8.24	7.17	7.09	11.73

BJH adsorption average pore diameter (4 V/A) (nm)	11.8	26.1	17.7	18.8	24.0

CHAPTER 4. DEVELOPMENT OF ANION EXCHANGE

MEMBRANES FOR FUEL CELL APPLICATION

4.1 Results and discussion

4.1.1 *Characterizations of QDPSU membranes*

The ^{1}HNMR spectra for pristine PSU and CM-PSU (DS 58 and 106) are shown in Figure 4-1a. In all spectra, characteristics of polysulfone backbone were found. The multi-peaks of protons (a, b, c, d, f, g and h position) on aromatic ring are in the region between 6.8 and 7.8 ppm [22, 23]. The proton peak at e position on CH_3 is at 1.7 ppm. The peaks at 7.3 ppm and 1.6 ppm are attributed by $CDCl_3$ and H_2O respectively. In the spectra of CM-PSU, the appearance of new peak (i) at 4.6 ppm indicates the formation of chloromethylated polysulfone (CH_2Cl), based on the calculation of integrated area of the peak, the degree of substitution (DS) was obtained using equation (1) [61]:

$$DS = 2 A_{H_i}/A_{H_g} \times 100 \% \qquad (1)$$

where A_{Hi} and A_{Hg} are integral area of H_i (i position) and H_g (g position) in the spectra of CM-PSU in Figure 4-1. A_{Hg} is divided by 2 due to there are two protons which adjacent to $-SO_2-$ group in the aromatic ring in each PSU molecular unit. Thus, the calculated DS represents the percentage of proton at H_i position against one PSU unit.

In Figure 4-1b, the QDPSU final product was dissolved in DMSO to conduct ^{1}H NMR analysis. The new emerging peak at 7.6 ppm suggests the success of quaternization reaction with DABCO (j position). The H_2O peak in DMSO is shifted to 3.3 ppm and the DMSO peak is at 2.7 ppm. The multi-peaks at around 4.0, 2.6 and 2.9 ppm may indicate the existence of CH_3CH_2OH and DABCO salt residual from washing

56

procedure.
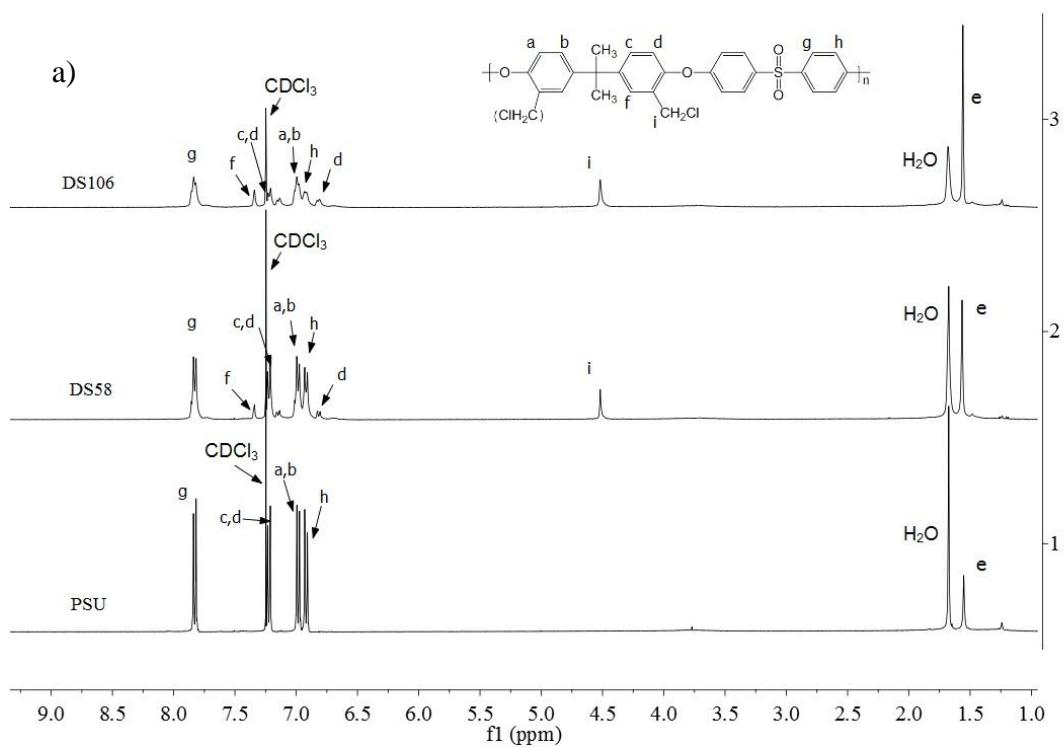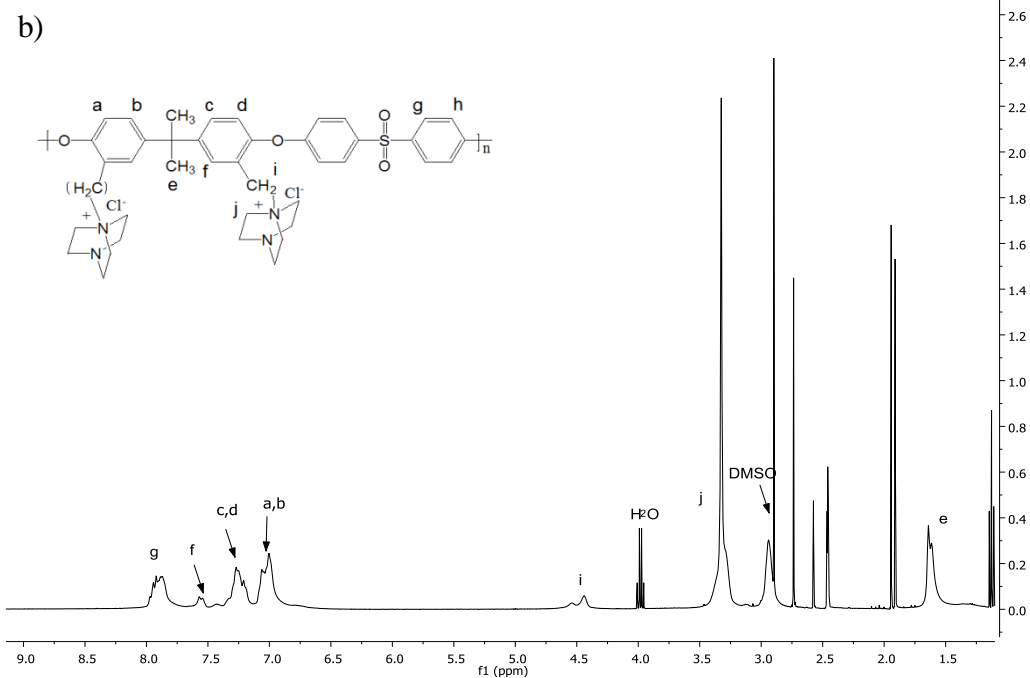
Figure 4-1 ^{1}H NMR of a) CM-PSU with different DS, b) final product-QDPSU in DMSO

In Figure 4-2, the degree of substitution increased with increased time of reaction. The obtained DS of CM-PSU were 58 %, 80 %, 106 % and 180 % for reaction times of 8h, 14h, 24h and 48 h, respectively. The DS of CM-PSU increases in a logarithm pattern rather than linear pattern which indicates the reaction rate decreased during the reaction due to the steric effect of chloromethylated groups. This phenomenon was also reported in the chloromethylation reaction of poly (aromatic ring) polymers [151, 152]. The mechanical property of the membrane with 180 % DS was found to be too brittle for use especially in the presence of water. Thus, it is was not possible to carry out any measurements for fuel cell application.
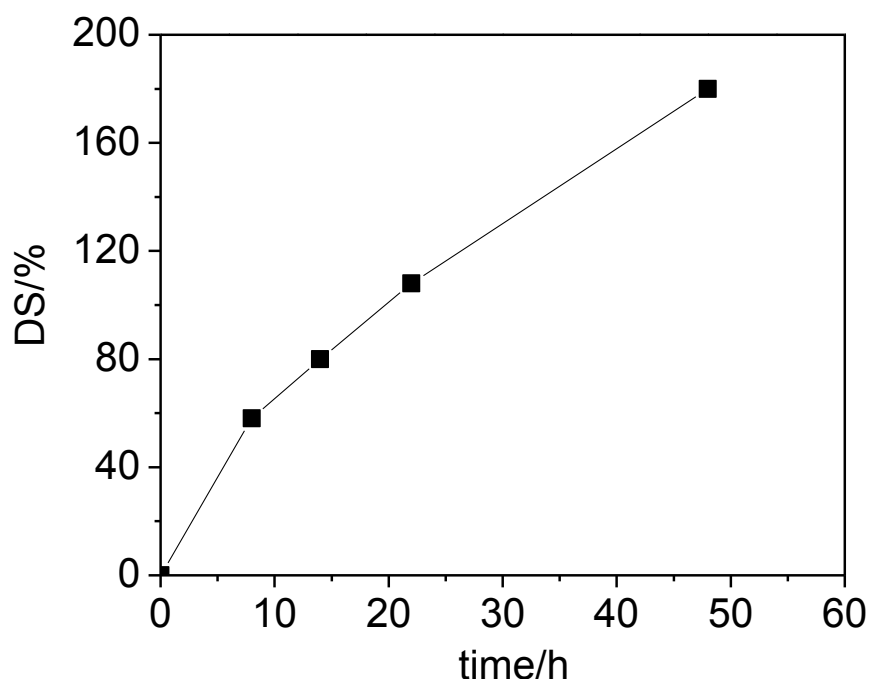
Figure 4-2 Time dependence of the degree of substitution

In Table 4-1, the mechanical strength, swelling degree and water uptake of all samples are listed. The pristine PSU film had a maximum strength of 28.8 MPa. With increasing DS, a trend of decreasing on maximum strength of membrane film was found in our result whilst the swelling degree and water uptake of membranes were increasing significantly to up to 24±2 and 81±6 %, respectively. This is caused by the increasing number of hydrophilic functional groups (quaternary DABCO groups) in the polymer matrix. In addition, the swelling degree and water uptake showed highly dependency

with each other and this behaviour was observed by other researchers on the quaternary ammonium polysulfone [22]. It reveals that the water content inside the membrane affect the dimension of membrane significantly.

Table 4-1 Physical properties of QDPSU membranes

Samples	Maximum strength /MPa	Maximum Extention /mm	Swelling degree/ %	Water uptake/ %
QDPSU-DS106	20.2	1.9	24±2	81±6
QDPSU-DS80	26.0	2.4	12.7±1	46.1±4
QDPSU-DS58	26.8	2.3	6.3±1	19.7±3
PSU	28.8	2.8	-	-
QDPSU-DS180	-	-	-	-

The thermal stability of QDPSU-DS106 and PSU were examined using TGA as shown in Figure 4-3. Before the experiment, the QDPSU was converted to the OH$^-$ form. The molecular structure of PSU was thermally stable at up to 500 $^{\circ}$C which showed a good agreement with the literature [153]. For QDPSU, the weight loss under 100 $^{\circ}$C is mainly attributed by free-water loss. At a temperature range between 100 and 200 $^{\circ}$C, the bonded water and QA group started decomposing [71]. The decomposition of QDPSU backbone occurred at the temperatures higher than around 200 $^{\circ}$C. The above data indicates that QDPSU is thermally stable under the operating temperature range of low temperature fuel cells ($< 100\,^{\circ}$C) which is suitable for the AAEMFC application.
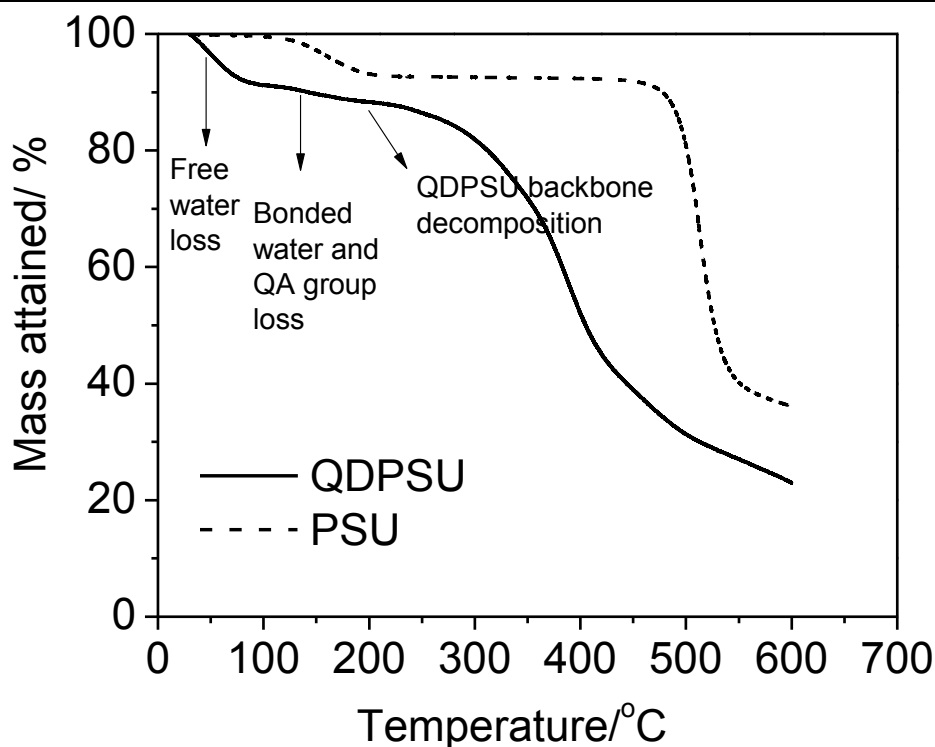
Figure 4-3 Thermogravimetric analysis of PSU and QDPSU

The solubility study of PSU, CM-PSU and QDPSU was conducted by immersing a small piece of membrane samples in different solvents and left overnight at room temperature. The solubility of different polysulfone materials are listed in Table 4-2. All samples were dissolved completely in dimethylacetamide (DMAc) and dimethyl sulfoxide (DMSO). However, the product QDPSU is insoluble in low-boiling point solvents used in this study. The low-boiling point of solvents indicates the bonds between molecules are weak which is unable to split the QDPSU polymer molecules. Based on the solubility study, the solvent for catalysts ink preparation was DMAc.

Table 4-2 Solubility of PSU, CM-PSU and QDPSU in different solvent at room temperature

Sample	PSU	CM-PSU	QDPSU
DI-water	-	-	-
Ethanol	-	-	-
Toluene	-	-	-
Chloroform	+	+	-
Tetrahydrofuran	+	+	-
Dimethylacetamide	+	+	+

Dimethyl sulfoxide	+	+	+

Note: + Soluble, - Insoluble

The morphology of QDPSU membrane was investigated using SEM. Figure 4-4a and b show that the surface and cross-section of membrane are dense and non-porous structure. The EDX element mapping of chlorine represents functional QA group and sulphur represents polysulfone backbone is shown in Figure 4-4c and d. These elements were dispersed homogeneously through the cross-section of the membrane. These results reveal that the obtained AAEM was uniform. These images indicate that the membrane is a suitable insulator for the gaseous reactant on the anode and the cathode and it can provide continuous pathways for conducting the ions.
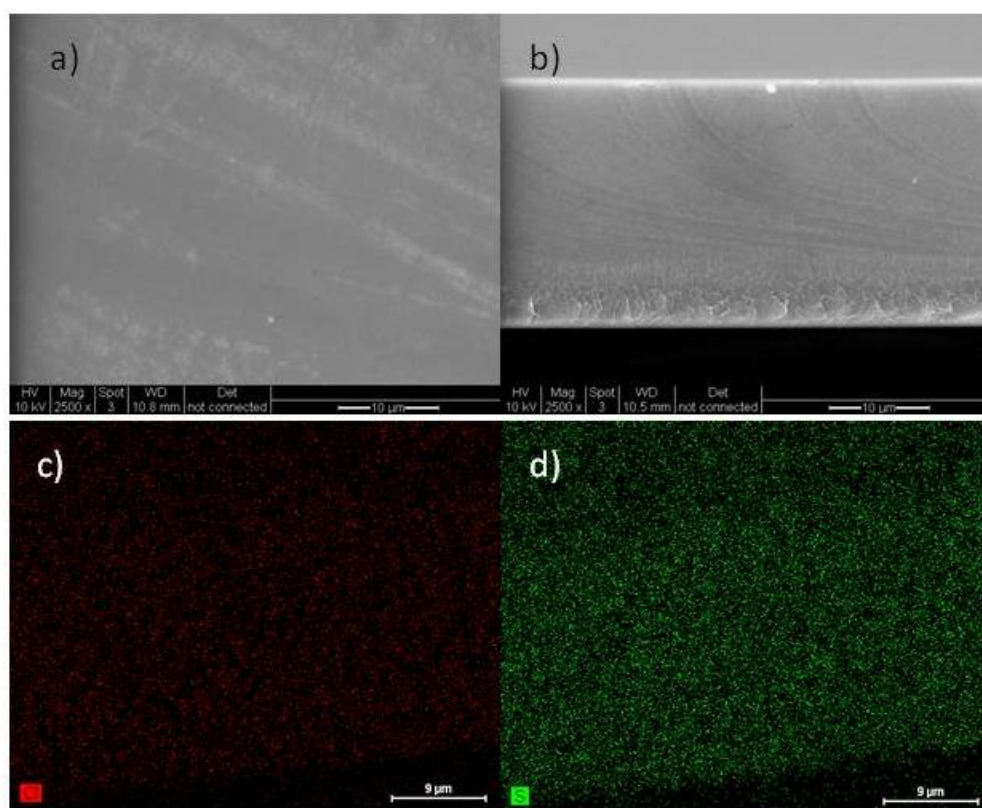
Figure 4-4 SEM images of QDPSU-DS106 a) surface, b) cross-section and element mapping of QDPSU membrane c) chlorine and b) sulphur

The ionic conductivity of a polyelectrolyte membrane is critical factor for fuel cell applications. The ionic conductivity of different DS of QDPSU was measured in a

temperature range of room temperature to up to 60 $^{\circ}$C under 100 % RH. Ionic conductivities of all membranes increased with increasing temperature. It shows a good agreement on the following equation (2) and literature reports [152, 154]:

$$\sigma = \sigma_0[1 + \alpha(T - T_0)] \qquad (2)$$

where σ is the membrane conductivity at certain temperature (S cm^{-1}), T is the temperature (K), T_0 is the reference temperature (K), σ_0 is the conductivity (S cm^{-1}) at the reference temperature (usually room temperature) and α is the temperature coefficient of conductance

At 50 $^{\circ}$C, the ionic conductivities of QDPSU-DS58, QDPSU-DS80 and QDPSU-DS016 were 0.015, 0.027 and 0.039 S cm^{-1}, respectively. Based on the equation of reaction rate as below:

$$\sigma \propto K[OH^-][N^+Me_4] \qquad (3)$$

where σ is the membrane conductivity (S cm^{-1}), [OH-] is the hydroxide concentration, [N$^+$Me$_4$] is the concentration of quaternary functional group

The data suggests that the higher DS of QDPSU membrane has higher ionic conductivity under the same operating condition. A highest ionic conductivity of 0.045 S cm^{-1} was achieved for QDPSU-DS106 membrane at 60 $^{\circ}$C and 100 % RH. This result is better than the latest publication on polysulfone based AAEM which is around 0.02 S cm^{-1} under the same conditions [22]. This is due to the higher DS (106 %) of QDPSU than the QAPSU (up to 80 % DS) in the literature [22].
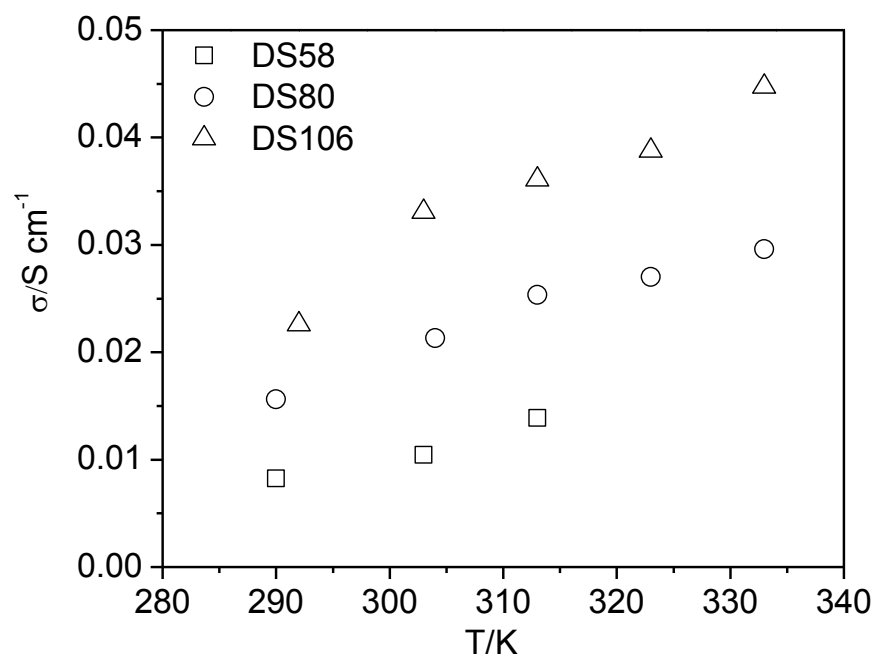
Figure 4-5 Ionic conductivities of QDPSU membranes at different temperatures and 100 % RH

4.1.2   Characterizations of PTFE-QDPSU composite membrane

Figure 4-6a shows the image of the micro-porous structure of the PTFE membrane. The dense structure of composite membrane cross-section, shown in Figure 4-6b, suggests the micro-porous PTFE sheet was filled with the QDPSU polymer. Figure 4-6c and d shows the chlorine and fluorine element mapping which indicates a homogenous structure of the composite membrane. Above images indicate that the membrane is a suitable insulator for the gaseous reactants on the anode and the cathode and it can provide continuous pathways for conducting the ions.

The fluorine peak at around 0.6 keV in EDX spectra on the cross-section of composite membrane further confirmed the successful preparation of PTFE-QDPSU composite membrane as shown in Figure 3-9e. Peaks of C, O and S at around 0.25, 0.5 and 2.4 keV are attributed to the pristine polysulfone backbone. The peak at around 2.6 keV is attributed to chlorine which was attached on the N bond of DABCO. Figure 4-6f shows that the chlorine element in the membrane was completely converted to hydroxide after 8 h in 1.0 M KOH at room temperature. The Al element peak was contributed by the

63

sample holder.
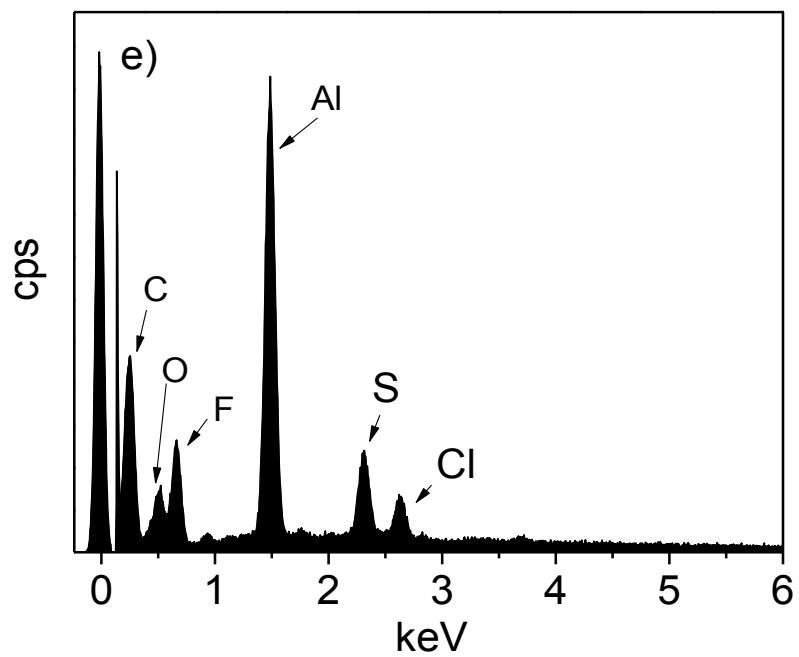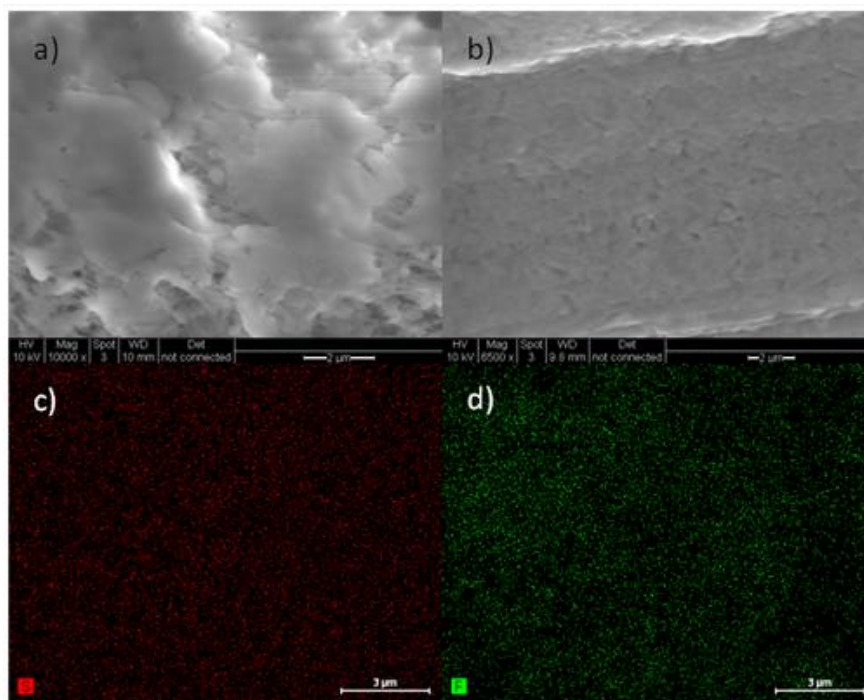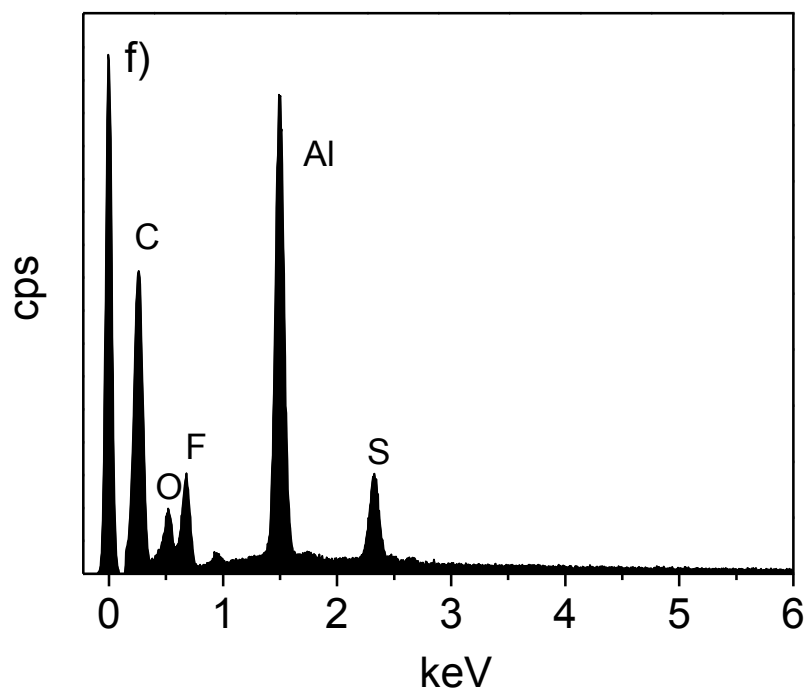
Figure 4-6 a) SEM image of cross-section PTFE sheet, b) SEM image of cross-section PTFE-QDPSU composite membrane, c) chlorine element mapping, d) fluorine element mapping, e) EDX spectra of chlorine form of membrane and f) EDX spectra of hydroxide form of membrane

Figure 4-7 shows infrared spectra of PTFE-QDPSU composite membrane and pristine QDPSU. Two new stretching vibration peaks at 1085 and 1058 cm^{-1} which is attributed by $-CF_2-$ symmetric were found after adding PTFE support to make the composite membrane with QDPSU polymer.
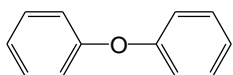
 and S=O vibration peaks are at 1241 and 1375 cm^{-1} [55]. The broad peak at around 3386 cm^{-1} was attributed by O-H and residual water. The quaternary ammonium group stretching vibration peaks are at 2924, 1617 and 1487 cm^{-1} [25]. The data suggests the successful synthesis of PTFE-QDPSU composite membrane.

65
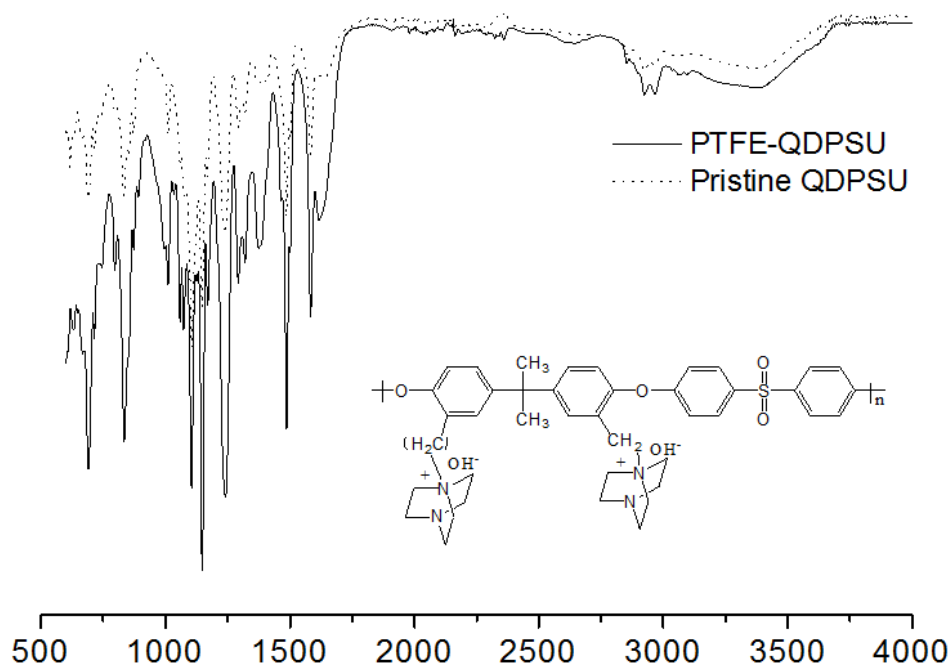
Figure 4-7 FT-IR of pristine QDPSU membrane and PTFE-QDPSU composite membrane in OH⁻ form

In Table 4-3, values of the swelling degree, water uptake and mechanical strength of PTFE-QDPSU composite and pristine QDPSU membrane are listed. The maximum strength of PTFE-QDPSU (32 ± 4 MPa) was greater than the pristine QDPSU (22 ± 3 MPa) due to the reinforcement of the PTFE substrate. Liu et al prepared a PTFE-Nafion composite membrane [68]. Compared to the wet form unsupported Nafion, the maximum strength of PTFE-Nafion was 19.1 MPa (100 % higher) higher in the same form. The swelling degree and water uptake of PTFE-QDPSU and pristine QDPSU membranes were 17 ± 2 % and 24 ± 2 %, 61 ± 3 % and 81 ± 4 %, respectively. The lower water uptake and swelling degree of the PTFE composite membranes was contributed by the hydrophobicity of PTFE material. The maximum extensions of PTFE-QDPSU and unsupported QDPSU were similar at 2.2 and 1.9 ± 0.3 mm.

Table 4-3 Physical properties of composite membrane and pristine QDPSU membrane

Samples	Maximum strength /MPa	Maximum Extention /mm	Swelling degree/ %	Water uptake/ %
PTFE-QDPSU	32.0	2.2	17±2	61±4
QDPSU-DS106	20.2	1.9	24±2	81±6

The ionic conductivity of PTFE-QDPSU composite and pristine QDPSU membrane was measured in a temperature range between 15 and 60 $^{\circ}$C. In Figure 4-8, the ionic conductivities of both membranes increased with increasing temperature. The PTFE-QDPSU composite membrane exhibited better conductivity than the pristine QDPSU membrane at different temperatures. This may be due to the combined hydrophobic (PTFE substrate) and hydrophilic (QDPSU) structure which improves the water transport and retention inside the membrane. The highest conductivity of 0.051 S cm^{-1} was achieved using PTFE-QDPSU composite membrane at 55 $^{\circ}$C and 100 % RH. Such ionic conductivity was superior to recently reported AAEM materials (up to 0.034 S cm^{-1} at 55 $^{\circ}$C in DI water) [22, 50, 57, 144]. Therefore, it is a promising candidate for the application of AAEMFCs.
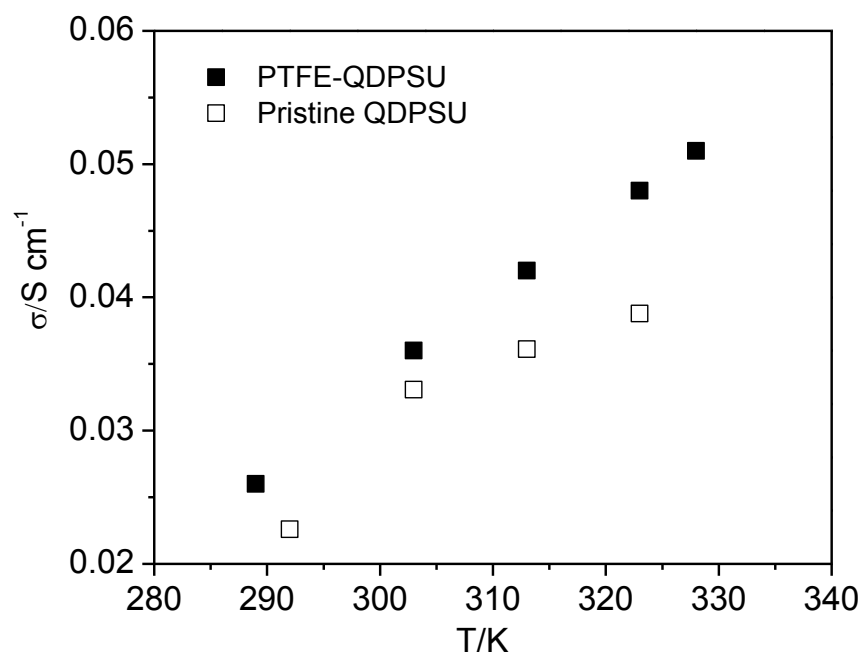
Figure 4-8 Ionic conductivities of QDPSU and PTFE-QDPSU composite membrane at different

temperatures and 100 % RH

Fuel cell performances are shown in Figure 4-9. All polarization curves showed a high open circuit potential, above 1.0 V, for a thin membrane (30 μm, fully hydrated) which indicates that the membrane had a low hydrogen permeability. The fuel cell performance improved with increasing temperature due to the higher conductivity of membrane (ionomer as well in the catalyst layer) and electro-catalytic activity of catalysts at elevated temperatures. A high peak power density of 146 mW cm^{-2} was achieved using hydrogen and pure oxygen at 50 $^{\circ}$C and atmospheric pressure. Such fuel cell performance is higher than the most AAEMFC using polysulfone based membranes (up to 120 mW cm^{-2} at 60 $^{\circ}$C) [22, 59, 61]. The combination of thin membrane and high conductivity of QDPSU contribute the most of the superior performance. Fuel cell performance using hydrogen and CO_2 free air was also investigated. Although the power density performance of 103 mW cm^{-2} with CO_2 free air was lower than the power output with pure oxygen due to the lower partial pressure of oxygen, it indicates the potential of membranes for the AAEMFC. The fuel cell polarisation curves showed signs of mass transport limitations below around 0.3 V. The catalyst ink based on the QDPSU ionomer may not have provided sufficient hydrophobicity for good gas access and water transport.

The internal cell conductivity estimated from the linear region of the polarisation curves obtained in Figure 3-12a at 50 $^{\circ}$C was 0.0024 S cm^{-1} for PTFE-QDPSU based MEAs. The value was much lower than the membrane conductivity, indicating significant voltage losses due to electrode polarisation and electrode layer resistances as well as mass transport limitations. These effects may in part be due to the MEA fabrication using cold-pressing of the MEA which may not have provided enough contact between the membrane and electrodes when they were assembled in the fuel cell.
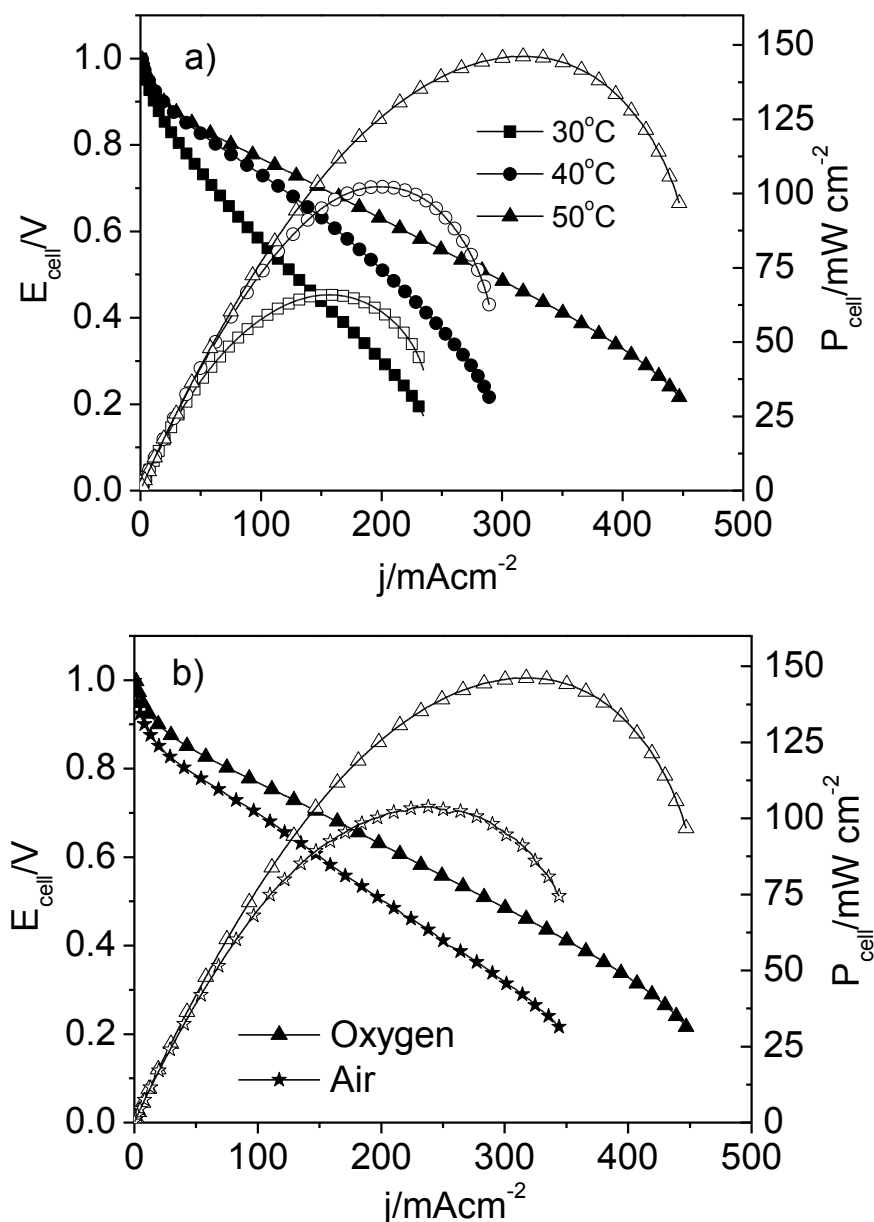
Figure 4-9 Fuel cell performances a) at different temperatures using hydrogen and pure oxygen, b) using pure O_2 and CO_2 free air at the cathode respectively, 50 °C, PTFE-QDPSU membrane thickness 30 μm, 0.5 mg$_{Pt}$ cm^{-2}, 6 wt % QDPSU in catalyst layers, atmospheric pressure, 100% RH at cathode.

4.1.3   Characterizations of KOH loaded PBI membrane

The PBI membrane used in these tests was immersed in 6.0 M and 4.0 M KOH for 9 days at room temperature. In Figure 3-13a, the conductivity of PBI in 6.0 M KOH was 0.035 S cm^{-1} which is around one order of magnitude higher than it is in 4.0 M KOH (0.0048 S cm^{-1}) at 60 °C. Figure 3-13b presents the ionic conductivities of membrane measured at different temperature under humidified or non-humidified condition. It was

found that the ionic conductivity of KOH loaded PBI under humidified condition is higher than the one under non-humidified condition (e.g. they are 0.035 and 0.02 S cm^{-1} at 60 ^{o}C, respectively).

Unfortunatly, an ammonia-like smell was released during the treatment of the PBI membrane with KOH which indicates degradation of PBI polymer structure after 9 days at room temperature. The unexpected non-linear increase of ionic conductivity might be contributed by the instability of KOH-PBI membrane. Specifically, the KOH inside the PBI matrix attacked the imidazole bond produces ammonia which causes the loss of OH^{-} groups and eventually the ionic conductivity fell.
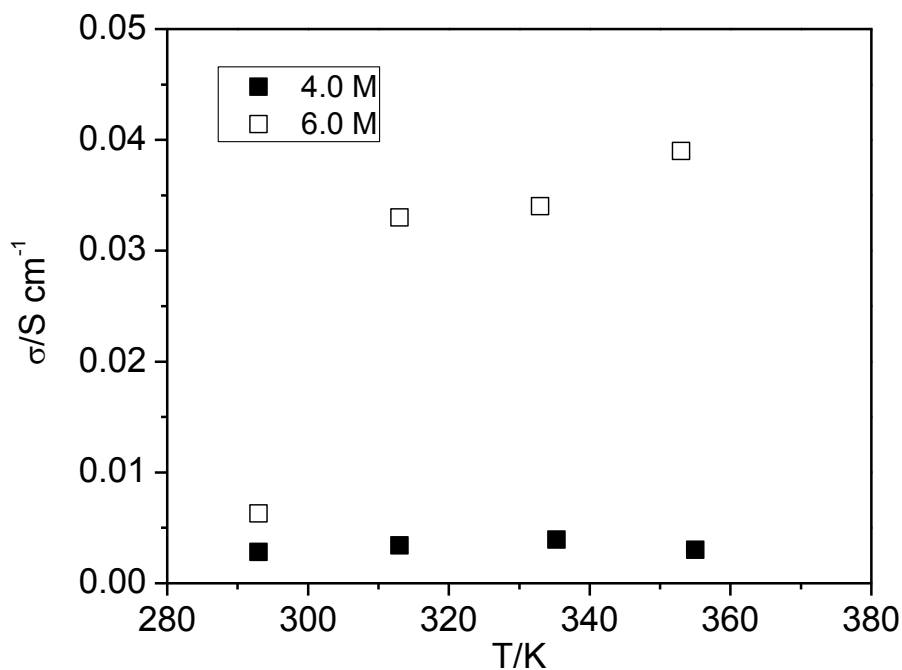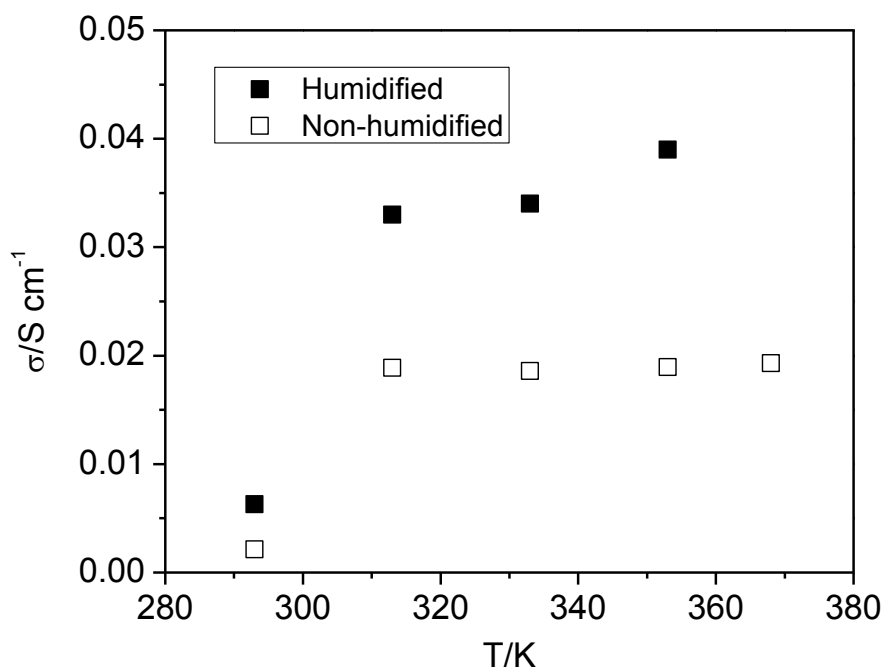
Figure 4-10 a) KOH concentration effect on ionic conductivity of KOH-PBI membrane for a doping duration of 9 days, b) Humidity effect on ionic conductivity of KOH-PBI membrane for a 6.0 M KOH and 9 days doping duration, the temperature of humidifier was either at room temperature so as the gas pipe (non-humidified) or at a temperature 10 ^{o}C higher than cell temperature and was maintain at 110 ^{o}C (humidified)

Figure 3-14 shows the polarization curves of DMFC at be specific and give more information. The low OCVs (around 0.52 V) were contributed by the sever methanol cross-over from the anode. It was higher at elevated temperature and they were 0.46, 0.50 and 0.52 V, at 60, 75 and 90 ^{o}C, respectively. This is due to the enhanced catalytic activity of both PtRu/C and Pt/C catalysts. A maximum power density and limiting current density of fuel cell reached 17.7 mW cm^{-2} and over 0.1 A cm^{-2} at 90 ^{o}C.

However, during the fuel cell test, the outlet of anode side where 1.0 M KOH and methanol solution turns yellow brown colour which indicates a severe degradation of KOH loaded PBI membrane at elevated temperatures.
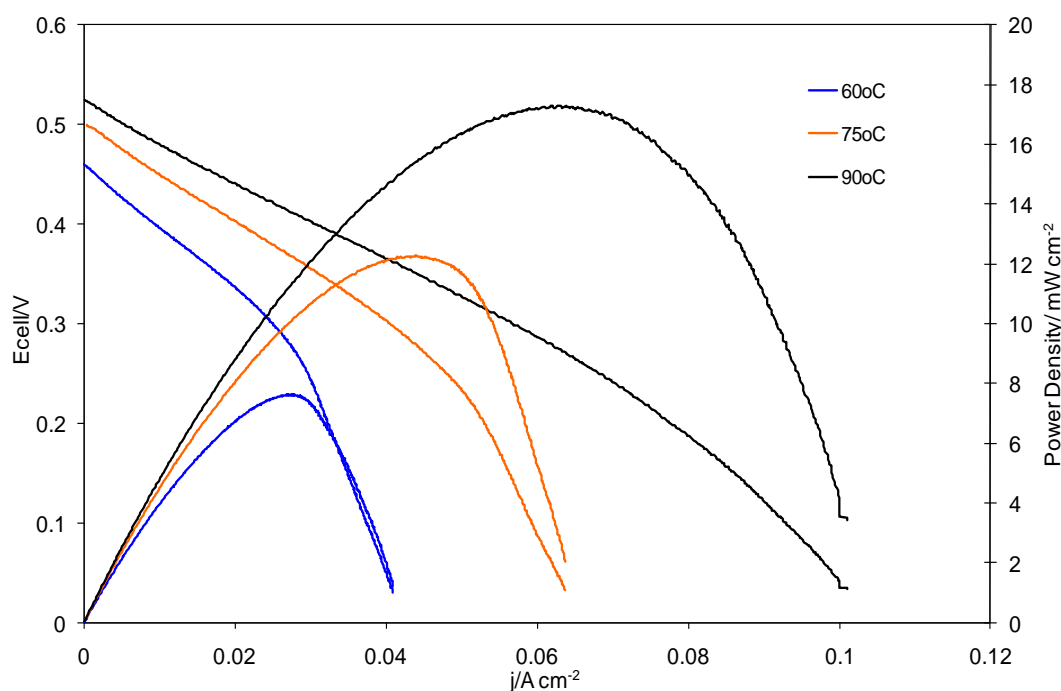
Figure 4-11 Direct methanol fuel cell performance using 6.0 M KOH doped PBI membrane after 9 days treatment at different temperatures and 100 % RH, 1.0 M KOH and methanol solution was circulating at the anode side, pure oxygen at the cathode, 60 µm membrane thickness, 1 mg cm^{-2} PtRu/C metal loading at anode, 1 mg cm^{-2} Pt/C metal loading for the cathode

4.2 Conclusions

Quaternary DABCO polysulfone was synthesised with different DS and characterized. Based on QDPSU, a thin PTFE-QDPSU composite membrane was prepared by using pre-treated PTFE impregnated with QDPSU polymer. The higher DS showed the better ionic conductivity. It was 0.015 S cm^{-1} for DS 58, 0.027 S cm^{-1} for DS 80 and 0.039 S cm^{-1} for DS 106 at 50 ^{o}C. The morphology of QDPSU and PTFE-QDPSU were both dense and homogenous structure. Compared to pristine QDPSU membrane, the composite membrane exhibited better mechanical strength (32 MPa, maximum strength), less swelling degree and lower water uptake. The ionic conductivity of the membrane was 0.051 S cm^{-1} at 55 ^{o}C and 100 % RH. In fuel cell tests, power outputs of 146 mW cm^{-2} and 103 mW cm^{-2} were achieved using oxygen and air, respectively. The good performance of such AAEM indicates the novel composite membrane is a promising material for AAEMFCs. Severe degradation was found during preliminary

experimental investigation on KOH loaded PBI membrane including
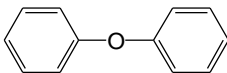
CHAPTER 5. PHOSPHORIC ACID LOADED QUATERNARY 1,4-DIAZABICYCLO-[2.2.2]-OCTANE POLYSULFONE MEMBRANE FOR INTERMEDIATE TEMPERATURE FUEL CELLS

5.1 Results and discussion

5.1.1 FT-IR

Figure 5-1 shows the infrared spectra of QDPSU and PA/QDPSU. For both membranes, the ⟨benzene⟩–O–⟨benzene⟩ and S=O vibration peaks were found at 1241 and 1375 cm^{-1}. The small peaks at 2924 cm^{-1}, 1617 cm^{-1} and the sharp peak at 1487 cm^{-1} are attributed to quaternary ammonium group stretching vibration [25]. For PA/QDPSU membrane, a significant vibration peak was found at 966 cm^{-1} and is attributed by the P=O vibration. The data suggests the successful preparation of QDPSU and PA/QDPSU membranes.
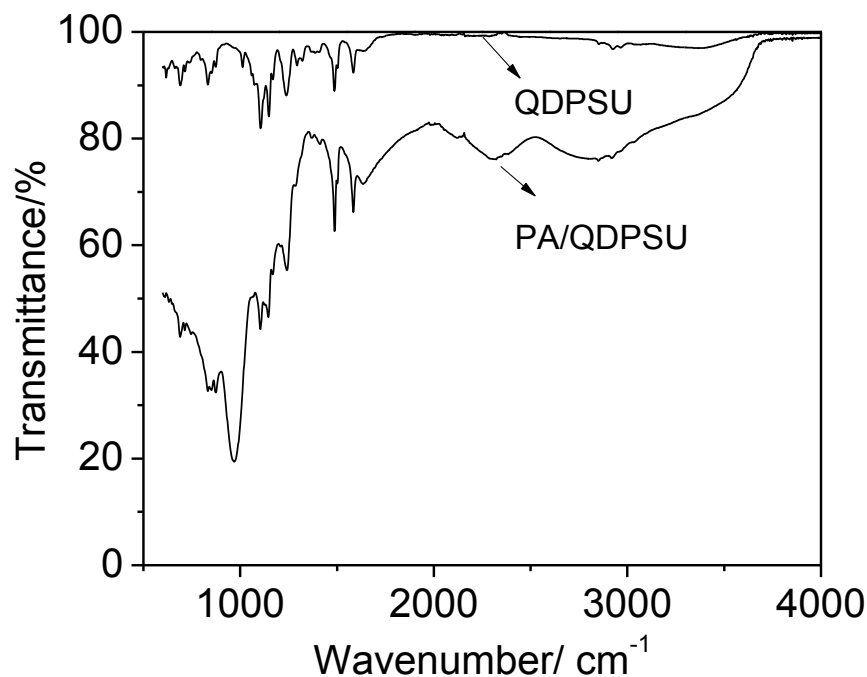
Figure 5-1 FT-IR spectra of QDPSU and PA/QDPSU

5.1.2   SEM and EDX

The morphology of PA/QDPSU membrane was investigated using scanning electron microscopy (SEM) and energy dispersive X-ray (EDX). The SEM images (Figure 5-2a) of the membrane cross-section reveal a dense and non-porous structure as shown in Figure 5-2a and b. The element mapping of P and S as shown in Figure 5-2c and d, further suggest that the homogenous structure of PA/QDPSU membrane was formed.

In Figure 5-2e, the EDX analysis of PA/QDPSU shows C, S element at 0.25 and 2.4 keV, respectively which were contributed by polysulfone. The Al element peak was contributed by the sample holder. The significant P element peak at 2.0 keV suggested a complete substitution of Cl$^-$ to H$_2$PO$_4^-$ after 3 days doping at room temperature. Thus, the degree of chloromethylation is the same as the degree of substitution (DS) after quaternization with DABCO.
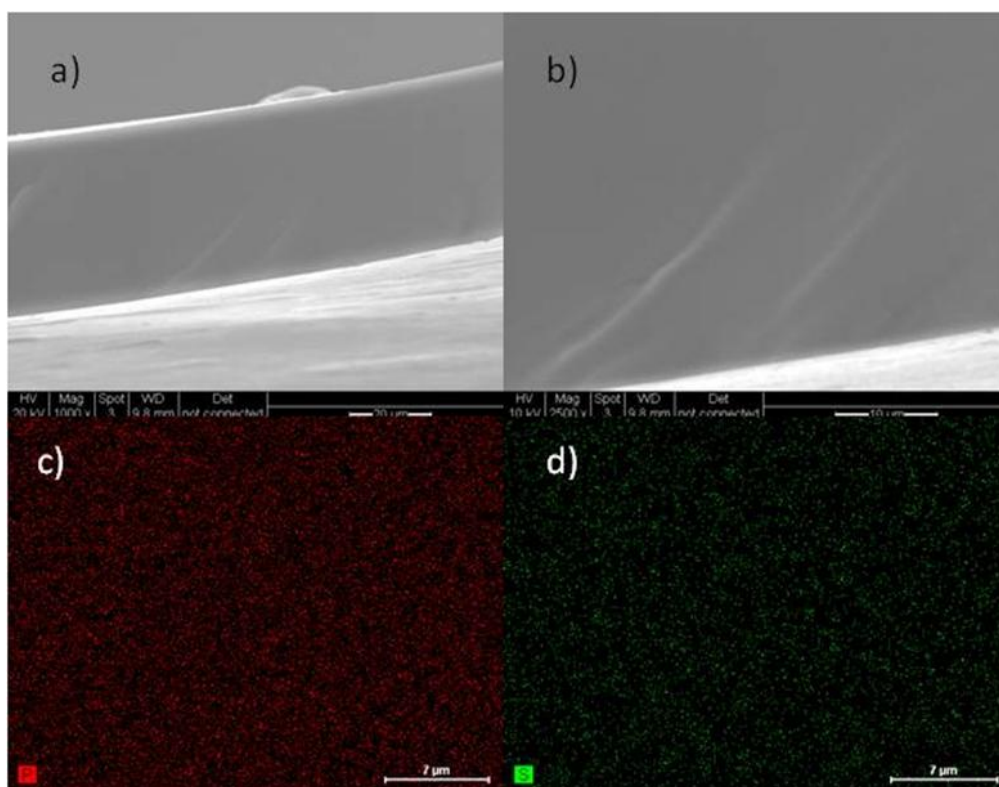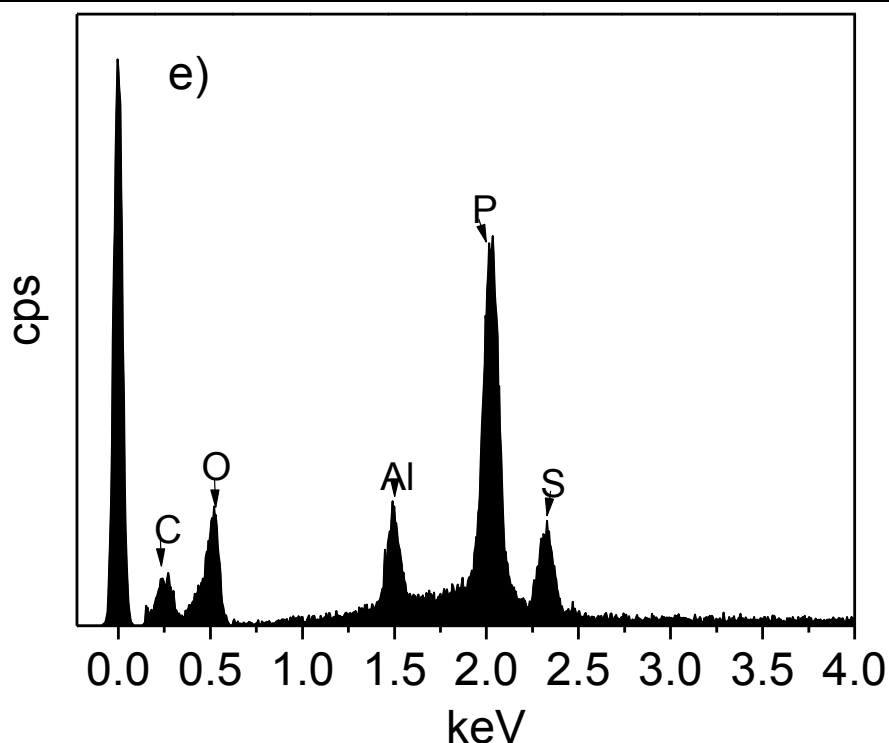
Figure 5-2 SEM images and element maps of PA/QDPSU-DS 58, a and b) cross-section view, c) phosphorous, d) sulfur and e) EDX analysis

5.1.3   Ionic conductivity

Figure 5-3a shows the variation of ionic conductivity with temperature for membranes prepared in this work. The conductivities of the DS106 membrane were approximately twice those of the DS58 membrane and increased with temperature in the range of 80-150 ^{o}C under a non-humidified condition. Conductivities of 0.12 and 0.064 S cm^{-1} were achieved for DS106 and DS58 at 150 ^{o}C, respectively. The data suggest that the ionic conductivity of QDPSU depended upon the DS of PSU. Higher DS of QDPSU was synthesised, however, DS180 membrane was too brittle in the presence of water and thus is not suitable for fuel cell applications.

Figure 5-3b shows Arrhenius plots of the conductivity data and the calculated activation energies using equation 1 of ion transport were 13.2 and 12.8 kJ mol^{-1}, respectively for DS58 and DS106 membranes.

$$E_a = -R \times T \times ln\sigma + lnA \qquad (1)$$

where Ea is the activation energy of ion transport (kJ mol^{-1}), R is the gas constant equals 8.314 J K^{-1} mol^{-1}, T is the temperature (K)

The data indicate that the ionic conductivity of PA/QDPSU was related to the number of function groups (degree of substitution) and was independent of the activation energy for ion transport. Thus, the ion conductivity of membrane only depends the number of functional group (equation 3 in Chapter 4). The properties of the membranes are listed in Table 5-1.
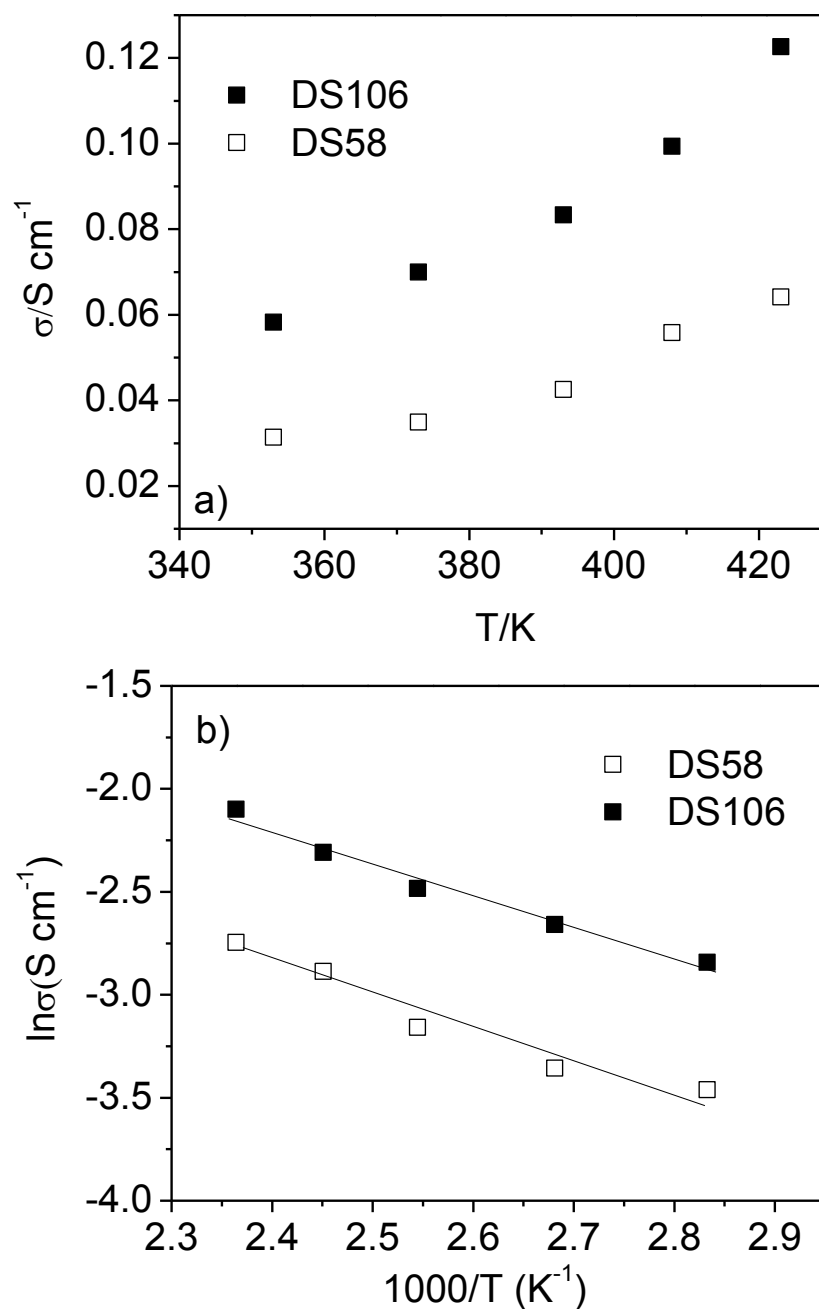
Figure 5-3 Ionic conductivity of a) different degree of substitution PA/QDPSU membrane and b)

Arrhenius plot obtained from ionic conductivity data

Table 5-1 Membrane properties of QDPSU

Sample	Degree of substitution /%	Doping level, %	Conductivity/Scm^{-1}, @150 ^{o}C	E$_a$/kJ mol^{-1}	Thickness/ μm
PA/QDPSU-58	58	102[b]	0.06	13.2	55
PA/QDPSU-106	106	193[c]	0.12	12.8	65
QDPSU-180[a]	180	-	-	-	-

a-brittle in the presence of water, b,c- equivalent to 4.6 and 8.6 per repeating unit (PRU)

5.1.4   Fuel cell performance

Figure 5-4a and b show polarization and power density curves of fuel cells using hydrogen and oxygen at different temperatures. Both MEAs with different DS of QDPSU showed increased fuel cell performance with increasing temperature due to higher catalytic activity and membrane conductivity at higher temperature. The open circuit potentials at temperatures of 150 ^{o}C were 0.97 and 0.90 V for the DS58 and DS106 membranes, respectively. The high DS of PA/QDPSU led to a superior fuel cell performance (400 mW cm^{-2}) than the low DS PA/QDPSU (323 mW cm^{-2}). The fuel cell performance was similar to the result published using greater catalyst loading (0.81 mg$_{Pt}$ cm^{-2}) and a thinner membrane of quaternary ammonium polysulfone (20 μm) [38].
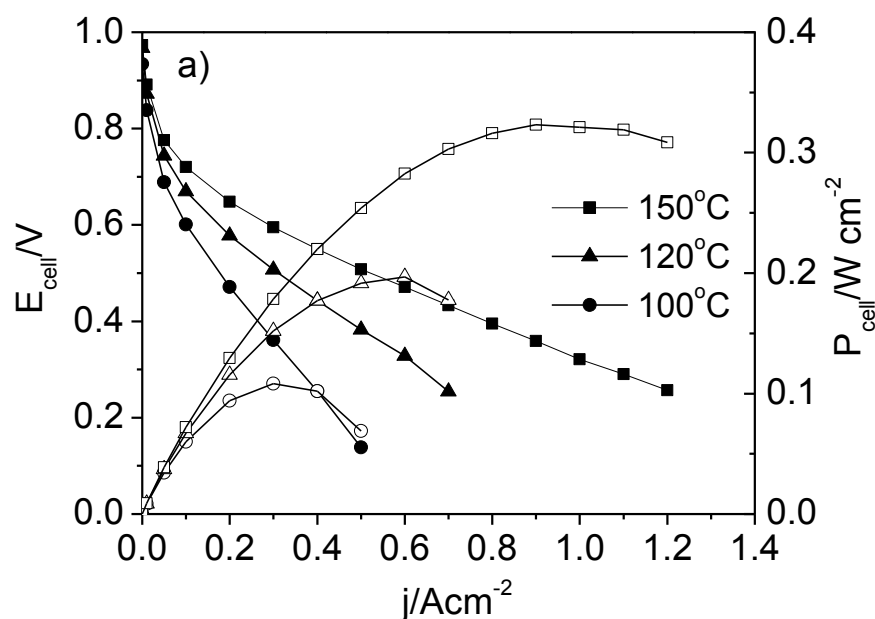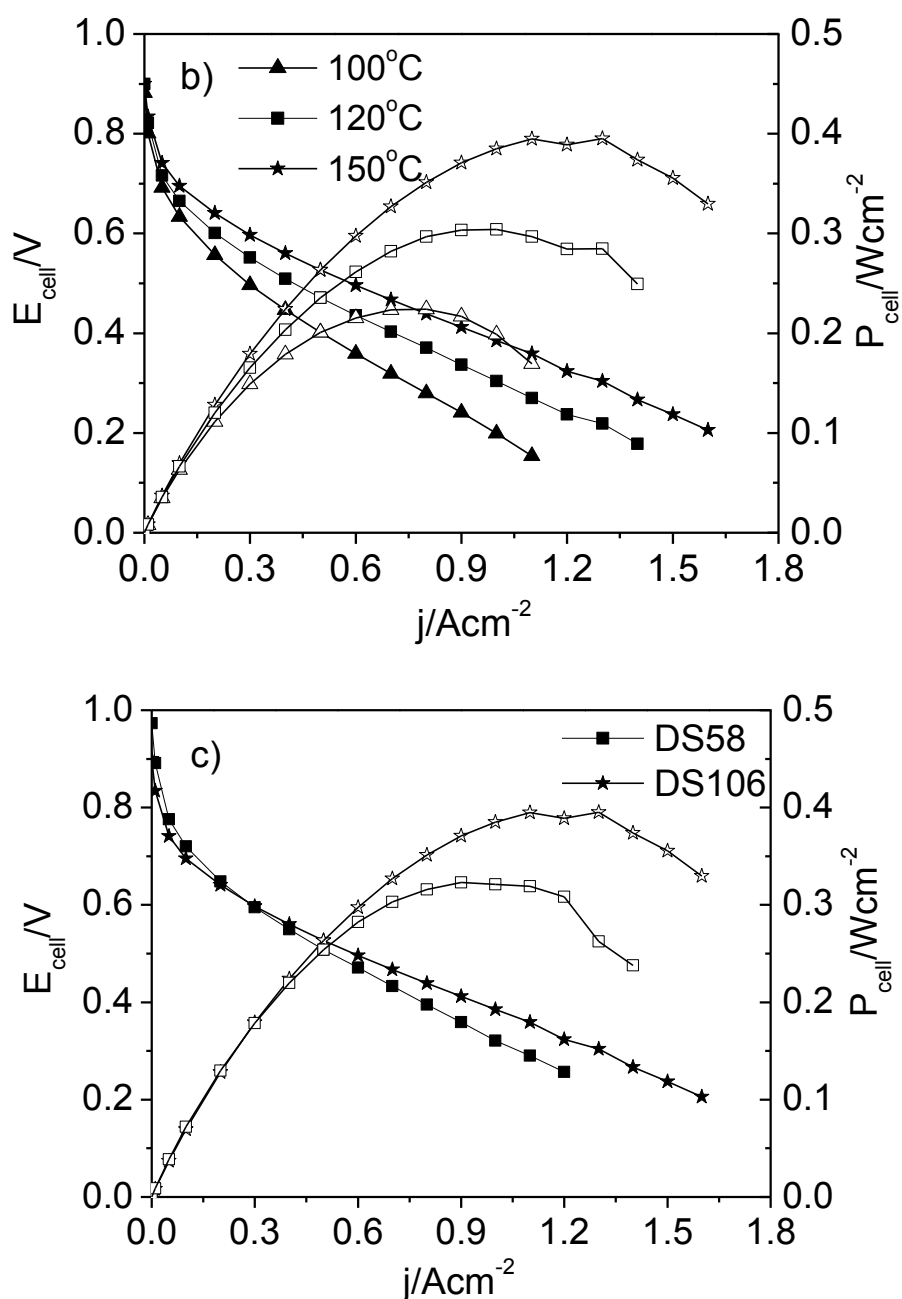
Figure 5-4 Fuel cell performance using different DS of PA/QDPSU, a) DS58, b) DS106, at 150 °C, 0.6 mg$_{Pt}$ cm^{-2} (50 wt % Pt/C) for both anode and cathode, under atmospheric pressure, dry gases

Internal cell conductivities estimated from the linear region of the polarisation curves obtained at 150 °C were 0.015 S cm^{-1} and 0.023 S cm^{-1} for the DS58 and DS106 membrane based MEAs respectively. These values are much lower than the membrane conductivities indicating significant voltage losses due to electrode polarisation and electrode layer resistances.

Figure 5-5a shows IR corrected polarisation curves of the fuel cells operated at 150 $^{\circ}$C. The IR correction was made by using following equation:

$$E = E_0 + I \times R \qquad (3)$$

where E is IR corrected cell voltage (V), E_0 is the cell voltage (V) from Figure 5-4, I is the current and R is the ohmic resistance (ohm) that calculated from linear region of the polarisation curves. From the plot of the IR correct voltage vs ln (j), the slope (Tafel type) of the lines were 120 and 103 mV per decade. Ignoring the contribution associated with the hydrogen oxidation reaction, these values are the same as literature reported for phosphoric acid loaded PBI fuel cells [29] which indicate the rate-determination reaction of overall fuel cell performance was the same. Above results suggest that the H₃PO₄ loaded QDPSU membrane showed a promising performance for ITFC applications.
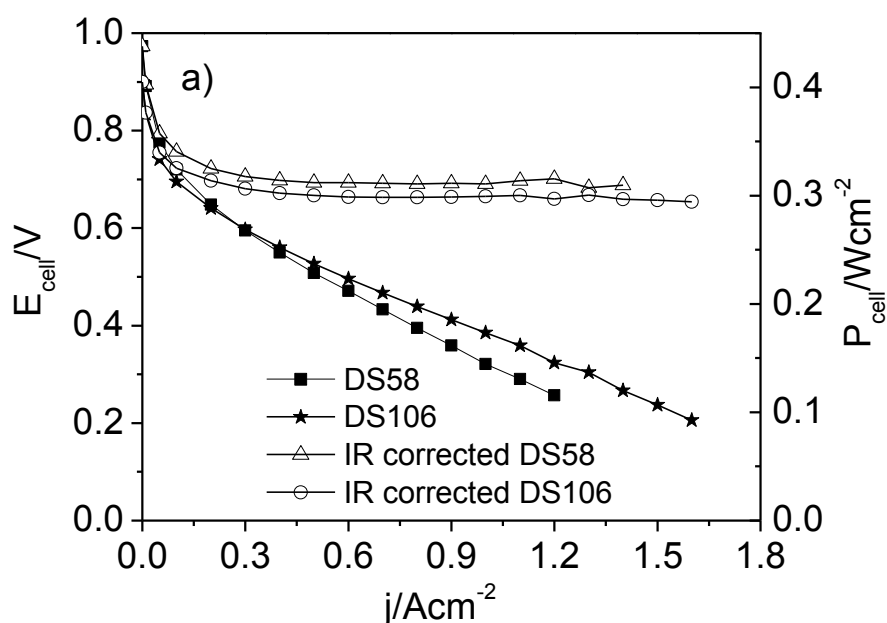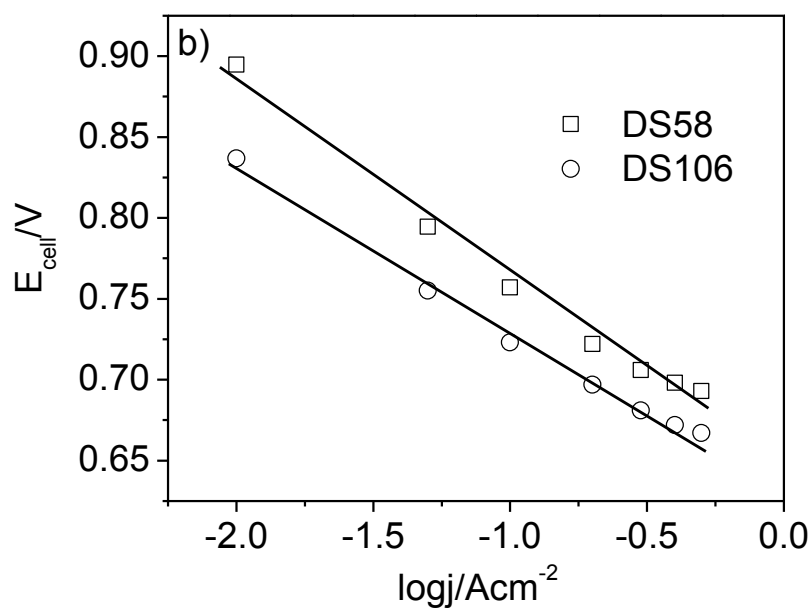
Figure 5-5 a) IR corrected polarization curves of DS58 and DS106 b) Tafel plots obtained from polarization curves in Figure 5-5a

5.2 Conclusions

A novel PA/QDPSU was prepared via a Friedel-Crafts like reaction followed by quaternization with DABCO, which is safe and easy to handle. Different degrees of substitution (DS) can be achieved by this method. The ionic conductivity and fuel cell performance are related to the DS. The higher DS of QDPSU results in significantly better ionic conductivity and fuel cell power density. However, too high of the DS (such as DS180) will compromise the membrane mechanical property which leads to the unfavourable results for fuel cell applications. A high power density output of 400 mW cm^{-2} can be achieved using DS106 of PA/QDPSU membrane at 150 $^{\circ}$C and atmospheric pressure.

CHAPTER 6. PALLADIUM SUPPORTED CATALYSTS FOR OXYGEN REDUCTION IN ALKALINE MEDIA

6.1 Results and discussion

6.1.1 Morphology of Pd/C catalysts

Figure 6-1 shows TEM images of Pd/C catalysts as prepared. Modifying the carbon support with either HNO_3 or H_2O_2 (Figure b and e) produced agglomeration of metal particles. This was probably due to change in some physical properties of the support (BET surface area, micropore volume and surface functional groups) which played a role in agglomeration of the metal particles. For instance, both the above treatment gave a lower BET surface area and micropore volume compared to the un-treated carbon support. It is well know that micropores are the dominant site for metal nano-particle deposition during reduction of the salt precursor which has passed through macro and mesopore [155]. The strong oxidative and corrosive nature of the above pre-treatments would eventually destroy the neighbouring micropore walls and merge them together into a larger dimensional pore void as provided in Table 3-4 Chapter 3. Such a colony of destroyed micropores favours formation of patches of agglomerated Pd nano-particles throughout the carbon support, as shown in Figure 6-1b and e. The nature and quantity of oxygen containing surface functional groups also plays an important role on the Pd nano-particle morphology and its distribution. However, this is difficult to assess since oxygen-containing groups behave as anchors for Pd particles and an increased dispersion of Pd supported on the oxidized carbons would be expected in this way. However, already published literature is quite ambiguous at this point; some data indicate an opposite effect, the absence of any effect at all or a volcano dependence of Pt dispersion on the concentration of chemisorbed oxygen [156].

a)

b)

c)

d)

e)
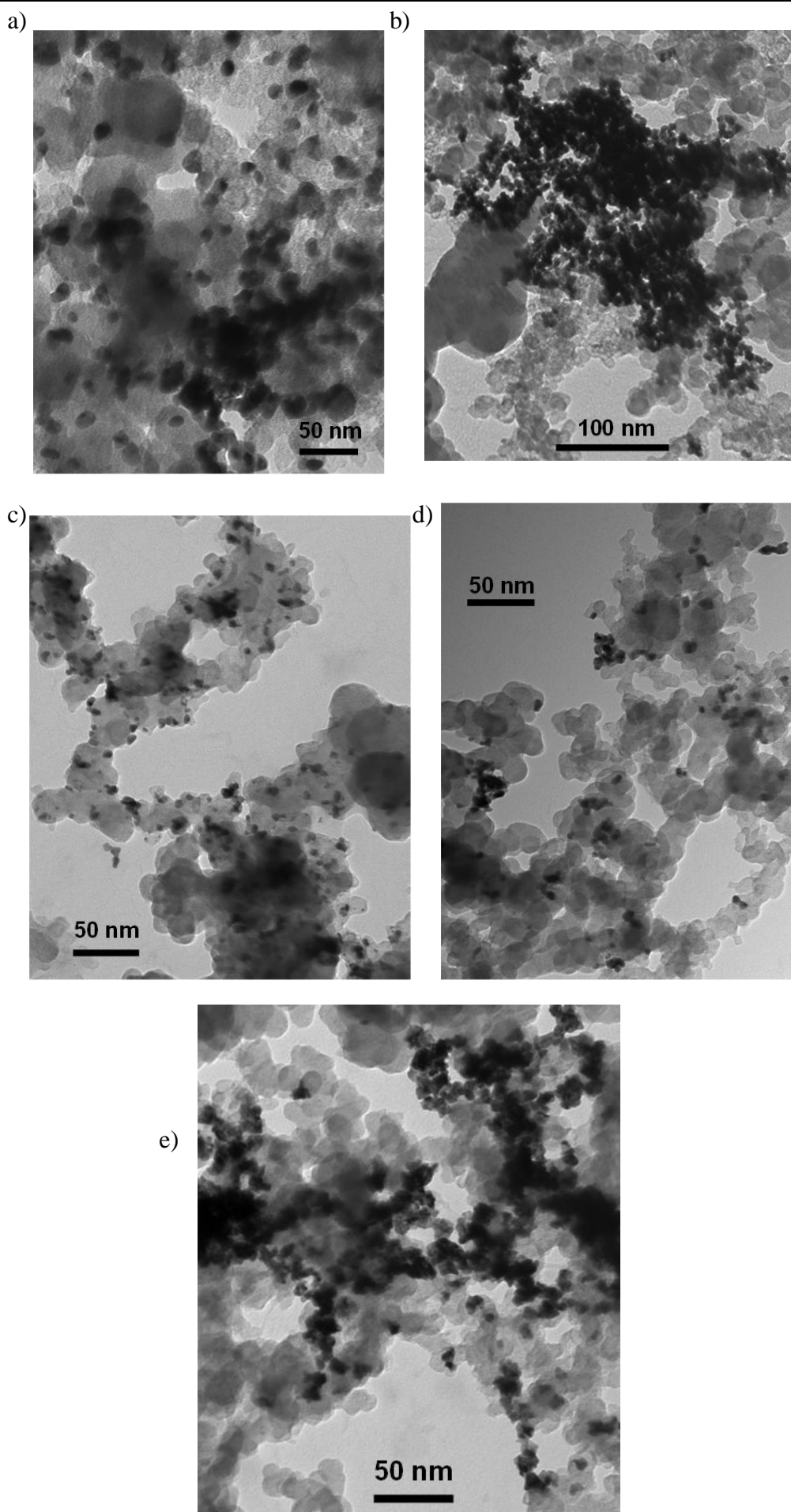
Figure 6-1 TEM images for Pd/C catalysts prepared with different kind of Vulcan XC-72R pretreatments (a) un-treated, (b) 5 % HNO_3, (c) 0.07 M H_3PO_4, (d) 0.2 M KOH and (e) 10 % H_2O_2

6.1.2   CV of Pd/C catalysts and Pt/C

Figure 6-2 shows CVs of Pt/C and Pd/C recorded at a scan rate of 5 mV s^{-1} in N_2 saturated 1.0 M KOH. The potential range for CVs was from -0.80 to 0.30 V. Peaks at a potential range between -0.60 and -0.70 V are attributed to either hydrogen adsorption or desorption. The double layer effect of the interface between electrolyte and electrode can be seen significantly (between -0.4 and -0.6 V). For the positive scan (potential increase), OH adsorption on Pt, described by equation (1) starts at -0.45 V:

$$Pt + OH^- \rightarrow Pt - OH + e^- \qquad (1)$$
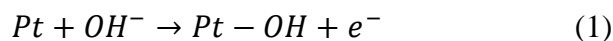
and above -0.20 V, the formation of oxides on Pt surface occurs:

$$Pt - OH + OH^- \rightarrow Pt - O^- + H_2O \qquad (2)$$
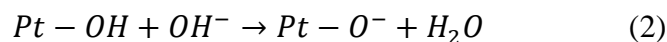
The current generated from species adsorption and desorption is a so-called non-Faradaic process [84]. During the negative scan, the significant broad peak between -0.45 and 0.25 V is mainly attributed to the reduction of oxide species (Pt-O$^-$) to Pt.

$$Pt - O + 2e^- + H_2O \rightarrow Pt + 2OH^- \qquad (3)$$
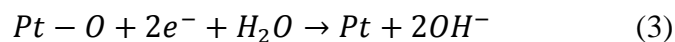
At potentials higher than 0.30 V, the oxygen evolution reaction starts and phase oxide formation on the Pt surface [18].

$$4OH^- \rightarrow 2H_2O + O_2 + 4e^- \qquad (4)$$
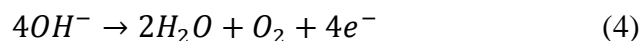
The hydrogen evolution reaction starts from the potential of -0.8 V:

$$H_2 + 2OH^- \rightarrow 2H_2O + 2e^- \tag{5}$$
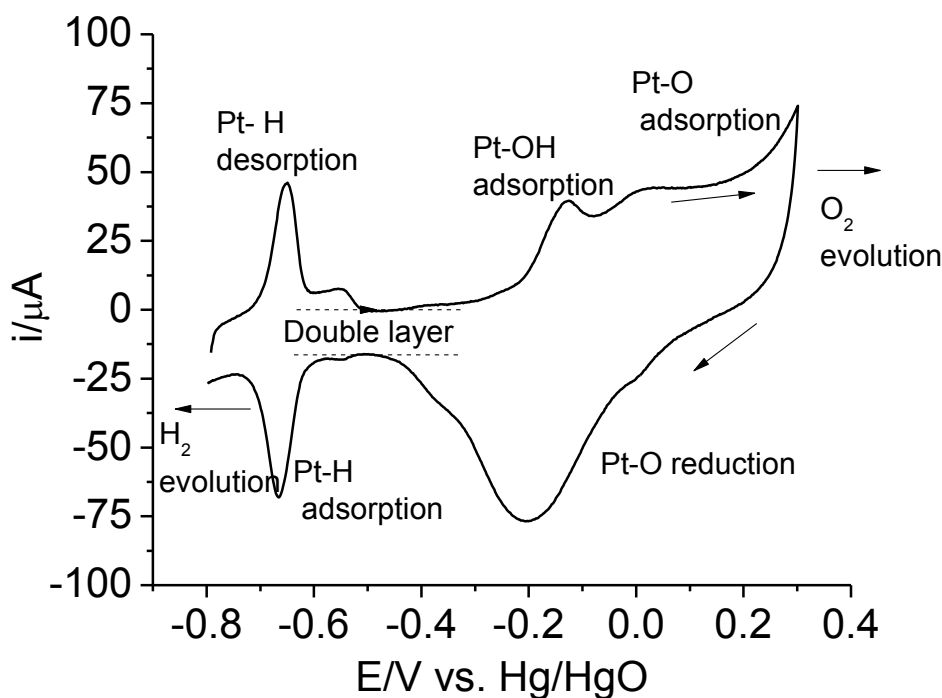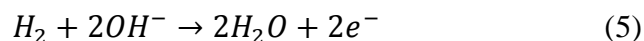
Figure 6-2 CVs of Pt/C in N_2 saturated 1.0 M KOH, 5 mV s^{-1} scan rate, at room temperature, the potential was measured against Hg/HgO in all voltammograms.

Figure 6-3 shows CVs of Pd/C samples all of which exhibited a poorly defined hydrogen adsorption region (-0.6 to -0.7 V) compare to Pt/C (in Figure 6-2) due to its dissolution into the bulk palladium metal [96, 97]. This feature makes it difficult to accurately determine the surface area from the area on the peaks. Therefore, the monolayer charge of chemisorbed oxygen was used to determine the Pd electrochemical surface area (ESA). Breiter reported the charge of Pd-O for the smooth Pd electrode was twice that (Q_H, 210 μC cm^{-2}) of the Pd-H hydrogen monolayer {i.e. $Q_H = 1/2 \ Q_O$ (E=1.27 V vs. RHE)} [157]. The obtained specific surface areas for all the Pd/C catalysts from CVs results are included in Table 3-2 Chapter 3. The integrated area of Pd-O reduction peaks of Pd/C catalysts (or ESA) showed a good agreement with their particle sizes obtained from TEM results. Overall the smaller particles size of Pd/C

catalyst, the higher the ESA.

The Pd/C catalysts, except for Pd/C-5 % HNO₃, had similar double layer region behaviour (between -0.50 to -0.30 V) which suggested that the catalysts had different transfer charges resistances. In the case of the 5% nitric acid treated carbon supported catalyst, the double layer was the widest of all other catalysts and exhibited its larger capacitance due to surface oxidation of the carbon surface.
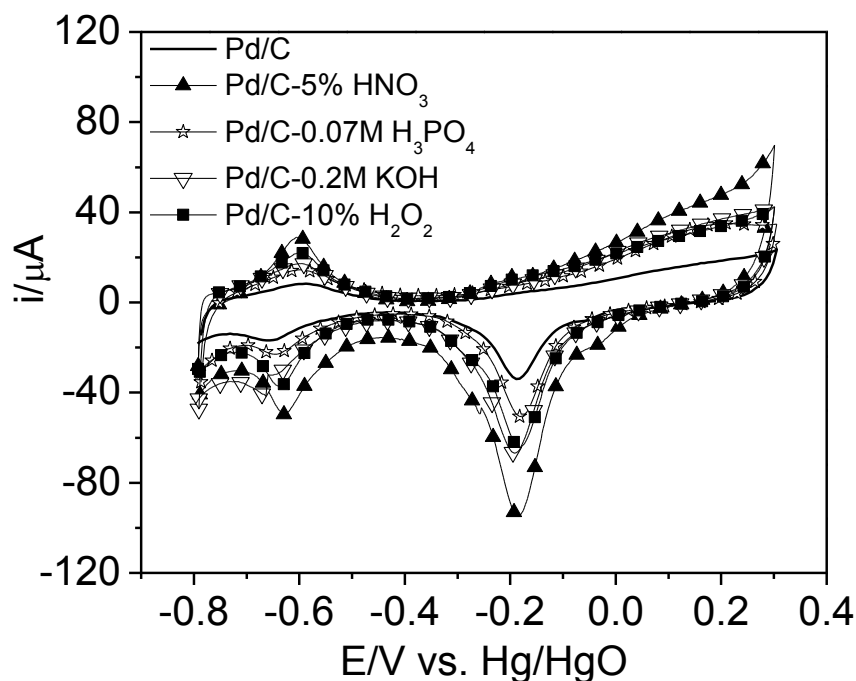
Figure 6-3 CVs of Pd catalysts with different carbon supports in N₂ saturated 1.0 M KOH, 5 mV s⁻¹ scan rate, room temperature

6.1.3 RRDE measurement

Figure 6-4 shows the polarization curve of Pd/C obtained in O₂ saturated 1.0 M KOH at a scan rate of 5 mV s⁻¹. The kinetic controlled region is in the potential range 0.15 and 0.05 V. At lower potentials, the nearly linear decline of polarization curve is the mixed kinetic-diffusion region. In this region, it clearly shows that the ORR current density during the positive scan was better than in negative scan. This was due to the nature of Pd which was easily oxidized at high potential and the presence of oxide on Pd or Pt surface decreases their activities for ORR [92]. At the negative scan, however, the Pd or

Pt surface was reduced to the metal phase at low potentials which then becomes available for ORR again. Thus, in this chapter, all polarisation curves for the Pd or Pt catalysts will use the positive scan. The current plateau is in the diffusion controlled region.
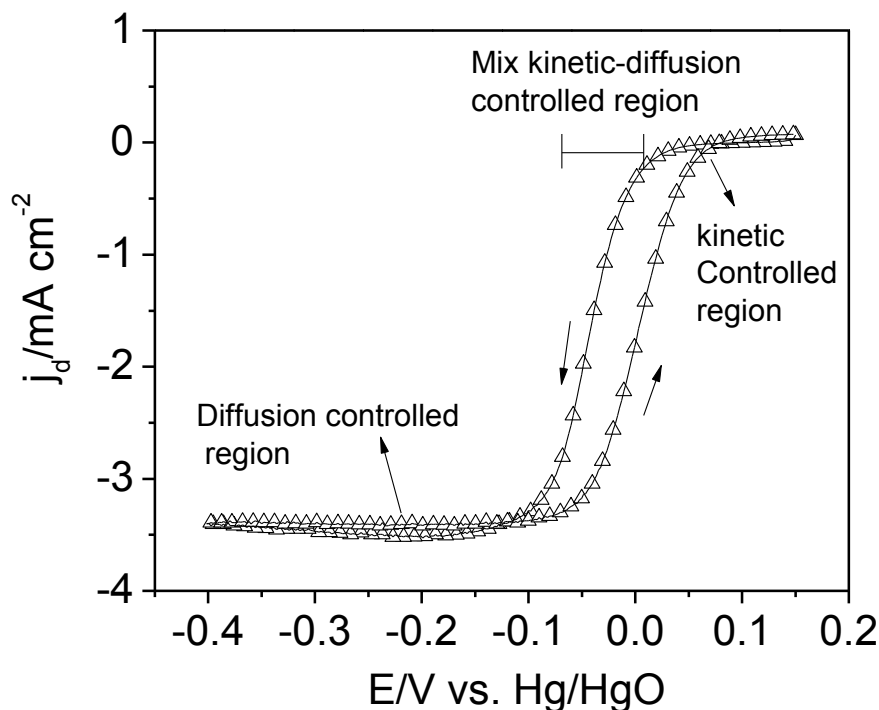
Figure 6-4 RRDE polarization curves of Pd/C in O_2 saturated 1.0 M KOH at 1600 rpm rotation rate, 5 mV s^{-1} scan rate, at room temperature

Figure 6-5a shows RRDE polarization curves of Pd/C catalysts and Pt/C for ORR in O_2 saturated 1.0 M KOH. Onset potentials of Pd/C, Pd/C-5 % HNO$_3$, Pd/C-0.07 M H$_3$PO$_4$, Pd/C-0.2M KOH, Pd/C-10% H$_2$O$_2$ and Pt/C were 0.078, 0.075, 0.085, 0.080, 0.078 and 0.078 V, respectively. The onset potential for the ORR on the Pd/C catalysts was similar to that on Pt/C (around 0.078 V vs. Hg/HgO) in alkaline media which agrees with published reports [92, 93].

Figure 6-5b shows the normalized mass activities with metal loading of catalysts. An increase trend of ORR activity with an order of Pt/C < Pd/C-10 % H$_2$O$_2$ < Pd/C-5 % HNO$_3$ < Pd/C < Pd/C- 0.07 M H$_3$PO$_4$ = Pd/C-0.2 M KOH at 0.025 V in the mixed kinetic-diffusion controlled region. Calculated mass activities of catalysts are listed in Table 6-1. All Pd/C catalysts (at least 3.9 mA mg^{-1} for Pd/C-10 % H$_2$O$_2$) exhibited

superior activity towards ORR than Pt/C (1.8 mA mg^{-1}) in O_2 saturated 1.0 M KOH solution. This behavior has been previously reported and is linked to the activation energy of ORR on Pd catalyst (39 kJ mol^{-1}) is lower than on Pt (48 kJ mol^{-1}) [92]. The lower mass activities of Pd support on 5 % HNO_3 and 10 % H_2O_2 treated carbons may be associated with the Pd metal agglomeration. Senthil et al explained that the strong interaction due to the high Pd agglomeration between Pd particles was prone to form Pd-O which reduced the reaction sites for ORR [97].

Figure 6-5a and c represent the ring current and percentage of H_2O_2 generated from ORR on all catalysts at different potentials. At lower potential, the higher production of H_2O_2 on Pd/C-5 % HNO_3, Pd/C-0.07 M H_3PO_4 and Pt/C in the diffusion controlled region resulted in lower limiting currents than the other catalysts. This behavior may be attributed to more oxygen groups on 5% HNO_3 and 0.07 M H_3PO_4 treated carbon support. For all catalysts, the ORR proceeds in a four-electron pathway at high potential which means negligible hydrogen peroxide yield until -0.15 V. As the potential goes more negative, the H_2O_2 yield of catalysts increases. At -0.4 V, the percentage of H_2O_2 yield on Pd/C-5 % HNO_3 , Pd/C-0.07 M H_3PO_4, Pt/C, Pd/C-10% H_2O_2, Pd/C and Pd/C-0.2 M KOH were 4.64 %, 3.43 %, 2.31 %, 2.06 %, 2 % and 1.18 %, respectively. Jiang et al reported that Pd/C catalyst with a particle size of around 5 nm produced no more than 2 % at -0.4 in O_2 saturated 0.1 M NaOH at 25 ^{o}C [94]. However, they found the H_2O_2 yield increased as the Pd particle size increases [94]. In the case of Pd/C-5 % HNO_3, although the Pd particle size is smallest (5.7 nm), the Pd metal particle agglomeration due to the low microspores area on the carbon surface caused a high yield of H_2O_2 [97].
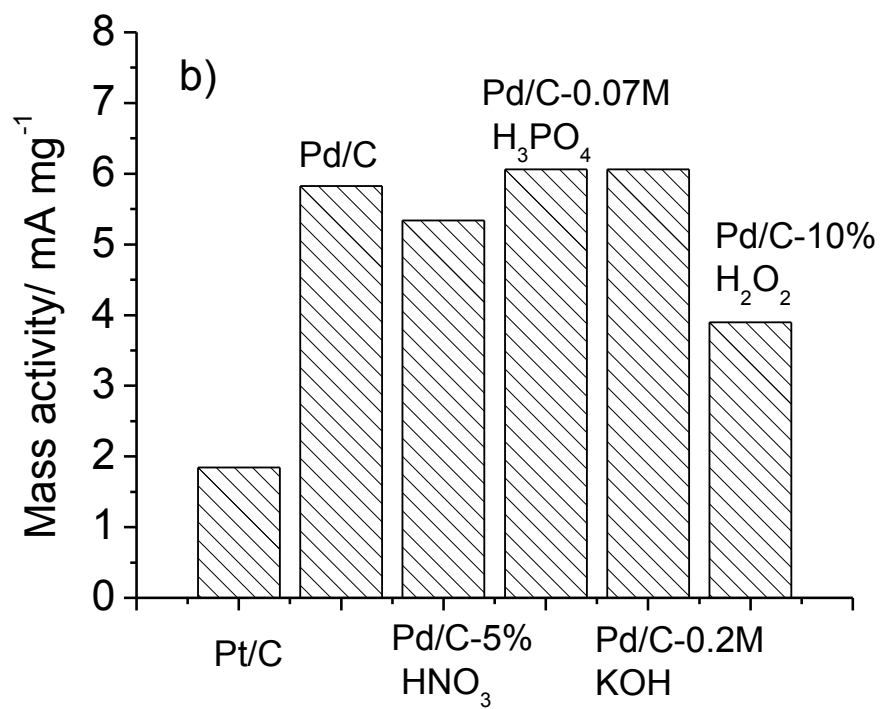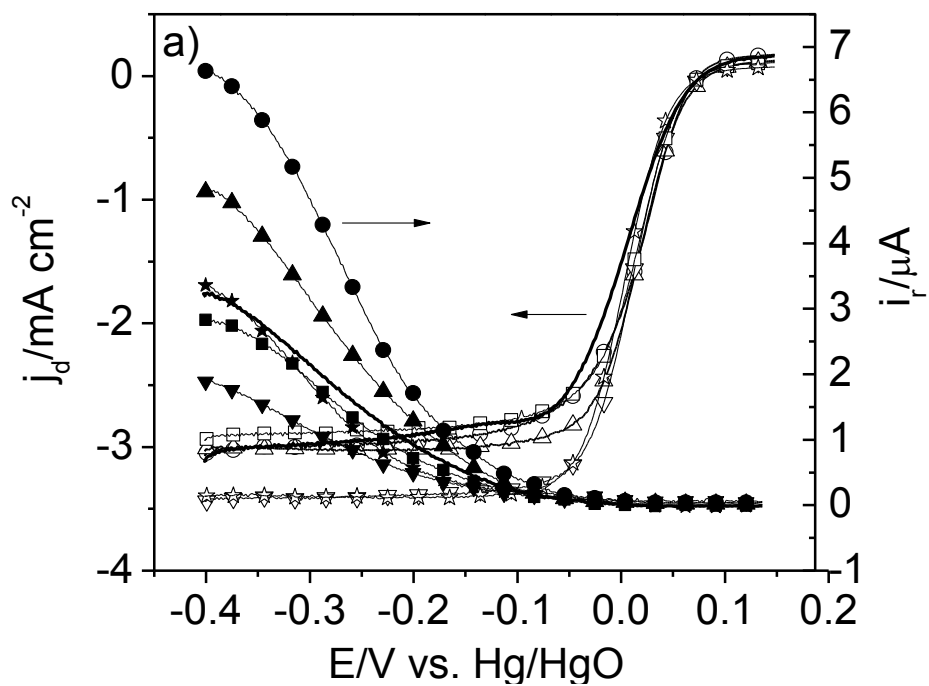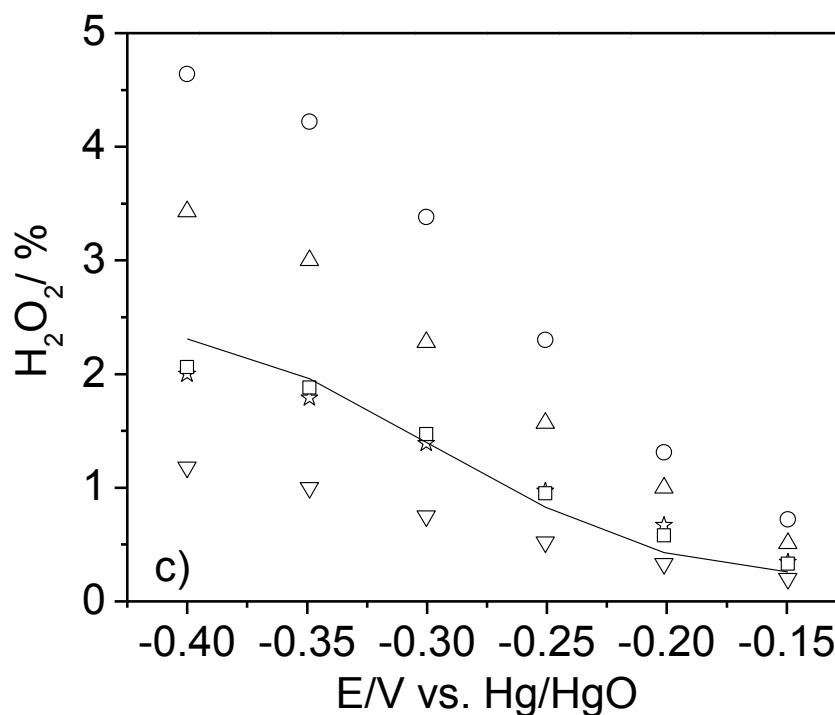
Figure 6-5 a) RRDE polarization curves of Pd/C catalysts and Pt/C at rotation rate of 1600 rpm in O_2 saturated 1.0 M KOH at room temperature, recorded at 5 mVs^{-1} scan rate, ($\square$) represent Pd/C-10% H_2O_2, (-) Pt/C, ($\triangle$) Pd/C-0.07M H_3PO_4,($\circ$) Pd/C-5% HNO$_3$, ($\triangledown$) Pd/C-0.2M KOH,($\star$) Pd/C, b) mass activities of Pd/C catalysts at 0 V, c) H_2O_2 fractional yields were calculated from polarization curves in Figure 4-5a at different potentials

Tafel plots were obtained from the linear-region as indicated by the solid line in Figure 6-6 of the plot from 0 to 80 mV. The observed Tafel slopes for various Pd/C catalysts were in the range of 50-60 mV/decade which are in good agreement with values reported by Jiang et al for Pd/C catalysts under similar experimental conditions (0.1 M NaOH at 25 ^{o}C) [92, 94]. Within experimental error Tafel plots are almost parallel, as shown in Figure 6-6 indicating that the rate-determining step was the same on all the catalysts which was consistent with a one-electron transfer reaction [84].
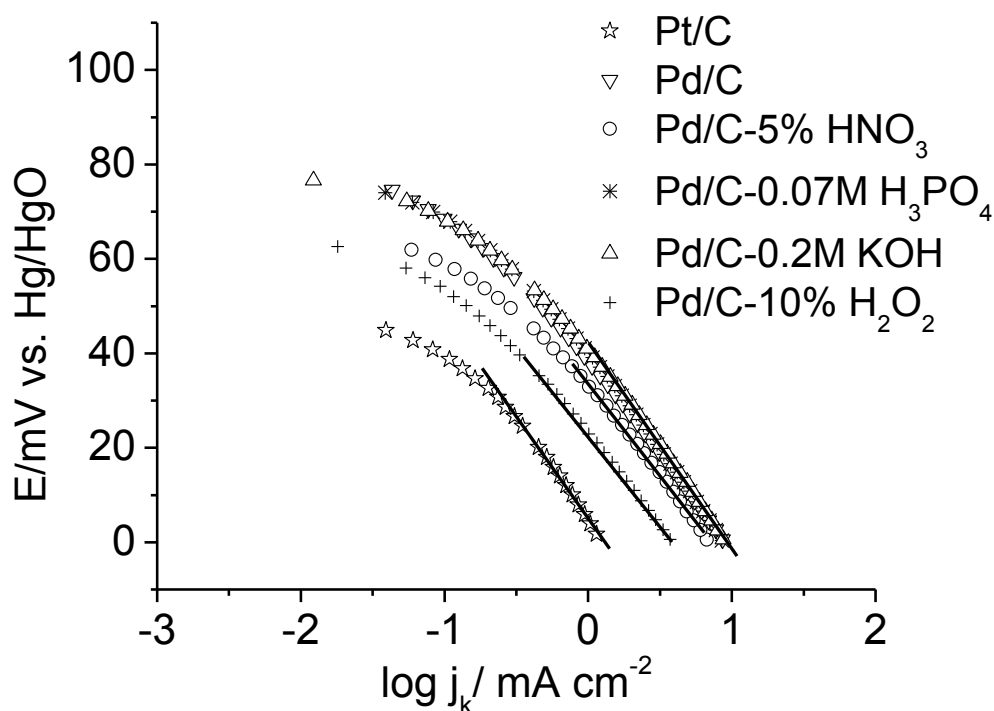
Figure 6-6 Tafel plots of all catalysts derived from Figure 4-5a

Polarization curves of all catalysts at five different rotation rates (100, 400, 900, 1600 and 2500 rpm) are shown in Figure 6-7. The expected increase in the diffusion limited current in the disk measurement was observed as a function of rotation rate. Based on the data, Figure 6-8 presents the inverse current density (i^{-1}) as a function of the inverse of the square root of the rotation rate ($\omega^{-1/2}$) which is so-called Koutecky-Levich equation (6):

$$1/i = 1/i_k + 1/B\omega^{1/2} \qquad (6)$$

where i is the measured current, i_k is the kinetic current, B is a constant ($B = 0.62nFAD_{O_2}^{2/3}v^{-1/6}C_{O_2}$), and ω is the rotation rate. The published value of the diffusion coefficient of O_2 in 1.0 M KOH solution (D_{O_2}= 1.59×10^{-5} cm^2 s^{-1}), the kinematic viscosity of the solution v =0.0095 cm^2 s^{-1}, and the concentration of dissolved O_2 in solution (C_{O_2}=0.88×10^{-3} mol L^{-1}) [158] F is the Faraday constant (96485) and A is the electrode geometric area (0.2475 cm^2). The calculated value of B is 0.072 mA s$^{-1/2}$ for a

91

four-electron exchange reaction (n=4).
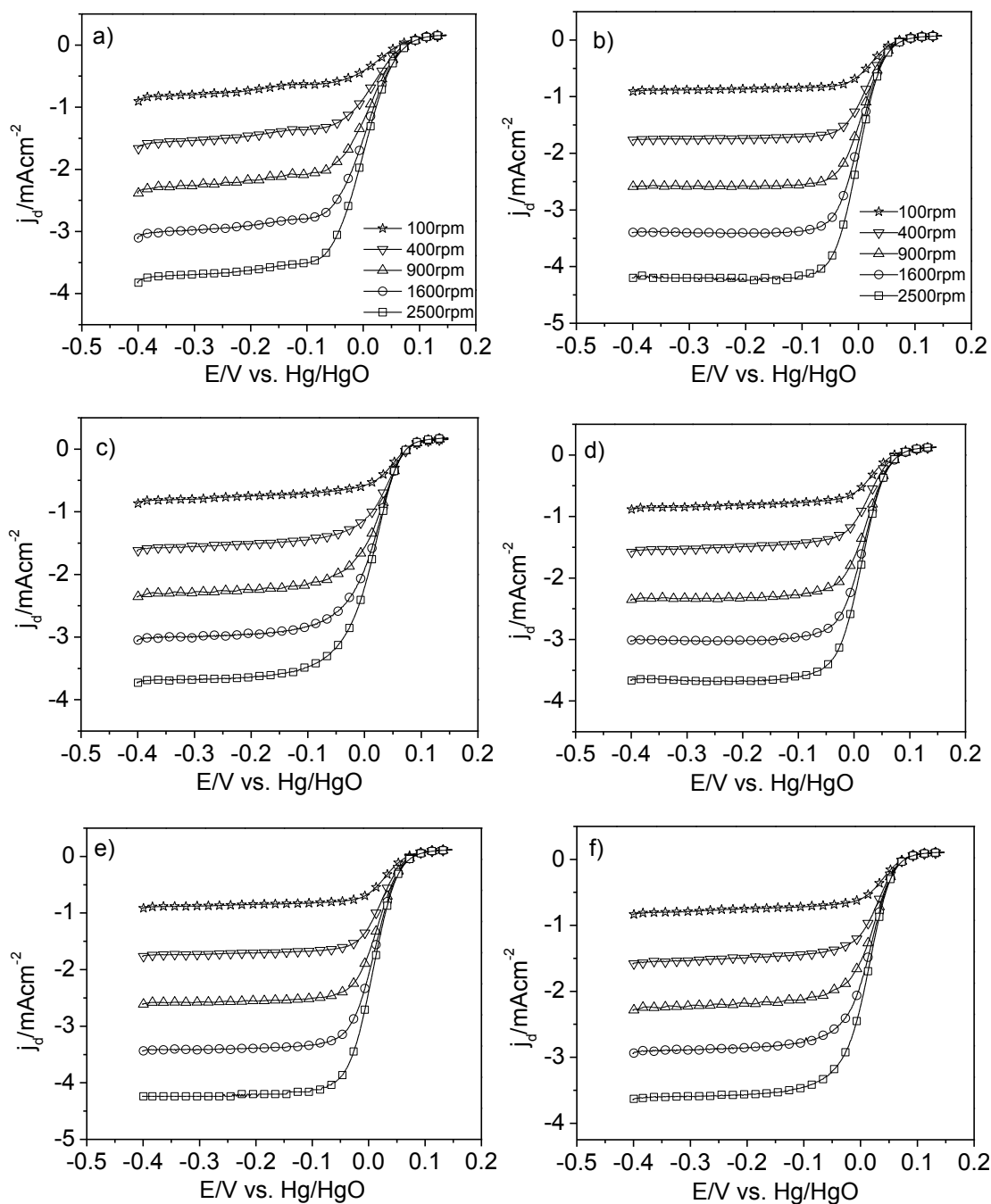
Figure 6-7 RRDE polarization curves of Pt/C and Pd/C catalysts at various rotation rates in O_2 saturated 1.0 M KOH at room temperature

The obtained Koutecky-Levich plot at -0.4 V is shown in Figure 6-8. The catalysts exhibited a four-electron transfer reaction pathway for the ORR in 1.0 M KOH except for Pd/C-5 % HNO_3 (3.9) and Pd/C-10 % H_2O_2 (3.8), however, these values are within the experimental error (5 %). Thus, all catalysts are considered that promotes an

effective ORR (four electrons transfer reaction) in alkaline media.
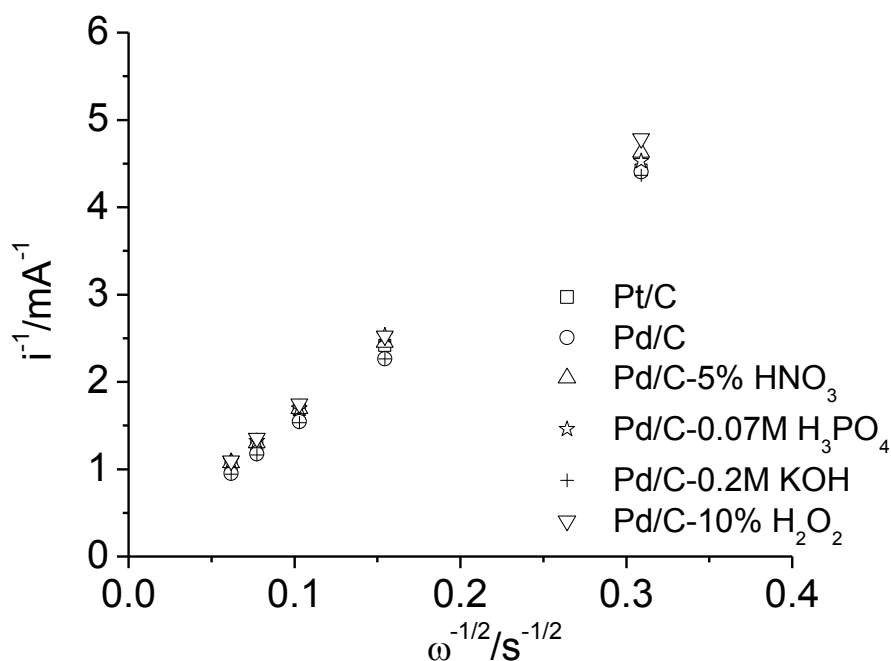
Figure 6-8 Koutecky-Levich plots derived from the results in Figure 4-6 extracted at a fixed potential of -0.4 V

Table 6-1 Kinetic parameters of all samples obtained from Koutecky-Levich plot

Sample	Mass activity[a]/mA mg^{-1}	Tafel slope, mV dec^{-1}	Electron number, n
Pt/C	1.84	-59.04	4.0
Pd/C	5.82	-54.44	4.0
Pd/C-5 % HNO$_3$	5.34	-50.31	3.9
Pd/C-0.07 M H$_3$PO$_4$	6.06	-61.88	4.0
Pd/C-0.2 M KOH	6.06	-55.74	4.0
Pd/C-10 % H$_2$O$_2$	3.90	-51.38	3.8

a-current was taken at a fixed potential (0.025 V) for different rotation rate, and it was normalized by the metal mass of catalysts

The Pd/C treated with 0.2 M KOH was selected for fuel cell test due to the high mass activity and lowest H$_2$O$_2$ production in half-cell tests compared to other Pd/C catalysts. Figure 6-9 shows the OCV of the MEA using the Pd catalyst at the cathode was 0.95 V,

only 0.05 V lower than that obtained with the Pt catalyst cathode. The maximum power density obtained by the MEA using commercial Pt/C catalyst was 30 mW cm^{-2} using the anion exchange membrane. The low fuel cell performance can be attributed mostly to the absence of ionomer in all catalyst layers. On the other hand, the Pd/C cathode electro-catalyst produced a power density of 20 mW cm^{-2} under identical experimental conditions. The lower power density of Pd/C than Pt/C might be attributed to the easy oxidation surface of Pd under a fuel cell operating conditions. Although the power density obtained was low in comparison to that typically obtained for PEMFCs, the data are encouraging for the potential application of Pd for the ORR, when taking into account the cost considerations where Pd is approximately 4 times cheaper than Pt metal. However to fully capitalize on the activity of Pd catalysts, by for example doubling the Pd loading, would require the use of a OH^{-} ion conducting ionomer in the catalyst layer.
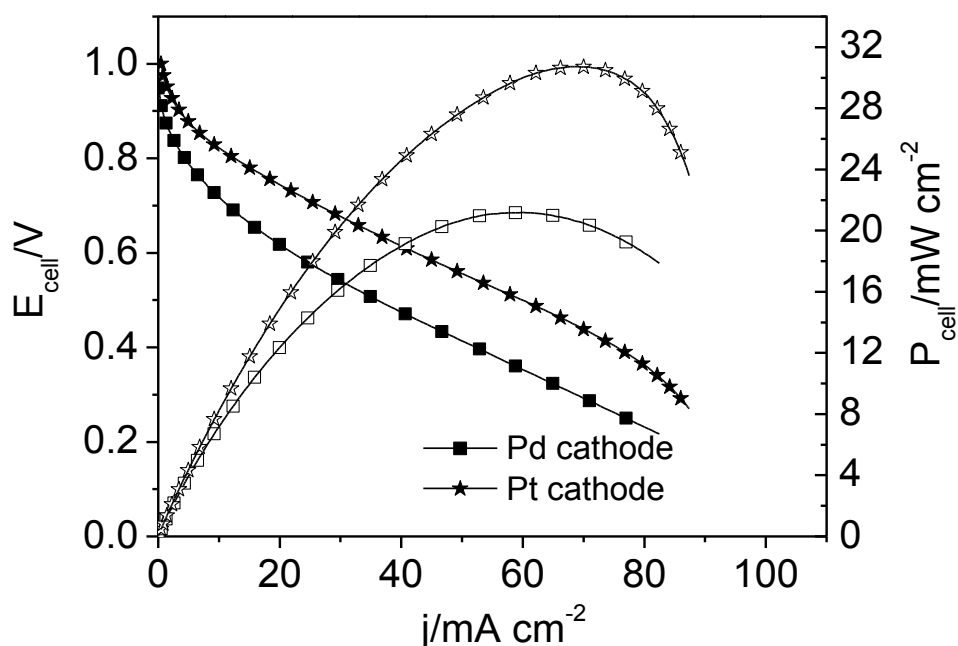
Figure 6-9 Fuel cell performances of MEAs using Pd/C-0.2 M KOH and Pt/C at the cathode metal loading 1 mg cm^{-2}, 1 mg cm^{-2} Pt/C at the anode, no ionomer for the both electrodes, room temperature, atmospheric pressure

6.2 Conclusions

This study demonstrated that the chemical pretreatment of the carbon support alters the

Pd nano-particle size and its distribution over the carbon surface. The resultant Pd/C catalysts were found to be very active towards the electrocatalytic oxygen reduction reaction compared to a commercial BASF 20 % Pt/C catalyst in alkaline solution. All Pd/C catalysts gave Tafel slopes close to 60 mV dec^{-1} which indicate a similar mechanism for the ORR as for Pt/C. Mass activities, measured at 0.025 V, for various Pd/C samples were superior to that for the commercial BASF 20% Pt/C. 0.07 M H_3PO_4 and 0.2 M KOH treated carbon deposited with Pd gave a mass activity of 6 mA mg$^{-1}_{Pd}$ is considered as the best catalyst studied in this work. The destructive pre-treatments (5 % HNO_3 and 10 % H_2O_2 treated carbons in this study) lead to an unfavorable effect on the morphology of Pd/C (metal particle agglomeration). The single fuel cell test obtained by employing 0.2 M KOH treated carbon supported Pd catalysts showed an inferior activity with the commercial BASF Pt/C under similar experimental conditions. However, the cost of Pd catalyst is much lower than Pt catalysts which make Pd a promising candidate for ORR in alkaline media.

CHAPTER 7. DEVELOPMENT OF METAL MACROCYCLE CATALYSTS FOR THE OXYGEN REDUCTION REACTION IN LAKALINE MEDIA

7.1 Results and discussion

7.1.1 Comparison of Metal macrocycle catalysts using RRDE measurements

RRDE polarization curves in O_2 saturated 1.0 M KOH of all catalysts are shown in Figure 7-1. Metal macrocycle catalysts gave lower onset potentials (in Table 7-1) than Pt/C (0.067 V). For FePc/VC and K-14, their onset potentials were 0.041 and 0.043 V. Literatures reported that onset potentials of Pt/C and FePc/C are around 0.05 V in 0.1 NaOH solution at 25 ^{o}C [93, 147]. Co based metal macrocycles (CoPc/VC, CoTMPP/VC) and Vulcan XC-72R carbon support (-0.05, -0.027 and -0.052 V, respectively) exhibited the much lower onset potential. Chen et al showed that the onset potential of CoPc is -0.05 V vs. Hg/HgO in 0.1 M NaOH solution at 25 ^{o}C. In the mixed kinetic-diffusion controlled region which extends from potentials of -0.1 to 0.1 V, mass activities (measured at 0.0 V) of all catalysts for the ORR were calculated from the mass transfer corrected kinetic currents divided with the total amount of catalysts including carbon support. The mass activity of FePc/VC (10.4 mA mg^{-1}) was higher than the commercial catalysts Pt/C (8.7 mA mg^{-1}) and K-14 (2.1 mA mg^{-1}). Activities of the other catalysts were too poor to measure at this potential. Recently, Chen et al reported the same observation of the catalytic activity of FePc and CoPc in 0.1 M NaOH [147]. This is due to the Co based metal macrocycles do not facilitate the cleavage reaction of O-O bond which lead to a two-electron transfer reaction, however, with a face-to-face structure of two Co metal centre, it promotes an effective ORR (four-electron transfer reaction) [113]. Tafel slopes of all catalysts (in Figure 7-1b) were around -50 mV dec^{-1} at low current density region which agrees well to the published reports in alkaline

media [112, 127, 147]. This slope value indicated that the mechanism of ORR at low current density is one-electron transfer reaction.

The ring current of catalysts in Figure 7-1c shows that Co based metal macrocycle catalysts and K-14 started generating H_2O_2 at higher potential (-0.04 V) than Pt/C and FePc/VC. At low potential region (-0.2 to -0.4 V), FePc/VC produced even less hydrogen peroxide than commercial 20 wt % Pt/C. For instance, the ring current of hydrogen peroxide oxidation from FePc/VC and Pt/C were 1.13 and 3.39 μA at -0.4 V. The Acta K-14 non-noble catalyst, however, produced hydrogen peroxide as high as CoPc and CoTMPP (up to 12 μA) which was one order magnitude higher than FePc/VC. Ring disk results of H_2O_2 production shows a good agreement of literatures which Fe based metal macocycles are more active for ORR and produce less H_2O_2 than Co based metal macrocycles in alkaline media [127, 147]. The H_2O_2 high yield of K-14 may originate from the carbon support.
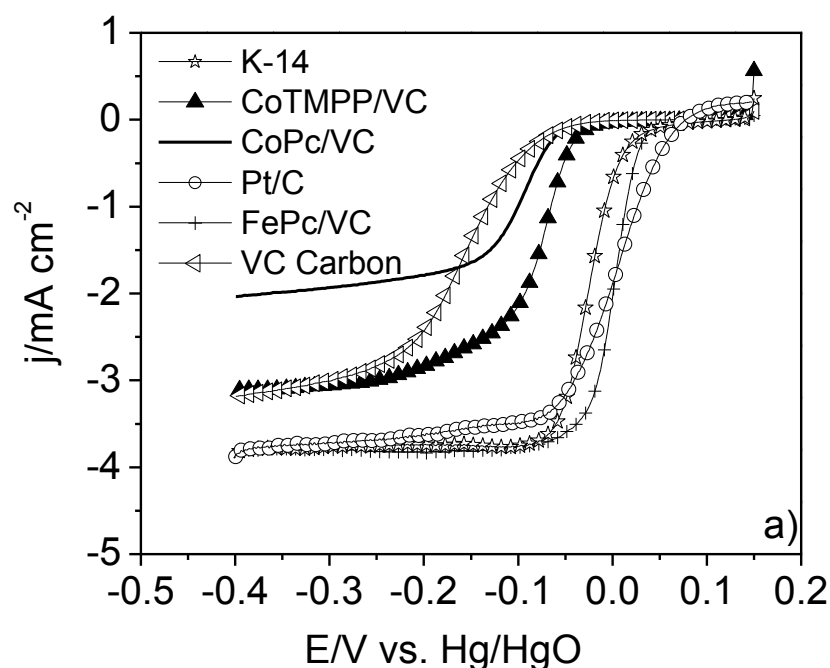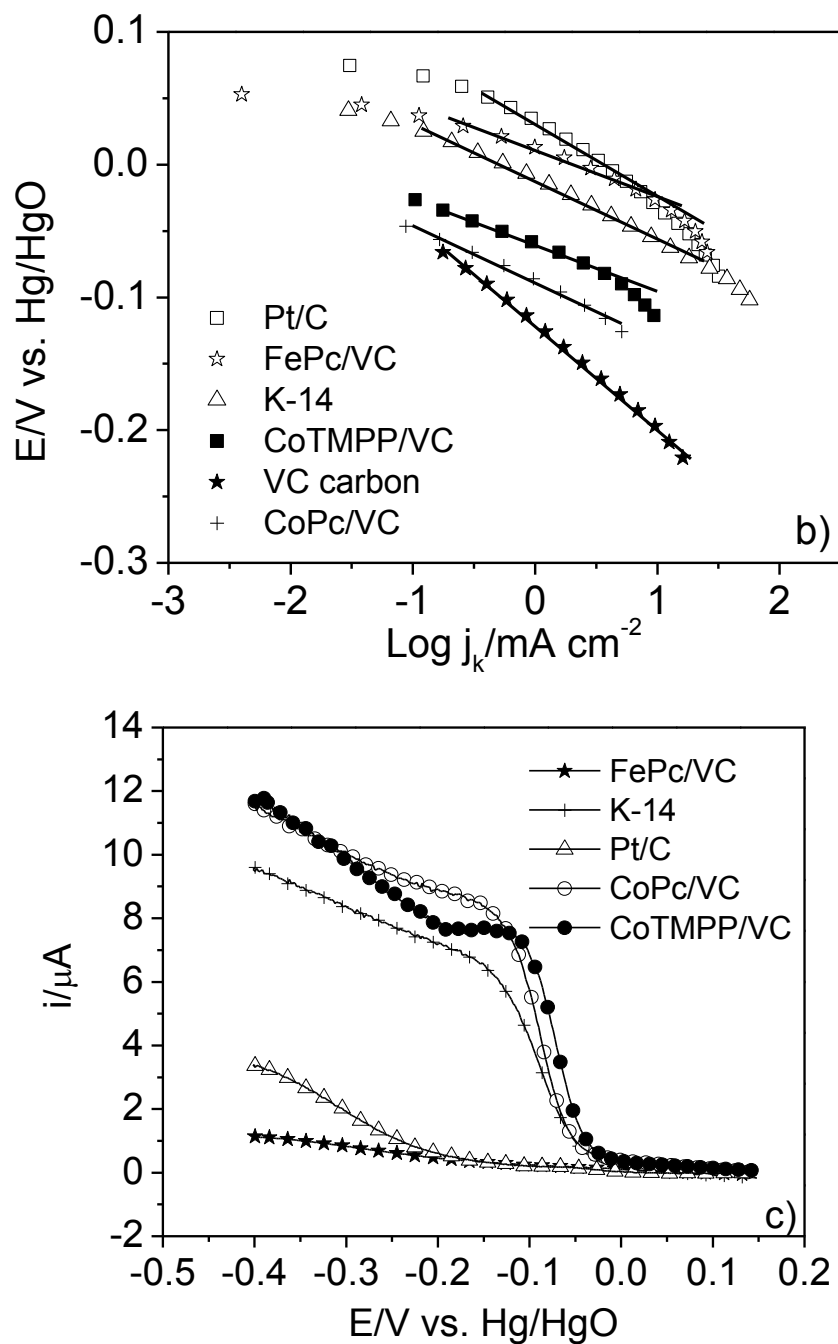
Figure 7-1 RRDE measurements of Pt/C, Vulcan carbon supported FePc, CoPc and CoTMPP in O_2 saturated 1.0 M KOH, 5 mV s^{-1} scan rate, 1600 rpm rotating speed and room temperature, a) disk current, b) Tafel plot of all catalysts derived from the polarization curves, c) corresponding ring current, the potential in half-cell test were measured against Hg/HgO reference electrode in 1.0 M KOH at 25 ^{o}C.

Table 7-1 Kinetic parameters of catalysts in O_2 saturated 1.0 M KOH at 25 $^{\circ}$C

Catalysts	Onset potential /V	Mass activity/mA mg^{-1}, @ 0 V	Tafel slope/mV dec^{-1}
Pt/C	0.067	8.7	-62
K-14	0.043	2.1	-53
CoPc/VC	-0.050	-	-43
FePc/VC	0.041	10.8	-42
CoTMPP/VC	-0.027	-	-45
VC carbon	-0.052	-	-78

7.1.2 Different carbon support for FePc

The ORR activity of FePc was affected by using different carbon supports (as shown in Figure 7-2). All onset potentials of catalysts were the same. In the mixed kinetic and mass transport controlled region, the KJB supported FePc exhibited the best ORR activity compared to the other two carbon supports. At a fixed potential of 0 V, the mass activities of FePc/KJB, FePc/VC and FePc/SP were 2.65, 2.15 and 1.36 mA cm^{-2}, respectively. The catalytic activity of FePc was improved by using higher surface area of carbon support. Although the higher ORR activity of KJB carbon support was found (in Figure 7-2b), the current densities at initial kinetic region that generated from carbons were negligible compared to the current from FePc catalysts at the same potential (in Figure 7-1b). Thus, the enhanced activity of FePc/KJB may be contributed by the higher surface area of catalyst not the current from KJB carbon support.
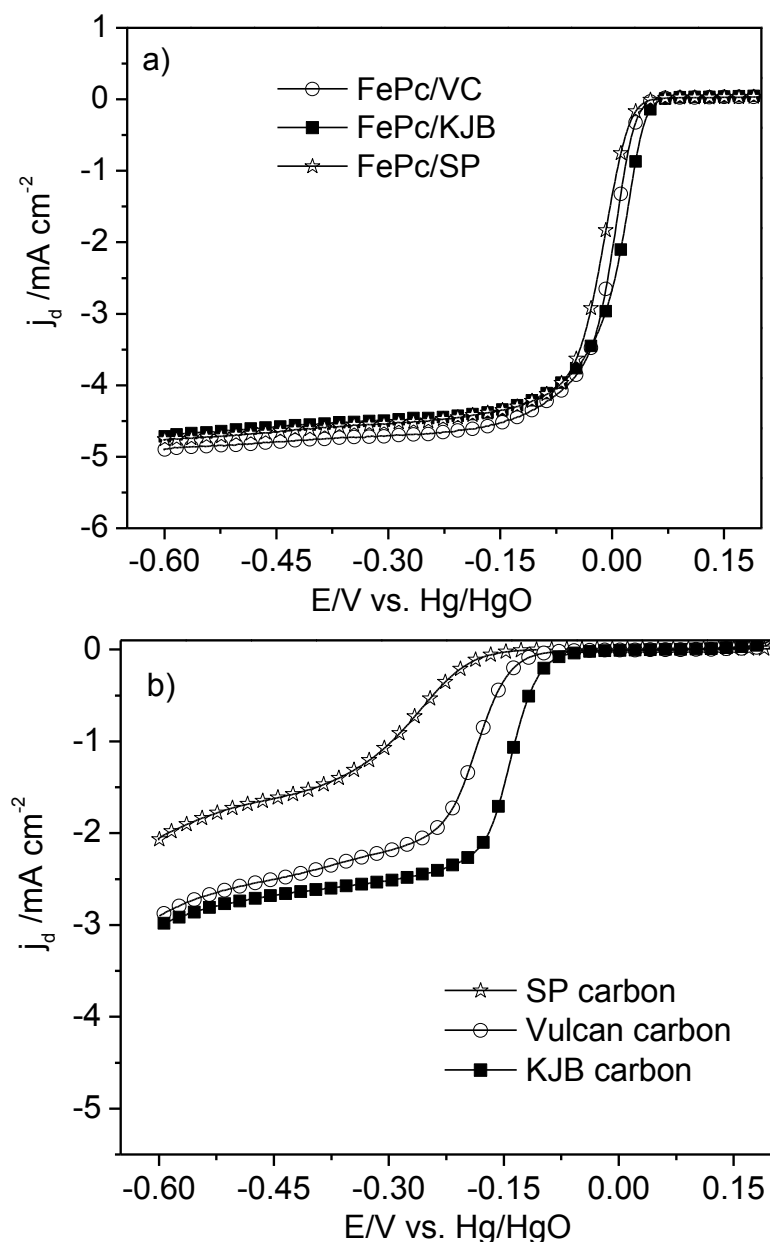
Figure 7-2 Polarization curves of a) FePc support on three different carbons, b) carbon supports, in O_2 saturated 1.0 M KOH, 5 mV s^{-1} scan rate, 2500 rpm rotating speed and 25 ^{o}C,

7.1.3   The determination of the kinetic parameters of the ORR on FePc/KJB catalyst

The morphology of FePc/KJB was investigated using ESEM (in Figure 7-3). The image reveals that FePc/KJB showed a porous structure with uniform fluffy small particles. The composition of metal iron was determined using Energy Dispersive X-ray (EDX) analysis which gave a value of ~ 2.7 wt %.
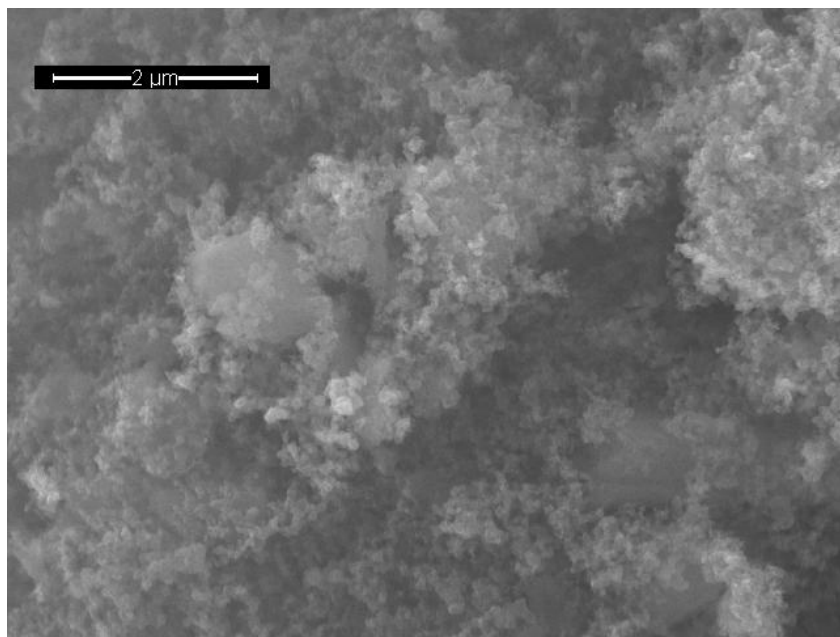
Figure 7-3 SEM image of FePc/KJB

Figure 7-4 shows LSVs at four different rotation rate (f = 400 rpm, 900rpm, 1600rpm and 2500 rpm) for the FePc/KJB catalyst in O_2 saturated 1.0 M KOH solution at 25 °C. The expected increase in the diffusion limited current in the disk measurement was observed as a function of rotation rate. The n number of FePc/KJB was calculated using the Koutecky-Levich plot according to the following equation:

$$1/j_d = 1/j_k + 1/B\omega^{1/2} \qquad (4)$$

where j_d is the disk current density (mA cm^{-2}), j_k is the kinetic current density (mA cm^{-2}), ω is the angular velocity ($\omega=2\pi f$ and f is rad s^{-1}) and B is a constant and B = $0.62nFAD_{O_2}^{2/3}v^{-1/6}C_{O_2}$ where n is the transferred electron number per O_2 molecule for ORR, F is the Faraday constant (96485 C mol^{-1}), A is the geometry area of the electrode (0.2475 cm^2), the published value of the diffusion coefficient of O_2 in 1.0 M KOH at 25 °C (D_{O_2}= 1.59 × 10^{-5} cm^2 s^{-1}), the kinematic viscosity (v = 0.0095 cm^2 s^{-1}) and the concentration of dissolved O_2 (C_{O_2}= 0.89 × 10^{-3} moL L^{-1}) [158].

For a four electrons transfer ORR, the constant value B is 0.072 mA s$^{-1/2}$ in 1.0 M KOH solution at 25 $^{\circ}$C. Based on this B value at low potential in diffusion controlled region (-0.3, -0.4 and -0.5 V), the average n numbers were calculated to be 4.0 ± 0.03 for both Pt/C and FePc/KJB. This is well-agreed with the literature [147].
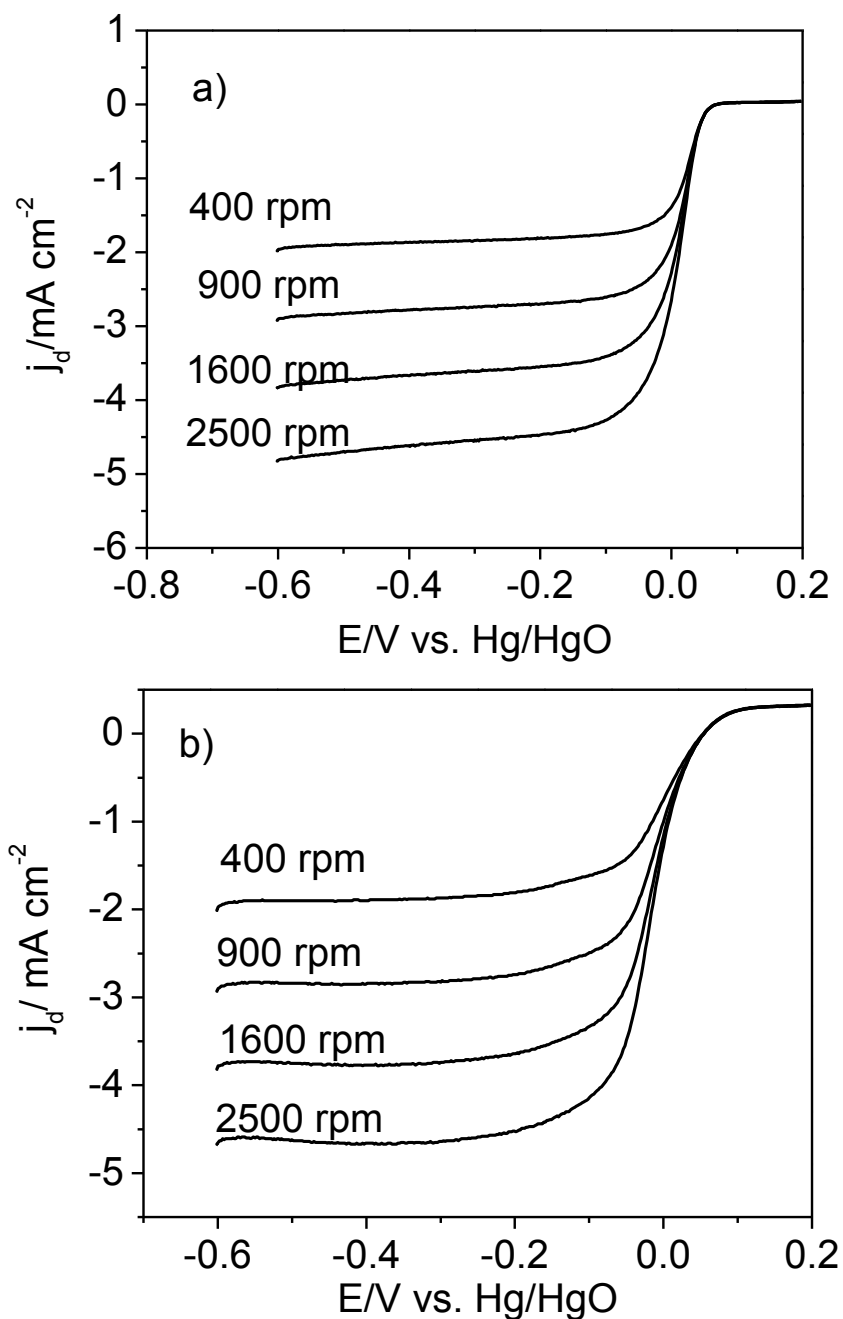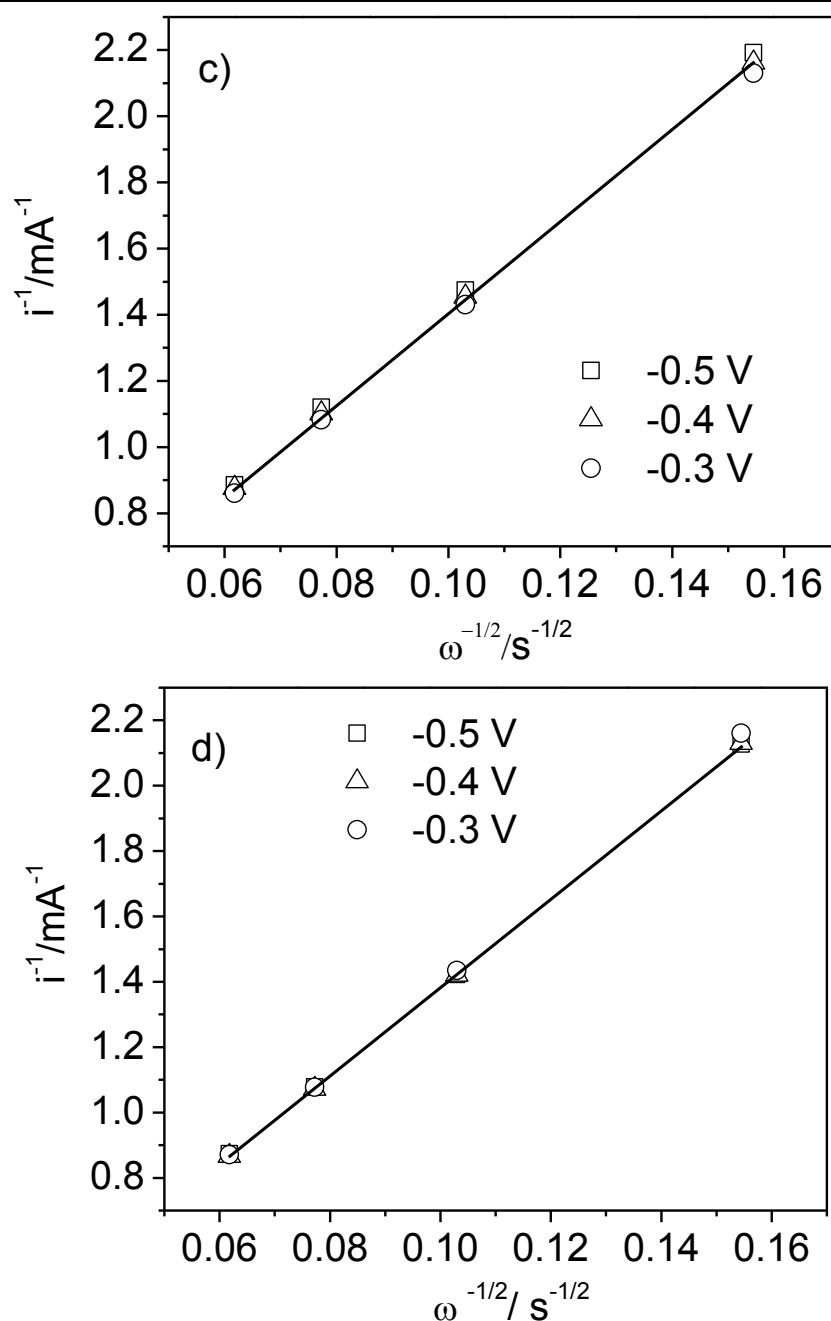
Figure 7-4 a,b) LSVs of FePc/KJB and Pt/C at four different rotation rate (400 rpm, 900 rpm, 1600 rpm and 2500 rpm) in O_2 saturated 1.0 M KOH at 25 $^{\circ}$C, recorded at 5 mVs^{-1} scan rate c,d) Koutecky-Levich plots of FePc/KJB and Pt/C at the potentials in mass transport controlled region (-0.3 V, -0.4 V and -0.5 V)

Figure 7-5 presents the mass transport corrected Tafel plots of logj_k versus against the electrode potential for the ORR on Pt/C and FePc/KJB in O_2 saturated 1.0 M KOH at 25 $^{\circ}$C. These Tafel curves were derived from the polarization curves of Figure 6-5. The Tafel slopes at high (> -50mV) and low potential (< -100 mV) were around 60 (one-electron transfer reaction) and 120 mV dec^{-1} (two-electron transfer reaction) for

both Pt/C and FePc/KJB. These results indicate the similar rate-determination reaction of ORR on both catalysts. It showed a good agreement of published reports of ORR on metal macrocycle catalysts in alkaline media [114, 147, 158].
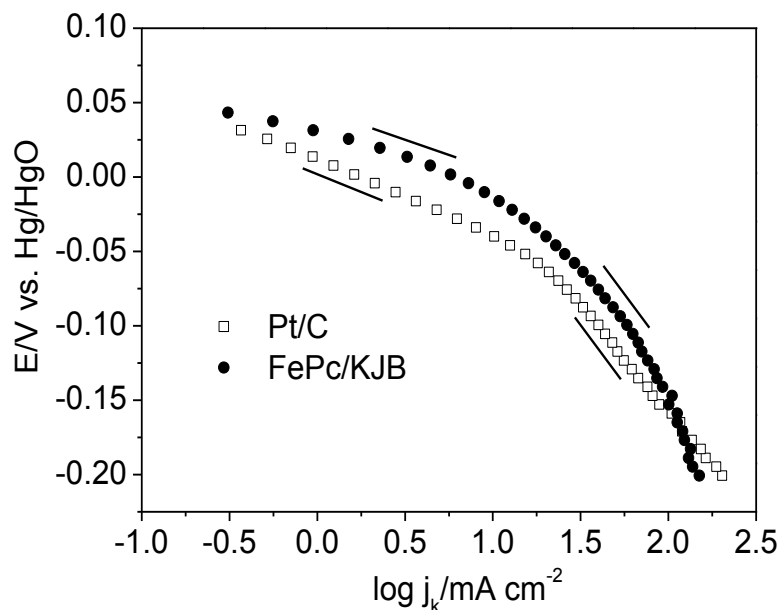
Figure 7-5 Tafel plots of Pt/C and FePc/KJB, log j_k was calculated from data in Figure 6-5 at a rotation rate of 2500 rpm, the short lines represent the slope of adjacent data points

The stability of FePc/KJB was investigated in half-cell using CV for 40 cycles in O_2 saturated 1.0 M KOH at a rotation rate of 2500 rpm (in Figure 7-6a). There was a steady decrease in the mass transport controlled current density with increasing number of cycles. However, there was no significant change in the kinetic and mixed kinetic-mass transport controlled regions. The data above suggest that the major loss in current density was contributed by the oxygen starvation due to the consumption of O_2 (the current generated from ORR for 40 cycles needs large amount of O_2 in the solution) in 1.0 M KOH faster than the O_2 diffusion (under O_2 atmosphere) into the solution. The stability result of this work is a contradiction of what reported in the literature that a rapid decline on ORR catalytic activity (especially in mixed diffusion and kinetic region) of FePc [147]. In order to verify the stability of FePc in O_2 saturated 1.0 M KOH solution, a further study using potentiostatic measurement was conducted by maintain the cell potential at 0.0 V for 24 h (in Figure 7-6b). The averaged data which indicated by a solid line confirm that there was no significant decay on ORR activity of FePc/KJB

during the 24 h test.
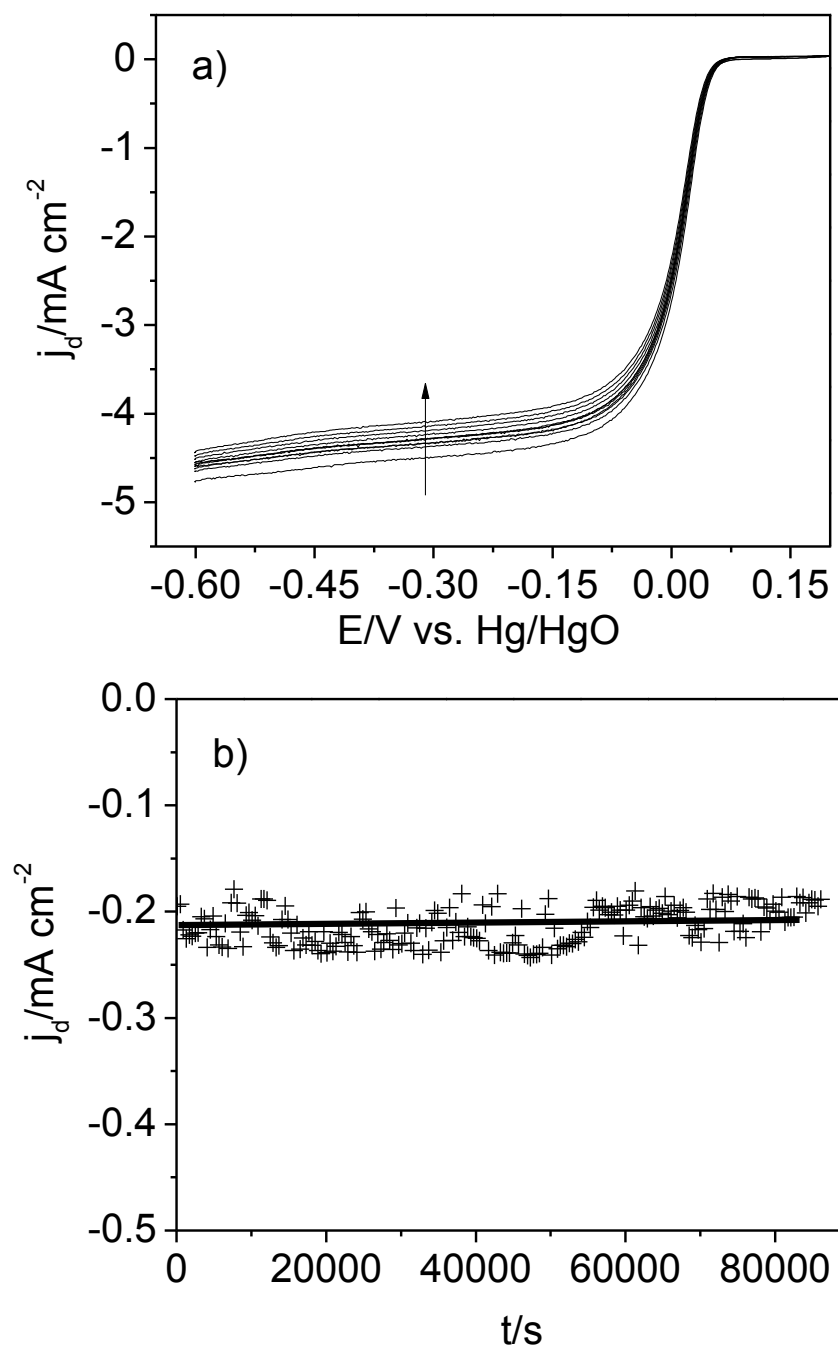
Figure 7-6 Stability test of FePc/KJB at 25 $^{\circ}$C using a) cyclic potential sweeping for 40 cycles at a rotation rate of 2500 rpm, 10 mV s^{-1} scan rate, , b) potentiostatic measurement at 0.0 V for 24 h

A number of reports on the stability test of FePc are listed in Table 7-2. Previous reports on the stability of FePc catalysts using different techniques were reasonable in low concentration or high concentration alkaline media. Chen et al reported the significant degradation (0.1 μA cm^{-2} s^{-1}) of FePc during CV test may be contributed by the loss of

catalysts on the RRDE electrode [147].

Table 7-2 The published stability studies on FePc in alkaline media

Electrodes	Conditions	Methods	Conclusions	References
FePc coated electrode	1.0 M KOH, 22 $^{\circ}$C	Open circuit aging, 24h	Slight degradation	[126]
FePc/Vulcan on glassy carbon	0.1 NaOH, 25 $^{\circ}$C	CV 30 cycles and Potentiostatic for 2h	Severe degradation	[147]
FePc on Ni foam in DBFC	6.0 M KOH, Room temperature	Potentiostatic for 50h	No degradation	[160]
FePc/KJB	1.0 M KOH, 25 $^{\circ}$C	CV 40 cycles and potentiostatic for 24 h	No degradation	This study

Based on half-cell tests above, FePc/KJB exhibited similar activity to commercial Pt/C. It is promising to utilize such low-cost, stable high electro-catalytic activity for ORR in AAEMFCs. For the further collaborated study with my colleague in single cell tests, we found that it is unstable in a quaternary ammonium solid state electrolyte environment [148]. The performance of the Fe-Pc catalyst under fuel cell conditions was found to fall with time due to an interaction of the catalyst with the ion-exchange group of the membrane and the ionomer used in the catalyst layer [148]. A heat treatment procedure will be carried out in order to stabilize the catalyst under the operating AAEMFC working condition.

7.1.4   *Characterizations of heat-treated FePc/KJB catalysts*

Figure 7-7 shows CVs of FePc/KJB and FePc/KJB-H8 in N_2 saturated 1.0 M KOH solution which were obtained in the potential range of -0.8 V to 0.3 V at a scan rate of 5 mVs^{-1}. The solid line represents the CV of FePc/KJB as prepared and two reversible peak couples at around -0.1 V was attributed to the Fe (II) /Fe (III) reversible reaction [127]. At more negative potential (around -0.55 V), the Fe (I)/Fe (II) reversible redox

peaks couple was observed. Redox couple peaks due to the changing oxidation states of the central metal ion were at same potentials in CV as reported in previous investigations [127]. After the heat-treatment at 800 $^{\circ}$C for 6 h, redox peaks disappeared which indicates the decomposition of FePc (in Figure 6-8b). The most recent review concluded that when the temperature of heat treatment reaches over 700 $^{\circ}$C, the only species which exists is the inorganic metal [124].
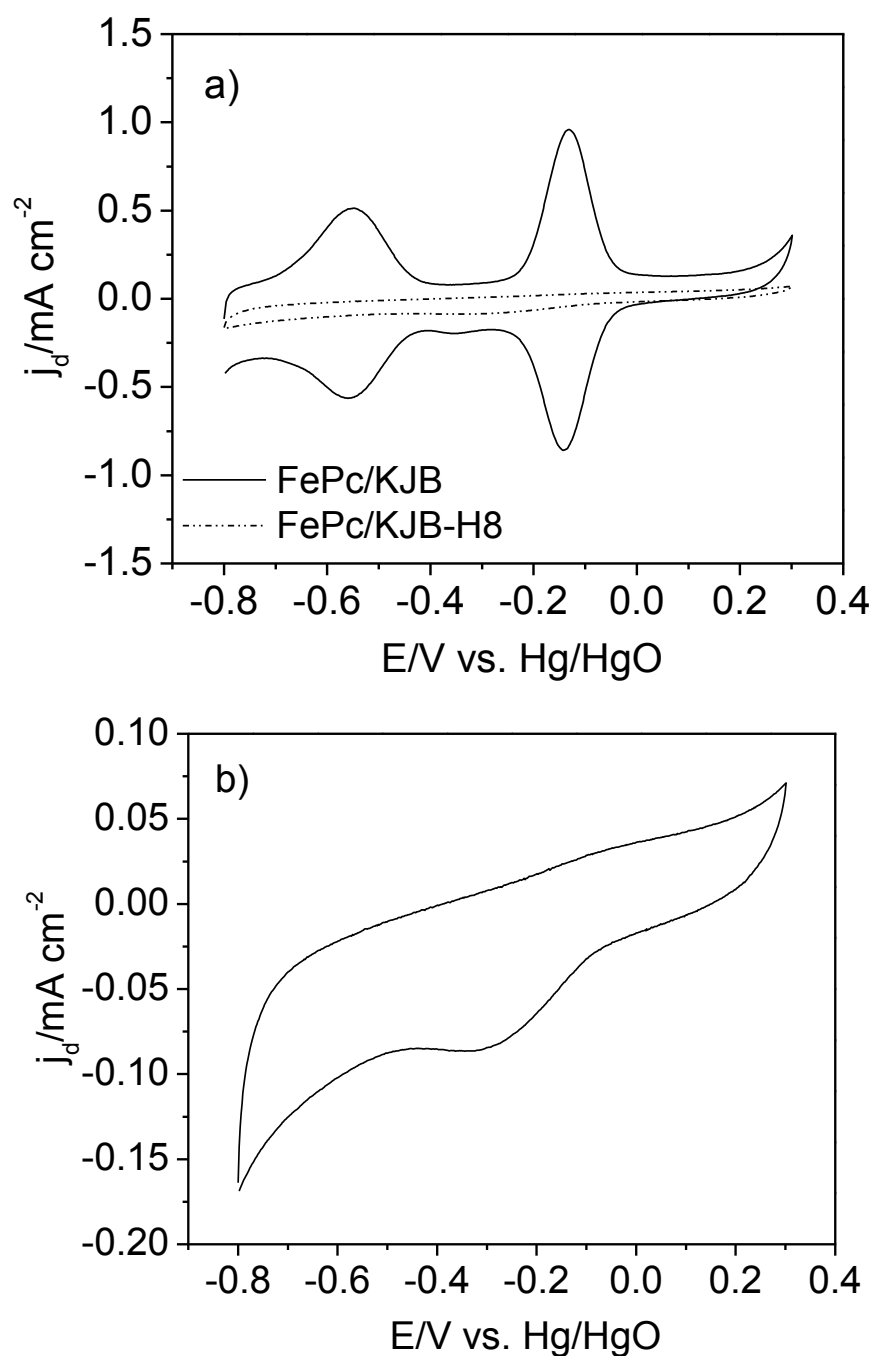
Figure 7-7 Cyclic voltammograms of a) FePc/KJB and FePc/KJB-H8, b) FePc/KJB-H8 in N$_2$ saturated 1.0 M KOH at 25°C, scan rate 25 mV s^{-1}

Figure 7-8a shows LSVs of Pt/C, FePc/KJB-H8 and KJB carbon in O_2 saturated 1.0 M KOH solution at a rotation rate of 2500 rpm. The onset potential of FePc/KJB-H8 was lower (0.027 V) than the commercial Pt/C [93]. At a fixed disk current density (2 mA cm^{-2}), the potential of FePc/KJB-H8 was shifted 0.05 V more negative than Pt/C in the mixed kinetic and diffusion controlled region. The performance of FePc/KJB-H8 was inferior to that of commercial Pt/C and FePc/KJB as prepared. Compared to KJB carbon, the FePc/KJB-H8 showed a significant higher activity for ORR. The lower activity of FePc/KJB-H8 may contributed by the lower activity of inorganic Fe metal compared to FePc ligand and mass loss of FePc [161].

Figure 7-8b and c shows data for hydrogen peroxide production for KJB, Pt/C and FePc/KJB-H8 in O_2 saturated 1.0 M KOH and at 25 ^{o}C. It can be observed from Fig 7-8b, the highest ring current of 93 μA produced from KJB indicating larger amount of H_2O_2 produced from O_2 reduction. It is well-known that the ORR proceeds mainly two-electron transfer reaction on carbon. Overall, FePc/KJB-H8 produced the lowest amount of H_2O_2 which indicates that the ORR on FePc/KJB-H8 was mainly a four-electron transfer reaction. Compared to the disk current, the fractional H_2O_2 yield of FePc (in Figure 6-9c) was less than 10 % which was similar to Pt/C (10.3 %) at low potential (-0.6 V).
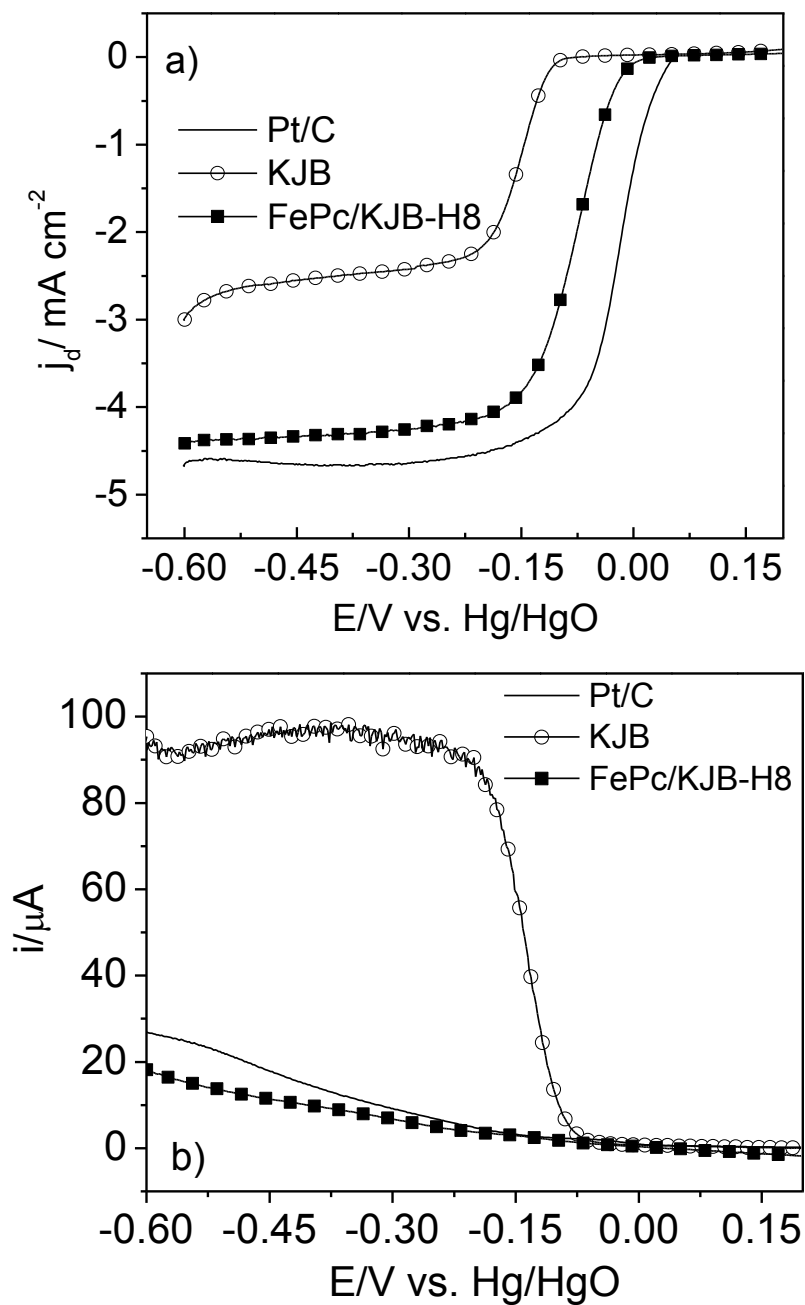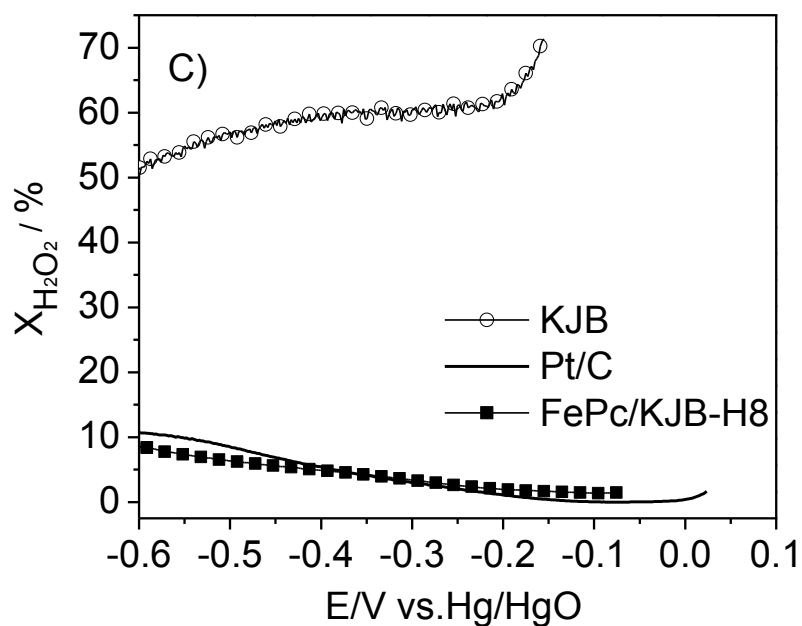
Figure 7-8 Polarization curves of KJB, Pt/C and FePc/KJB a) disk current, b) ring current, c) percentage of ring current

Kinetic current densities (j_k) were calculated using equation 5 in Chapter 3 from the data in Figure 7-8a and used to produce Tafel plots (Figure 7-9). Two Tafel slopes at regions of low and high overpotential were observed for Pt/C, which was close to values of 0.05 Vdec^{-1} and 0.12 Vdec^{-1}, respectively. The same Tafel slope values were reported by other researchers, derived from steady state polarization curves of Pt/C in O_2 saturated 1.0 M NaOH solution at 25 $^{\circ}$C [147, 162]. For the FePc/KJB-H8 catalyst, values of Tafel slope were 0.062 V dec^{-1} at high potential and 0.118 V dec^{-1} at low potential. The data suggests that the same rate-determining reaction of ORR on both catalysts.
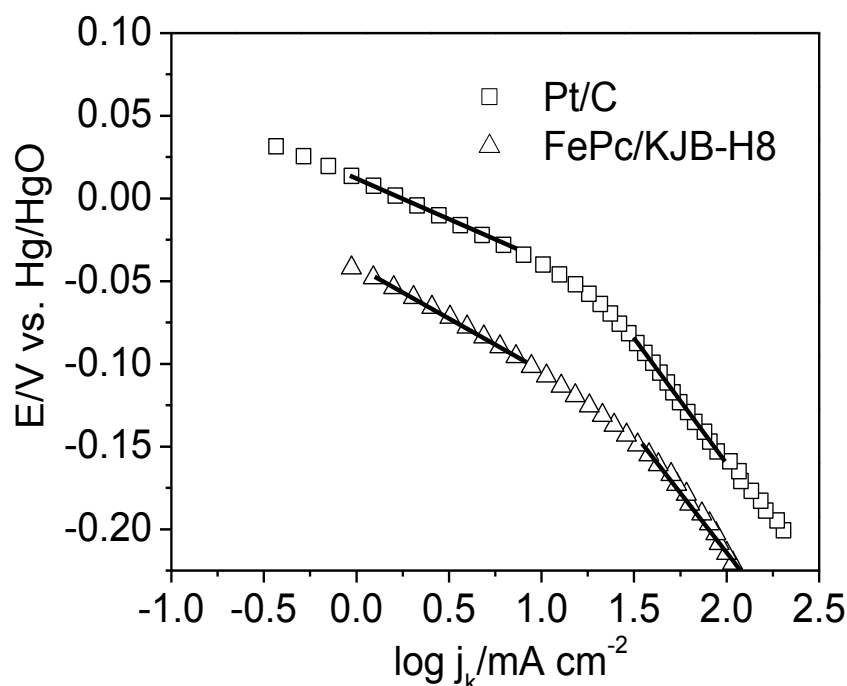
Figure 7-9 Tafel plots of Pt/C and FePc/KJB-H8, $\log j_k$ was calculated from data in Figure 3a.

Figure 7-10 shows fuel cell performance using a radiation-grafted AAEM. The anode for both MEAs was the same (0.33 mg cm^{-2} Pt). The noble metal catalyst (Pt/C) showed better performance than the non-noble metal catalyst (FePc/KJB-H8) throughout the polarization curve. The cell open circuit potential (OCP) of Pt/C and FePc/KJB-H8 were 1.0 and 0.9 V, respectively. The lower OCP of the MEA using FePc/KJB-H8 at cathode showed an agreement on previous half-cell data. In the kinetic region (0.7 V), the current density of Pt/C is 11.3 mA cm^{-2} which was approximately one order magnitude higher than FePc/KJB-H8 (1.69 mA cm^{-2}). The sharper decrease with FePc/KJB-H8 than with Pt/C was expected from the ORR half-cell data and confirmed the lower catalytic activity towards ORR in the AAEMFC. The peak power densities obtained from fuel cells using Pt/C and FePc cathode catalysts with solid state AAEM were 13.5 and 9.2 mWcm^{-2}, respectively. Recently, Piana et al. demonstrated a commercial non-noble metal catalyst (Acta, 4020) which produced around half the power density (200 mW cm^{-2}) compared to Pt/C eletrodes (around 400 mW cm^{-2}) [27]. Furthermore, taking into account the much thicker catalyst layer of FePc/KJB-H8 than Pt/C due to the low metal loading of FePc/KJB-H8 (3.8 wt %), the actual performance of FePc/KJB-H8 in AAEMFC could be significantly improved after optimising the

structure of the catalyst layer. Note that in this work the catalyst layer contained no ionomer or ion conductor and thus the relatively low fuel cell performance (peak power of around 9 mW cm^{-2} for the FePc/KJB) was a result primarily of the activity of catalysts adjacent the membrane. Varcoe et al addressed the ionomer in the catalyst layer as a critical factor in fuel cell performance [47, 61, 163].
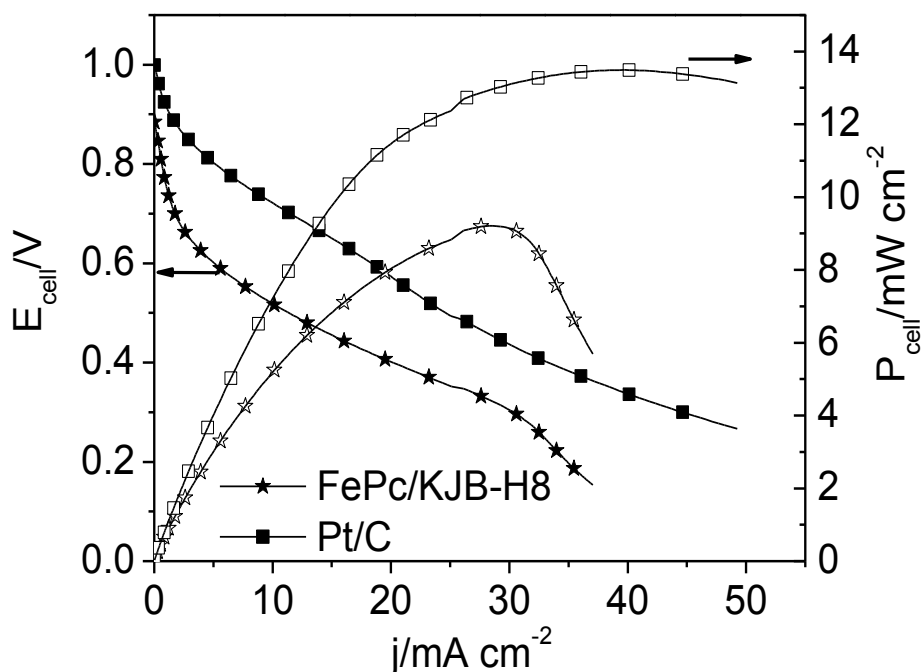
Figure 7-10 Fuel cell performance using hydrogen and pure oxygen, 0.33 mg cm^{-2} Pt/C catalyst loading for anode, FePc/KJB-H8 0.6 mg cm^{-2} catalyst loading for cathode, at 20 $^{\circ}$C, 100 % RH and no back-pressure

The MEA's stability with FePc/KJB-H8 was investigated using a potentiostatic measurement at a cell potential of 0.7 V (as shown in Fig 7-11) for 48 h. There was some initial fall in fuel cell performance during the first 20 hours of the test after which the performance stabilised for the duration. There are several possible reasons for the initial decline in fuel cell activity. These include a gradual flooding of anode electrode due to water accumulation from the humidifier and the reaction itself, after which the fuel cell system established a new equilibrium condition. This behaviour may be improved upon by modifying the catalyst layer by introducing a new binder, e.g. PTFE to repel excessive water from the system.
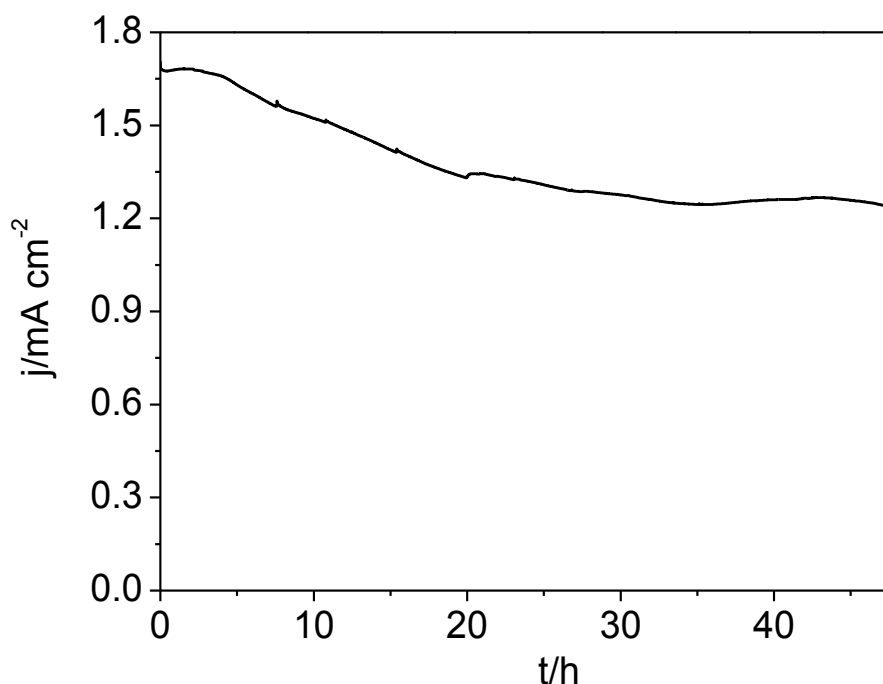
Figure 7-11 Stability measurement of MEA with 0.33 mg cm^{-2} Pt/C anode and 0.6 mgcm^{-2} FePc/KJB-H8 cathode for 48 hours, maintained at a cell potential of 0.7 V, 20 $^{\circ}$C, 100 % RH and no back-pressure

7.2 Conclusions

Metal macrocycles based catalysts were examined for AAEMFC application. FePc/KJB was found more active catalyst among the other metal macrocycles (CoPc, CoTMPP). The stability study in half cell suggests that the FePc/KJB catalyst is reasonable for a cathode catalyst. However, the latter discovery of instability in single cell test using a radiation-grafted membrane was firstly reported by us [148].

The FePc/KJB was heat-treated under N$_2$ atmosphere and 800 $^{\circ}$C. The electrochemical behaviour for ORR was characterised in half cell and single cell tests. The n number of FePc/KJB-H8 was calculated to be 3.90 for ORR at -400 mV (vs. Hg/HgO). In the AAEMFC test, the peak power densities obtained were 13.5 and 9.2 mW cm^{-2} for Pt/C and FePc/KJB-H8, respectively. There was some initial performance loss of the fuel cell with the FePc catalysts which stabilised during the stability test of FePc/KJB-H8 for 48 hours. Future work will focus on development of ionomer and optimising the structure

of catalyst layer to improve the performance of AAEMFC with a non-noble metal catalyst cathode.

CHAPTER 8. DIRECT METHANOL CARBONATE FUEL CELLS

USING ANION EXCHANGE MATERIALS AND NON-NOBLE

METAL CATHODE CATALYST

8.1 Results and discussion

Figure 8-1 shows hydroxide and carbonate conductivities of radiation-grafted LDPE at various temperatures. The ionic conductivity of membrane in both forms increased as temperature increased. At 53 ^{o}C and 100 % RH, the hydroxide conductivity of membrane (0.036 S cm^{-1}) was 42 % higher than that of carbonate form membrane. The expected lower conductivity of carbonate ions than that of hydroxide ions is well agreed with the literature report [144]. Ionic conductivity values radiation-grafted poly (ethylene-co-tetrafluoroethylene) in hydroxide and carbonate forms reported by Varcoe et al were 0.034 and 0.022 S cm^{-1} at 50 ^{o}C [144]. In Figure 8-1b, Arrhenius plot of anion conducting membrane in hydroxide and carbonate form was obtained using the same equation in Chapter 5 below:

$$E_a = -R \times T \times ln\sigma + lnA \qquad (1)$$

where R is the gas constant equals 8.314 J K^{-1} mol^{-1}, T is the thermal dynamic temperature (K)

The obtained activation energy E_a of ion transport from the slope of the liner regression of lnσ versus 1000/T (E_a in kJ mol^{-1}) was 13.3 kJ mol^{-1} for hydroxide and 15.4 kJ mol^{-1} for carbonate ions. The reported activation energy values of hydroxide and carbonate transport in a radiation-grafted poly (ethylene-co-tetrafluoroethylene) anion exchange membrane were similar (12.6±0.6 kJ mol^{-1} and 16.1±0.4 kJ mol^{-1}, respectively)

115

[144]. The results suggest a potential application for direct alcohol fuel cells using carbonate form of anion exchange membrane.
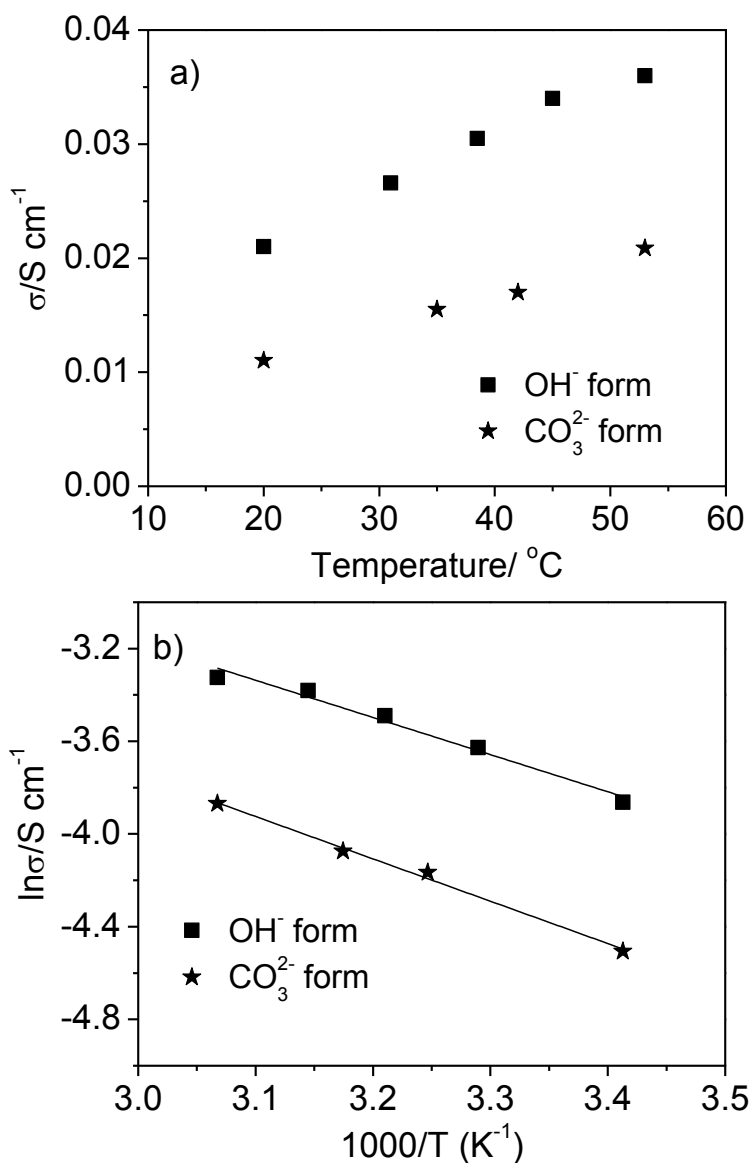
Figure 8-1 a) Ionic conductivity measurements of radiation-grafted LDPE in the form of hydroxide and carbonate at various temperatures and 100 % RH, b) Arrhenius plot of membrane conductivities

Figure 8-2a compares the fuel cell performance using Pt/C and Acta 4020 catalyst at the cathode. The OCV of MEA using Acta 4020 at the cathode (0.54 V) was much higher than the MEA using Pt/C cathode (0.41 V). This was due to the high tolerance of methanol of the non-noble metal catalyst (Acta 4020). The resulting poor fuel cell performance on power density (0.5 mW cm^{-2}) and OCV using Pt/C was attributed to the

methanol crossover through the thin membrane (50 μm) from the anode causing a mixed potential on the cathode. In Figure 8-2b, the polarization curves of Acta 4020 based MEA was obtained at temperatures up to 60 ^{o}C. The OCVs of the fuel cell at 30, 50 and 60 ^{o}C were 0.50, 0.54 and 0.56 V, respectively. The increasing OCV with higher temperature indicates the enhanced activity of catalysts at higher temperatures. A higher power density of 3.0 mW cm^{-2} using non-noble metal catalyst Acta 4020 than Pt/C was achieved at 60 ^{o}C. It is significantly higher than the previous literature report (i.e. 8 μW cm^{-2}) [14]. The improvement in this work is mainly due to several factors including the application of novel materials, i.e. (1) methanol tolerant and more selective to ORR cathode catalyst Acta 4020, which was also low cost compared to Pt; (2) thinner anion exchange membranes, 50 instead of 150 μm, which largely improve the ionic conductivity. The other important factor was the use of CO_3^{2-} in the anode as the reactant for methanol oxidation [14]. The dehydration of the membrane and the MEA was eliminated by supplying humidified gas on the cathode side.

With K_2CO_3 circulating at the anode, it gradually reacts with CO_2 and produces $KHCO_3$. This will lead to the decrease on ionic conductivity and pH which will affect the catalytic activity for both anode and cathode reactions. $KHCO_3$ is unstable at elevated temperatures and decompose to CO_2 and K_2CO_3, therefore it is desirable to operate fuel cell at temperatures higher than 60 ^{o}C. However, the OCVs of fuel cell at the temperature range of 70 to 80 ^{o}C decreased from 0.53 V to 0.48 V which is a contrary of the OCV behaviour at temperatures below 60 ^{o}C (as shown in Figure 8-2c). At a fixed cell potential (0.3 V), the current densities at 70 ^{o}C, 80 ^{o}C-run1 and 80 ^{o}C-run2 were 10.65, 11.45 and 7.62 mA cm^{-2}, respectively. At the temperatures above 60 ^{o}C, the fuel cell performance at 80 ^{o}C was lower than the performance at 70 ^{o}C. This may be contributed by the QDPSU ionomer degradation in high pH environment at this temperature range and the resulting lower utilization of catalyst lead to OCV and current density drop. The performance loss also may be associated with membrane degradation as the performance for 80 ^{o}C run2 exhibited a shaper decline in the ohmic dominate region. The degradation in DMCFC is similar to the operating temperature

limitation of AAEMFCs which is below 60 $^{\circ}$C to minimize the S$_N$2 attack on the
quaternary ammonium functional group [3].
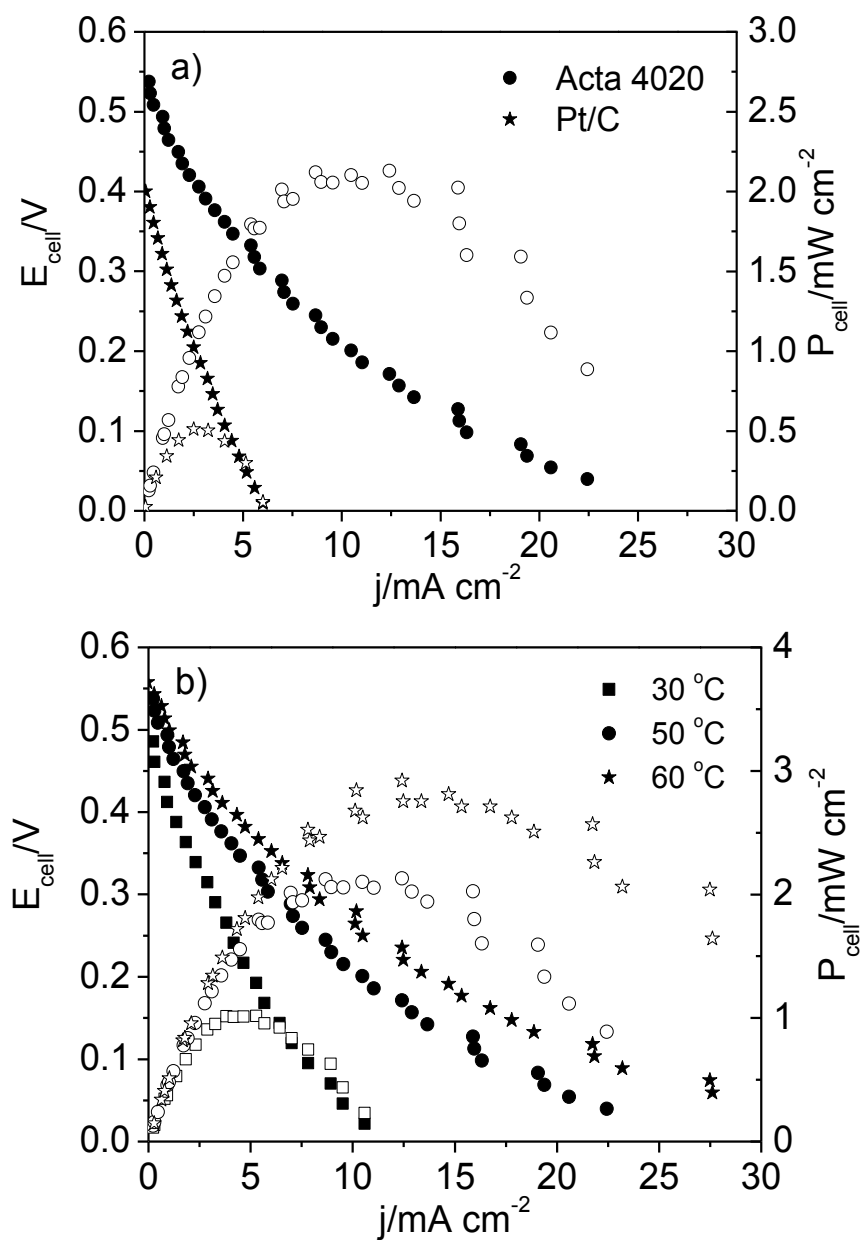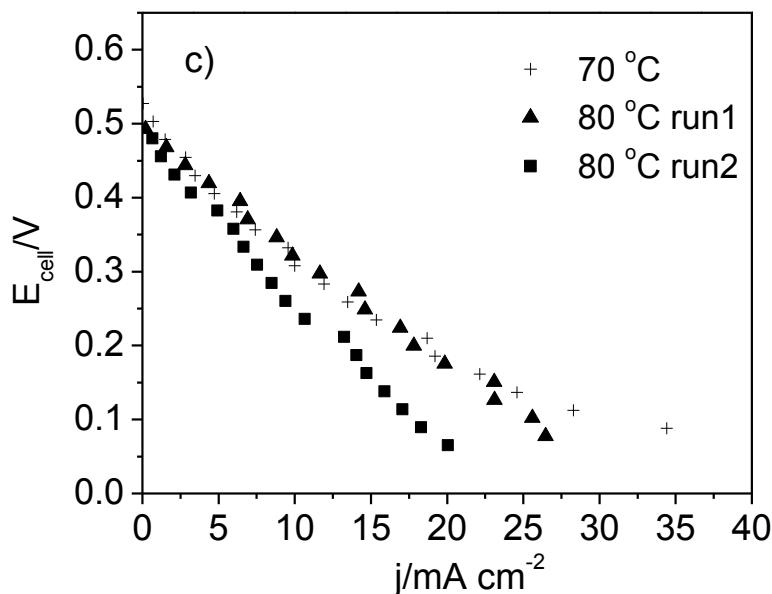
Figure 8-2 Polarization curves of the low temperature carbonate fuel cell, membrane thickness 50 μm (fully hydrated), 2.0 M Methanol and K_2CO_3 at the anode, CO_2 and O_2 at the cathode were 40 and 20 mL min^{-1}, respectively. a) comparison of Pt/C cathode and Acta 4020 cathode, same anode Pt/C (40 wt %) 1.0 mg$_{Pt}$ cm^{-2}, b) Anode Pt/C (40 wt %) 1.0 mg$_{Pt}$ cm^{-2}, cathode Acta 4020 1.0 mg cm^{-2} catalyst loading, at different temperatures c) cell performance at temperature higher than 60 °C, the cell performance named after 80 °C run2 was recorded after 10 min of 80 °C run1

The fuel cell test on hydrogen was conducted to investigate the anode limitation on cell performance compared to the methanol oxidation reaction (as shown in Figure 8-3). The power density of fuel cell with hydrogen (8.8 mW cm^{-2}) was eight times higher than methanol at the anode (1.0 mW cm^{-2}) at a cell temperature of 30 °C. The data suggests a much slower kinetic of methanol oxidation than hydrogen using Pt/C as anode in low temperature carbonate fuel cell. The fuel cell performance using hydrogen and pure oxygen is much lower than the performance in alkaline media from my pervious publication which is as much as 60 mW cm^{-2} under the same operating condition. The significant low performance maybe not only associated to the lower ionic conductivity of membrane in carbonate form but also the lower ORR activity of Acta 4020 catalyst.
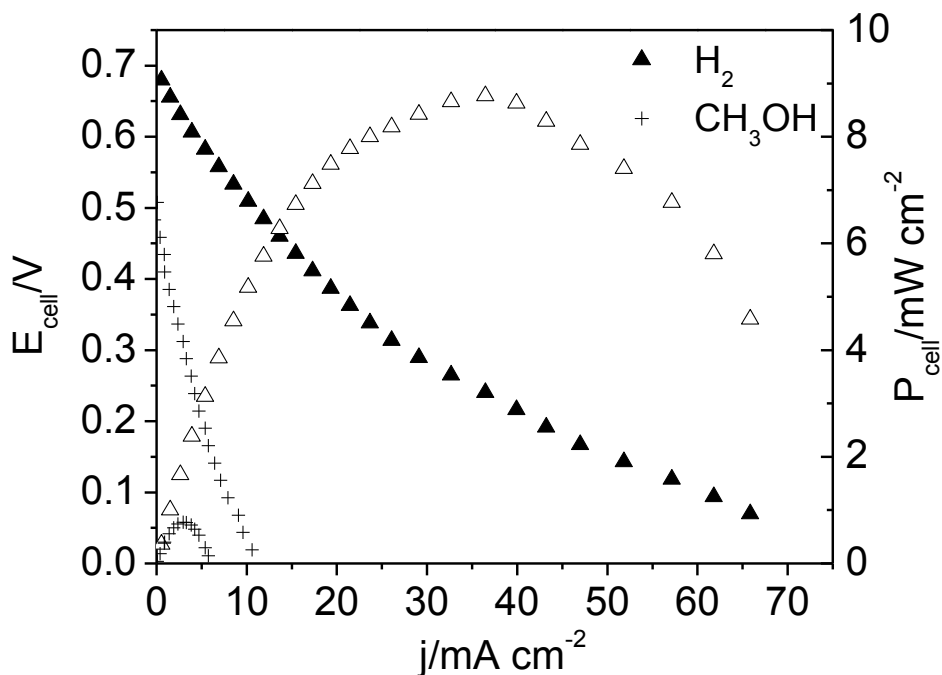
Figure 8-3 Fuel cell test using hydrogen and methanol at the anode and gas mixture as the cathode was kept the same, at 30 $^{\circ}$C 2.0 M Methanol and K_2CO_3 at the anode, CO_2 and O_2 at the cathode were 40 and 20 mL min^{-1}, respectively Anode Pt/C (40 wt %) 1.0 mg$_{Pt}$ cm^{-2}, cathode Acta 4020 1.0 mg cm^{-2} catalyst loading

Figure 8-4a shows the effect of ionomer content in the catalyst layer on the fuel cell performance. Compared to the MEAs using 1 mg cm^{-2} metal loading Pt/C for the anode and 1 mg cm^{-2} catalyst loading Acta 4020 for the cathode, the OCV was significantly increased using higher loading of catalysts for both anode (2 mg cm^{-2} metal loading Pt/C) and cathode (3 mg cm^{-2} catalyst loading Acta 4020). The power density of fuel cell using 15 wt % ionomer reached 4.0 mW cm^{-2} more than one order magnitude higher than the MEA without ionomer (0.2 mW cm^{-2}). In a hydrogen and oxygen fuelled AAEMFC, it was found that there was a substantial increase in the peak power density at 50 $^{\circ}$C (from 1.6 to 55 mW cm^{-2}) on simply adding the interface polymer [163]. With increasing ionomer loading (0 to 15 wt %) in the catalyst layer, the fuel cell performance improved due to the better ultilization of catalyst. However, when ionomer loading was higher than 22 wt %, it was found that electrodes de-attached from the membrane after cold-pressed due to the thin film were formed on the electrode surface. This will cause high ohmic resistance in the MEA. For Nafion based PEMFC systems, this can be solved by hot-pressing at glassy transition temperature (130 $^{\circ}$C).

Figure 8-4b shows the data for the direct methanol carbonate fuel cell operated using different concentrations (up to 6.0 M) of methanol in 2.0 M K_2CO_3. OCVs of fuel cell were the same using different concentration of methanol because of the high methanol tolerance of the Acta 4020 catalyst at the cathode. The MEA performance was slightly better using higher concentration of methanol. A highest power density of 4.5 mW cm^{-2} was achieved using 6.0 M methanol and 2.0 M K_2CO_3 at 50 $^{\circ}$C. It is still much lower than DAAFCs (49 mW cm^{-2} at 60 $^{\circ}$C) [88]. This is mainly attributed to the low mobility of carbonate ion and the limitation of anode catalyst.
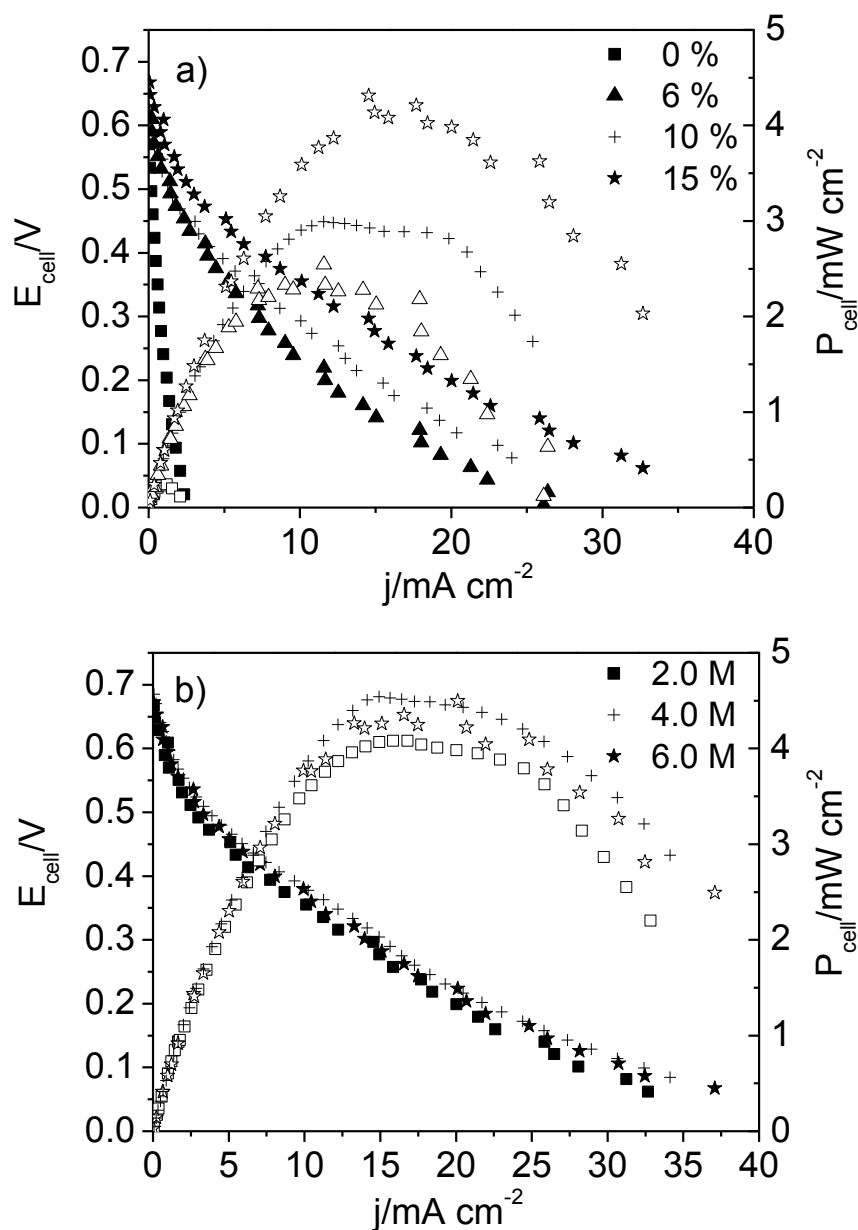
Figure 8-4 Fuel cell polarization curves of a) 0 %, 6 %, 10 %, 15 % ionomer in catalyst layer, anode 2 mg cm^{-2} metal loading Pt/C, cathode 3 mg cm^{-2} catalyst loading Acta 4020, 2.0 M

Methanol and K_2CO_3 at anode , atmospheric pressure, 50 ^{o}C, b) different fuel concentrations (2.0, 4.0 and 6.0 M methanol and 2.0 M K_2CO_3) circulating at anode side, 15 % ionomer for both electrodes, anode 2 mg cm^{-2} metal loading, cathode   Acta 4020 3 mg cm^{-2} catalyst loading, at 50 ^{o}C and atmospheric pressure

The stability test of DMCFC was conducted using potentiostatic method at a cell potential of 0.4 V for 13 h as shown in Figure 8-6. The degradation rate of cell performance was around 2.52 μA cm^{-2} min^{-1}. The formation of KHCO$_3$ might be mainly contributed to the performance loss due to the low operating temperature (50 ^{o}C). Additionally, Scott et al also reported that the cell potential fell from 250 to 195mV at a fixed current density after 15 h due to the fuel consumption at the anode [164]. For a new fuel cell system, the preliminary durability study showed a reasonable performance.
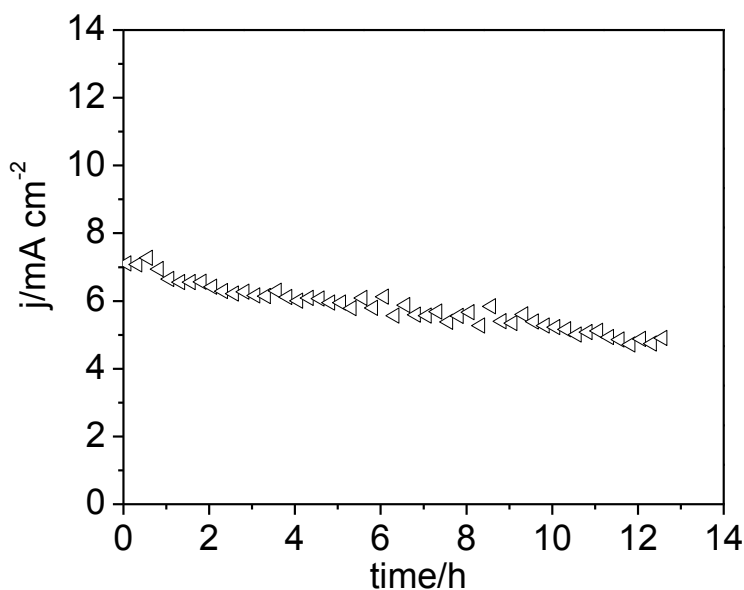
Figure 8-5 Stability test of MEA at 0.4 V, anode 2 mg cm^{-2} metal loading Pt/C, cathode 3 mg cm^{-2} catalyst loading Acta 4020, 15 wt % ionomer, 6.0 M Methanol and 2.0 M K_2CO_3 at 50 ^{o}C for 13 h

8.2 Conclusions

The direct methanol carbonate fuel cell using anion exchange materials and non-noble catalyst was demonstrated. The MEA performance using non-noble catalyst Acta 4020 and was superior to Pt/C electrodes. Compared to non-ionomer MEA, the MEA with a

starting ionomer loading of 6 wt % gave a power density (around 2.1 mW cm^{-2}) which is one order magnitude higher. A maximum power density of 4.5 mW cm^{-2} was achieved at 50 ^{o}C using 6.0 M methanol and 2.0 M K$_2$CO$_3$. For the stability study, the MEA exhibited a degradation rate of 2.52 μA cm^{-2} min^{-1}. For the future work, in order to improve the fuel cell performance and stability, it is desirable to use highly thermally and chemically stable membrane (e.g. Tokuyama A201) and ionomer especially at temperatures above 60 ^{o}C.

CHAPTER 9. CONCLUSIONS AND PERSPECTIVES

9.1 Conclusions

Proton exchange membrane fuel cells (PEMFCs) are currently based on high cost materials such as Nafion® membrane and Pt based catalysts. The high cost and limited abundance of noble metal hinder the commercialization of fuel cell. For the future hydrogen economy, alkaline anion exchange membrane fuel cell offers advantages of the utilization of non-Pt group metal catalysts, low-cost membranes (e.g. polysulfone based) and bipolar plate (e.g. stainless steel). In a direct alcohol fuel cell, the revered osmsis drag of anion exchange membrane fuel cells eases the fuel-cross over effect and usage of highly selective catalysts towards ORR further improves the performance. This thesis explored the possibility of using low-cost materials in fuel cells.

QDPSUwas synthesised with different DS and characterized using different techniques. The higher degree of DS showed the better ionic conductivity. A thin PTFE-QDPSU composite membrane was prepared by using pre-treated PTFE impregnated with QDPSU polymer. Compared to pristine QDPSU membrane, the composite membrane exhibited better mechanical strength (32 MPa, maximum strength), less swelling and lower water uptake. The ionic conductivity of the composite membrane was 0.051 S cm^{-1} at 55 °C and 100 % RH. The membrane showed superior conductivity than the literature reported [22]. In fuel cell tests, power densities of 146 mW cm^{-2} and 103 mW cm^{-2} were achieved using oxygen and air, respectively. Severe degradation was found during preliminary experimental investigation on KOH loaded PBI membrane including an ammonia smell came out the bottle and anode methanol solution turned yellow brown color in fuel cell test which make PBI unsuitable candidate for alkaline anion exchange membrane fuel cells (AAEMFCs).

The phosphoric acid loaded polysulfone was used for an intermediate temperature fuel

cell. It was found that the higher DS, the higher membrane conductivity. When the DS reached 180 %, the QDPSU polymer cannot form a film with a suitable mechanical strength for fuel cell applications. The derived Tafel slope for the MEA using phosphoric acid loaded polysulfone fuel cell was the same as reported in the literature. Preliminary fuel cell test exhibited a promising power density. A high power density of 400 mW cm^{-2} was achieved using DS106 of PA/QDPSU membrane at 150 ^{o}C and atmospheric pressure.

Pd supported on various pre-treated carbons showed different mass activity for ORR in alkaline media. All Pd/C catalysts showed better performance than the commercial Pt/C. All catalysts promote a four-electron transfer reaction. It was found that 5 % HNO_3 and 10 % H_2O_2 treatments destroyed the pore structure on Vulcan XC-72R carbon support which lead to a sever Pd agglomeration. The resulting activity of both catalysts was worse than un-treated Pd/C in terms of mass activity and production of hydrogen peroxide. Pd/C-0.2 M KOH gave the best performance in term of the ORR activity and hydrogen peroxide production.

Several metal macrocycles based catalysts were prepared by impregnation method. FePc was the most active catalyst among others (CoPc, CoTMPP and the commcerical K-14 catalyst). Un-treated FePc/C was instable for the AAEMFC test due to the interaction with ionomer and membrane materials. A heat-treatment under N_2 gas at 800 ^{o}C successfully stabilized the catalyst with a certain compromise on the ORR activity. The electron transfer number (n) of FePc and FePc/KJB-H8 of ORR was four which is the same to Pt/C. In AAEMFC tests, the peak power densities were 13.5 and 9.2 mW cm^{-2} for Pt/C and FePc/KJB-H8, respectively. Further fuel cell stability test confirmed that the FePc/KJB-H8 was stable for a 48 h potentiostatic measurement using hydrogen and pure oxygen.

Performance of the direct methanol carbonate fuel cell using a radiation-grafted anion exchange membrane, ionomer and commercial non-noble metal catalyst (Acta 4020)

was studied. The MEA using Acta 4020 gave a better OCV and power density than Pt based MEA. The ionomer loading of 15 wt % in the catalyst layer exhibited the best performance. A maximum power density of 4.5 mW cm^{-2} was achieved at 50 ^{o}C using 6.0 M methanol and 2.0 M K$_2$CO$_3$. The operating temperature of the DMCFC limited below 60 ^{o}C. The stability of such fuel cell system was reasonable for 13 h.

9.2 Perspectives

The development of anion exchange membrane fuel cells (AEMFCs) is still in infancy compared to PEMFCs. Recommendations on future development of anion exchange membrane fuel cells can be briefly addressed as below:

1. High thermal and chemical stability of anion conducting materials especially at temperatures higher than 60 ^{o}C. Operating fuel cells at higher temperature offers faster kinetics for both anode and cathode reactions and better membrane conductivity which improve significantly on the fuel cell performance. For example, self-humidification developed for the Nafion membrane can be considered to apply to AEMs [165].

2. A detailed study on anode oxidation reaction in hydrogen and oxygen fuelled AAEMFC needs to be carried out in order to understand the rate-determination step on fuel cell performances. This will help to optimise the electrodes and MEA design for AEMFCs.

3. Engineering property: good solubility of anion ionomers and electrode processing of AEMs [26]. In order to minimize the resistance between electrodes and polymer membranes. For instance, a catalyst ink with certain ionomer loading can be sprayed onto the membrane directly which is so-called catalyst coated membrane (CCM).

4. Developing low cost non-Pt catalysts for the anode oxidation of direct oxidation fuel cells (e.g. alcohols). Current catalysts are not effective to oxidise alcohols to release more electrons which will improve the fuel cell performance. Novel catalysts such as ternary Pd alloy are promising for the anode oxidation in direct oxidation alkaline fuel cells [26].

In addition, developing a mathematic model on the water transport inside membrane, investigating new applications for anion exchange membrane (e.g. electrolyser, metal-air batteries) are also recommended for future works.

REFERENCES

1.   Gülzow, E., *Alkaline fuel cells: a critical view.* Journal of Power Sources, 1996. **61**(1–2): p. 99-104.

2.   Blomen, L.J.M.J. and M.N. Mugerwa, *Fuel Cell Systems*1993, New York: Plenum Press. 42.

3.   Varcoe, J.R. and R.C.T. Slade, *Prospects for alkaline anion-exchange membranes in low temperature fuel cells.* Fuel Cells, 2005. **5**(2): p. 187-200.

4.   Adzic, R.R., M.L. Avramovivic, and A.V. Tripkovic, *Structural Effects in Electrocatalysis - Oxidation of Formaldehyde on Gold and Platinum Single-Crystal Electrodes in Alkaline-Solution.* Electrochimica Acta, 1984. **29**(10): p. 1353-1357.

5.   Taraszewska, J. and G. Roslonek, *Electrocatalytic oxidation of methanol on a glassy carbon electrode modified by nickel hydroxide formed by ex situ chemical precipitation.* Journal of Electroanalytical Chemistry, 1994. **364**(1-2): p. 209-213.

6.   Chen, Y.G., L. Zhuang, and J.T. Lu, *Non-Pt anode catalysts for alkaline direct alcohol fuel cells.* Chinese Journal of Catalysis, 2007. **28**: p. 870-874.

7.   Miyazaki, K., N. Sugimura, K. Matsuoka, Y. Iriyama, T. Abe, M. Matsuoka, and Z. Ogumi, *Perovskite-type oxides La1-xSrxMnO3 for cathode catalysts in direct ethylene glycol alkaline fuel cells.* Journal of Power Sources, 2008. **178**(2): p. 683-686.

8.   Yu, E.H. and K. Scott, *Direct methanol alkaline fuel cell with catalysed metal mesh anodes.* Electrochemistry Communications, 2004. **6**(4): p. 361-365.

9.   Avram, E., M.A. Brebu, A. Warshawsky, and C. Vasile, *Polymers with pendent functional groups. V. Thermooxidative and thermal behavior of chloromethylated polysulfones.* Polymer Degradation and Stability, 2000. **69**(2): p. 175-181.

10.   Bauer, B., H. Strathmann, and F. Effenberger, *Anion-exchange membranes with improved alkaline stability.* Desalination, 1990. **79**(2-3): p. 125-144.

11.   Hou, H., G. Sun, R. He, B. Sun, W. Jin, H. Liu, and Q. Xin, *Alkali doped polybenzimidazole membrane for alkaline direct methanol fuel cell.* International Journal of Hydrogen Energy, 2008.

12.   Hou, H., G. Sun, R. He, Z. Wu, and B. Sun, *Alkali doped polybenzimidazole membrane for high performance alkaline direct ethanol fuel cell.* Journal of Power Sources, 2008. **182**(1): p. 95-99.

13.   Xing, B. and O. Savadogo, *Hydrogen/oxygen polymer electrolyte membrane fuel cells (PEMFCs) based on alkaline-doped polybenzimidazole (PBI).* Electrochemistry Communications, 2000. **2**(10): p. 697-702.

14.   Lang, C.M., K. Kim, and P.A. Kohl, *High-Energy Density, Room-Temperature Carbonate Fuel Cell.* Electrochemical and Solid-State Letters, 2006. **9**(12): p. A545-A548.

15.   (EIA), E.I.A. *International Energy Annual 2003*. 2003; Available from: http://www.eia.doe.gov/iea/.

16.   Barbir, F., *PEM Fuel Cells: Theory and Practice*, ed. R.C. Dorf2005: Elsevier.

17.   Li, Z.P., B.H. Liu, K. Arai, and S. Suda, *Development of the direct borohydride fuel cell.* Journal of Alloys and Compounds, 2005. **404-406**(0): p. 648-652.

18.   *Handbook of Fuel Cells - Fundamentals Technology and Applications*, ed. Wolf Vielstich, Arnold Lamm, and H.A. Gasteiger. Vol. 1. 2003: John Wiley & Sons Ltd,.

19.   Quanxing, Z., *Introduction of Electrode Kinetics*. 3rd ed2002: Science Beijing.

20.   Antolini, E. and E.R. Gonzalez, *Alkaline direct alcohol fuel cells.* Journal of Power Sources, 2010. **195**(11): p. 3431-3450.

21.   Lu, S., J. Pan, A. Huang, L. Zhuang, and J. Lu, *Alkaline polymer electrolyte fuel cells completely free from noble metal catalysts.* Proceedings of the National Academy of Sciences of the United States of America, 2008. **105**(52): p. 20611-20614.

22.   Pan, J., S. Lu, Y. Li, A. Huang, L. Zhuang, and J. Lu, *High-Performance alkaline polymer electrolyte for fuel cell applications.* Advanced Functional Materials, 2010. **20**(2): p. 312-319.

23.   Wang, X., M. Li, B.T. Golding, M. Sadeghi, Y. Cao, E.H. Yu, and K. Scott, *A polytetrafluoroethylene-quaternary 1,4-diazabicyclo-[2.2.2]-octane polysulfone composite membrane for alkaline anion exchange membrane fuel cells.* International Journal of Hydrogen Energy, 2011. **36**(16): p. 10022-10026.

24.   Gong, K., F. Du, Z. Xia, M. Durstock, and L. Dai, *Nitrogen-doped carbon nanotube arrays with high electrocatalytic activity for oxygen reduction.* Science, 2009. **323**(5915): p. 760-764.

25.   An, L. and T.S. Zhao, *An alkaline direct ethanol fuel cell with a cation exchange membrane.* Energy & Environmental Science, 2011. **4**(6): p. 2213-2217.

26.   Yu, E.H., X. Wang, U. Krewer, L. Li, and K. Scott, *Direct oxidation alkaline fuel cells: from materials to systems.* Energy & Environmental Science, 2012.

27.   Piana, M., M. Boccia, A. Filpi, E. Flammia, H.A. Miller, M. Orsini, F. Salusti, S. Santiccioli, F. Ciardelli, and A. Pucci, *H2/air alkaline membrane fuel cell performance and durability, using novel ionomer and non-platinum group metal cathode catalyst.* Journal of Power Sources, 2010.

28.   Li, Q., R. He, J.O. Jensen, and N.J. Bjerrum, *PBI-Based Polymer Membranes for High Temperature Fuel Cells – Preparation, Characterization and Fuel Cell Demonstration.* Fuel Cells, 2004. **4**(3): p. 147-159.

29.   Zecevic, S.K., J.S. Wainright, M.H. Litt, S.L. Gojkovic, and R.F. Savinell, *Kinetics of O2 reduction on a Pt electrode covered with a thin film of solid polymer electrolyte.* Journal of the Electrochemical Society, 1997. **144**(9): p. 2973-2982.

30.   Wang, J.T., R.F. Savinell, J. Wainright, M. Litt, and H. Yu, *A H2O2 fuel cell using acid doped polybenzimidazole as polymer electrolyte.* Electrochimica Acta, 1996. **41**(2): p. 193-197.

31.   Bezerra, C.W.B., L. Zhang, K. Lee, H. Liu, J. Zhang, Z. Shi, A.L.B. Marques, E.P. Marques, S. Wu, and J. Zhang, *Novel carbon-supported Fe-N electrocatalysts synthesized through heat treatment of iron tripyridyl triazine complexes for the PEM fuel cell oxygen reduction reaction.* Electrochimica Acta, 2008. **53**(26): p. 7703-7710.

32.   Oh, S.-Y., T. Yoshida, G. Kawamura, H. Muto, M. Sakai, and A. Matsuda, *Inorganic-organic composite electrolytes consisting of polybenzimidazole and Cs-substituted heteropoly acids and their application for medium temperature fuel cells.* Journal of Materials Chemistry, 2010. **20**(30): p. 6359-6366.

33.   Lobato, J., P. CaÃ±izares, M.A. Rodrigo, D. Ãšbeda, and F.J. Pinar, *A novel titanium PBI-based composite membrane for high temperature PEMFCs.* Journal of Membrane Science, 2010. **369**(1â€"2): p. 105-111.

34.   Zaidi, S.M.J., S.D. Mikhailenko, G.P. Robertson, M.D. Guiver, and S. Kaliaguine, *Proton conducting composite membranes from polyether ether ketone and heteropolyacids for fuel cell applications.* Journal of Membrane Science, 2000. **173**(1): p. 17-34.

35.   Xing, D. and J. Kerres, *Improvement of synthesis procedure and characterization of sulfonated poly(arylene ether sulfone) for proton exchange membranes.* Journal of New Materials for Electrochemical Systems, 2006. **9**(1): p. 51-60.

36.   Xing, D., G. He, Z. Hou, P. Ming, and S. Song, *Preparation and characterization of a modified montmorillonite/sulfonated polyphenylether sulfone/PTFE composite membrane.* International Journal of Hydrogen Energy, 2010. **36**(3): p. 2177-2183.

37.   Li, M., H. Zhang, and Z.-G. Shao, *Quaternized Poly(phthalazinone ether sulfone ketone) Membrane Doped with H[sub 3]PO[sub 4] for High-Temperature PEMFC Operation.* Electrochemical and Solid-State Letters, 2006. **9**(2): p. A60-A63.

38.   Li, M., K. Scott, and X. Wu, *A poly(R1R2R3)â€"N+/H3PO4 composite membrane for phosphoric acid polymer electrolyte membrane fuel cells.* Journal of Power Sources, 2009. **194**(2): p. 811-814.

39.   Li, M. and K. Scott, *A polytetrafluoroethylene/quaternized polysulfone membrane for high temperature polymer electrolyte membrane fuel cells.* Journal of Power Sources, 2010. **196**(4): p. 1894-1898.

40.   Scott, K., W.M. Taama, and P. Argyropoulos, *Performance of the direct*

methanol fuel cell with radiation-grafted polymer membranes. Journal of Membrane Science, 2000. **171**(1): p. 119-130.

41.   Yu, E.H. and K. Scott, *Development of direct methanol alkaline fuel cells using anion exchange membranes.* Journal of Power Sources, 2004. **137**(2): p. 248-256.

42.   Yu, E.H. and K. Scott, *Direct methanol alkaline fuel cells with catalysed anion exchange membrane electrodes.* Journal of Applied Electrochemistry, 2005. **35**(1): p. 91-96.

43.   Yu, E., K. Scott, and R. Reeve, *Application of sodium conducting membranes in direct methanol alkaline fuel cells.* Journal of Applied Electrochemistry, 2006. **36**(1): p. 25-32.

44.   Shen, M., S. Roy, J.W. Kuhlmann, K. Scott, K. Lovell, and J.A. Horsfall, *Grafted polymer electrolyte membrane for direct methanol fuel cells.* Journal of Membrane Science, 2005. **251**(1-2): p. 121-130.

45.   Danks, T.N., R.C.T. Slade, and J.R. Varcoe, *Comparison of PVDF- and FEP-based radiation-grafted alkaline anion-exchange membranes for use in low temperature portable DMFCs.* Journal of Materials Chemistry, 2002. **12**(12): p. 3371-3373.

46.   Danks, T.N., R.C.T. Slade, and J.R. Varcoe, *Alkaline anion-exchange radiation-grafted membranes for possible electrochemical application in fuel cells.* Journal of Materials Chemistry, 2003. **13**(4): p. 712-721.

47.   Varcoe, J.R. and R.C.T. Slade, *An electron-beam-grafted ETFE alkaline anion-exchange membrane in metal-cation-free solid-state alkaline fuel cells.* Electrochemistry Communications, 2006. **8**(5): p. 839-843.

48.   Poynton, S.D., J.P. Kizewski, R.C.T. Slade, and J.R. Varcoe, *Novel electrolyte membranes and non-Pt catalysts for low temperature fuel cells.* Solid State Ionics, 2010. **181**(3-4): p. 219-222.

49.   Zhang, J., L. Zhang, C.W.B. Bezerra, H. Li, Z. Xia, J. Zhang, A.L.B. Marques, and E.P. Marques, *EIS-assisted performance analysis of non-noble metal electrocatalyst (Fe-N/C)-based PEM fuel cells in the temperature range of*

23-80°C. Electrochimica Acta, 2009. **54**(6): p. 1737-1743.

50.   Wu, L., T. Xu, D. Wu, and X. Zheng, *Preparation and characterization of CPPO/BPPO blend membranes for potential application in alkaline direct methanol fuel cell.* Journal of Membrane Science, 2008. **310**(1-2): p. 577-585.

51.   Wu, L. and T. Xu, *Improving anion exchange membranes for DMAFCs by inter-crosslinking CPPO/BPPO blends.* Journal of Membrane Science, 2008. **322**(2): p. 286-292.

52.   Wu, Y., C. Wu, T. Xu, F. Yu, and Y. Fu, *Novel anion-exchange organic-inorganic hybrid membranes: Preparation and characterizations for potential use in fuel cells.* Journal of Membrane Science, 2008. **321**(2): p. 299-308.

53.   Wu, Y., C. Wu, J.R. Varcoe, S.D. Poynton, T. Xu, and Y. Fu, *Novel silica/poly(2,6-dimethyl-1,4-phenylene oxide) hybrid anion-exchange membranes for alkaline fuel cells: Effect of silica content and the single cell performance.* Journal of Power Sources, 2010. **195**(10): p. 3069-3076.

54.   Li, L. and Y. Wang, *Quaternized polyethersulfone Cardo anion exchange membranes for direct methanol alkaline fuel cells.* Journal of Membrane Science, 2005. **262**(1-2): p. 1-4.

55.   Fang, J. and P.K. Shen, *Quaternized poly(phthalazinon ether sulfone ketone) membrane for anion exchange membrane fuel cells.* Journal of Membrane Science, 2006. **285**(1-2): p. 317-322.

56.   Wang, G., Y. Weng, D. Chu, R. Chen, and D. Xie, *Developing a polysulfone-based alkaline anion exchange membrane for improved ionic conductivity.* Journal of Membrane Science, 2009. **332**(1-2): p. 63-68.

57.   Yan, J. and M.A. Hickner, *Anion exchange membranes by bromination of benzylmethyl-containing poly(sulfone)s.* Macromolecules, 2010. **43**(5): p. 2349-2356.

58.   Hwang, G.-J. and H. Ohya, *Preparation of anion-exchange membrane based on block copolymers: Part 1. Amination of the chloromethylated copolymers.* Journal of Membrane Science, 1998. **140**(2): p. 195-203.

59.   Park, J.-S., S.-H. Park, S.-D. Yim, Y.-G. Yoon, W.-Y. Lee, and C.-S. Kim,

Performance of solid alkaline fuel cells employing anion-exchange membranes. Journal of Power Sources, 2008. **178**(2): p. 620-626.

60. Hickner, M.A., G.J. Tudryn, T.M. Alam, M.R. Hibbs, and C.H. Fujimoto, *Polymers with tethered anionic and cationic groups as membranes for fuel cells.* Macromolecular Symposia, 2009. **279**(1): p. 59-62.

61. Gu, S., R. Cai, T. Luo, Z. Chen, M. Sun, Y. Liu, G. He, and Y. Yan, *A soluble and highly conductive ionomer for high-performance hydroxide exchange membrane fuel cells.* Angewandte Chemie - International Edition, 2009. **48**(35): p. 6499-6502.

62. Guo, M., J. Fang, H. Xu, W. Li, X. Lu, C. Lan, and K. Li, *Synthesis and characterization of novel anion exchange membranes based on imidazolium-type ionic liquid for alkaline fuel cells.* Journal of Membrane Science, 2010. **362**(1-2): p. 97-104.

63. Luo, Y., J. Guo, C. Wang, and D. Chu, *Quaternized poly(methyl methacrylate-co-butyl acrylate-co-vinylbenzyl chloride) membrane for alkaline fuel cells.* Journal of Power Sources, 2010. **195**(12): p. 3765-3771.

64. Piana, M., M. Boccia, A. Filpi, E. Flammia, H.A. Miller, M. Orsini, F. Salusti, S. Santiccioli, F. Ciardelli, and A. Pucci, *H2/air alkaline membrane fuel cell performance and durability, using novel ionomer and non-platinum group metal cathode catalyst.* Journal of Power Sources, 2010. **195**(18): p. 5875-5881.

65. Robertson, N.J., H.A. Kostalik, T.J. Clark, P.F. Mutolo, H.c.D. Abrunìƒa, and G.W. Coates, *Tunable High Performance Cross-Linked Alkaline Anion Exchange Membranes for Fuel Cell Applications.* Journal of the American Chemical Society, 2009. **132**(10): p. 3400-3404.

66. Elabd, Y.A. and M.A. Hickner, *Block Copolymers for Fuel Cells.* Macromolecules, 2011. **44**(1): p. 1-11.

67. Merle, G., M. Wessling, and K. Nijmeijer, *Anion exchange membranes for alkaline fuel cells: A review.* Journal of Membrane Science, 2011. **377**(1-2): p. 1-35.

68. Liu, F., B. Yi, D. Xing, J. Yu, and H. Zhang, *Nafion/PTFE composite membranes*

for fuel cell applications. Journal of Membrane Science, 2003. **212**(1-2): p. 213-223.

69. Li, M. and K. Scott, *A polymer electrolyte membrane for high temperature fuel cells to fit vehicle applications.* Electrochimica Acta, 2010. **55**(6): p. 2123-2128.

70. Li, M. and K. Scott, *A polytetrafluoroethylene/quaternized polysulfone membrane for high temperature polymer electrolyte membrane fuel cells.* Journal of Power Sources, 2010.

71. Zhang, F., H. Zhang, J. Ren, and C. Qu, *PTFE based composite anion exchange membranes: thermally induced in situ polymerization and direct hydrazine hydrate fuel cell application.* Journal of Materials Chemistry, 2010. **20**(37): p. 8139-8146.

72. Matsuoka, K., Y. Iriyama, T. Abe, M. Matsuoka, and Z. Ogumi, *Alkaline direct alcohol fuel cells using an anion exchange membrane.* Journal of Power Sources, 2005. **150**(1-2): p. 27-31.

73. Li, Y.S., T.S. Zhao, and Z.X. Liang, *Performance of alkaline electrolyte-membrane-based direct ethanol fuel cells.* Journal of Power Sources, 2009. **187**(2): p. 387-GIF.

74. Yamada, K., K. Yasuda, N. Fujiwara, Z. Siroma, H. Tanaka, Y. Miyazaki, and T. Kobayashi, *Potential application of anion-exchange membrane for hydrazine fuel cell electrolyte.* Electrochemistry Communications, 2003. **5**(10): p. 892-896.

75. Asazawa, K., K. Yamada, H. Tanaka, A. Oka, M. Taniguchi, and T. Kobayashi, *A Platinum-Free Zero-Carbon-Emission Easy Fuelling Direct Hydrazine Fuel Cell for Vehicles.* Angewandte Chemie International Edition, 2007. **46**(42): p. 8024-8027.

76. Agel, E., J. Bouet, and J.F. Fauvarque, *Characterization and use of anionic membranes for alkaline fuel cells.* Journal of Power Sources, 2001. **101**(2): p. 267-274.

77. Stoica, D., L. Ogier, L. Akrour, F. Alloin, and J.F. Fauvarque, *Anionic membrane based on polyepichlorhydrin matrix for alkaline fuel cell: Synthesis, physical and electrochemical properties.* Electrochimica Acta, 2007. **53**(4): p. 1596-1603.

78. Sollogoub, C., A. Guinault, C. Bonnebat, M. Bennjima, L. Akrour, J.F. Fauvarque, and L. Ogier, *Formation and characterization of crosslinked membranes for alkaline fuel cells.* Journal of Membrane Science, 2009. **335**(1-2): p. 37-42.

79. Yang, C.C., Y.J. Lee, S.J. Chiu, K.T. Lee, W.C. Chien, C.T. Lin, and C.A. Huang, *Preparation of a PVA/HAP composite polymer membrane for a direct ethanol fuel cell (DEFC).* Journal of Applied Electrochemistry, 2008. **38**(10): p. 1329-1337.

80. Xiong, Y., J. Fang, Q.H. Zeng, and Q.L. Liu, *Preparation and characterization of cross-linked quaternized poly(vinyl alcohol) membranes for anion exchange membrane fuel cells.* Journal of Membrane Science, 2008. **311**(1-2): p. 319-325.

81. Chempath, S., B.R. Einsla, L.R. Pratt, C.S. Macomber, J.M. Boncella, J.A. Rau, and B.S. Pivovar, *Mechanism of Tetraalkylammonium Headgroup Degradation in Alkaline Fuel Cell Membranes.* The Journal of Physical Chemistry C, 2008. **112**(9): p. 3179-3182.

82. MacOmber, C.S., J.M. Boncella, B.S. Pivovar, and J.A. Rau, *Decomposition pathways of an alkaline fuel cell membrane material component via evolved gas analysis.* Journal of Thermal Analysis and Calorimetry, 2008. **93**(1): p. 225-229.

83. Yeager, E., *Electrocatalysts for O2 reduction.* Electrochimica Acta, 1984. **29**(11): p. 1527-1537.

84. Bard, A.J. and L.R. Faulnker, *Electrochemical methods: Fundamentals and Applications*. 2nd ed2001: John Wiley & Sons, Inc.

85. Damjanovic, A. and V. Brusic, *Electrode kinetics of oxygen reduction on oxide-free platinum electrodes.* Electrochimica Acta, 1967. **12**(6): p. 615-628.

86. Damjanovic, A., M.A. Genshaw, and J.O.M. Bockris, *The Mechanism of Oxygen Reduction at Platinum in Alkaline Solutions with Special Reference to H[sub 2]O[sub 2].* Journal of the Electrochemical Society, 1967. **114**(11): p. 1107-1112.

87. Bianchini, C. and P.K. Shen, *ChemInform Abstract: Palladium-Based Electrocatalysts for Alcohol Oxidation in Half Cells and in Direct Alcohol Fuel*

Cells. ChemInform, 2010. **41**(3): p. no-no.

88.   Shen, S., T.S. Zhao, J. Xu, and Y. Li, *High performance of a carbon supported ternary PdIrNi catalyst for ethanol electro-oxidation in anion-exchange membrane direct ethanol fuel cells.* Energy & Environmental Science, 2011. **4**(4): p. 1428-1433.

89.   Antolini, E., *Catalysts for direct ethanol fuel cells.* Journal of Power Sources, 2007. **170**(1): p. 1-12.

90.   Suo, Y., L. Zhuang, and J. Lu, *First-principles considerations in the design of Pd-alloy catalysts for oxygen reduction.* Angewandte Chemie - International Edition, 2007. **46**(16): p. 2862-2864.

91.   Shao, M.H., K. Sasaki, and R.R. Adzic, *Pd-Fe nanoparticles as electrocatalysts for oxygen reduction.* Journal of the American Chemical Society, 2006. **128**(11): p. 3526-3527.

92.   Jiang, L., A. Hsu, D. Chu, and R. Chen, *Oxygen reduction reaction on carbon supported Pt and Pd in alkaline solutions.* Journal of the Electrochemical Society, 2009. **156**(3).

93.   Jiang, L., A. Hsu, D. Chu, and R. Chen, *Oxygen reduction on carbon supported Pt and PtRu catalysts in alkaline solutions.* Journal of Electroanalytical Chemistry, 2009. **629**(1-2): p. 87-93.

94.   Jiang, L., A. Hsu, D. Chu, and R. Chen, *Size-dependent activity of palladium nanoparticles for oxygen electroreduction in alkaline solutions.* Journal of the Electrochemical Society, 2009. **156**(5): p. B643-B649.

95.   Lima, F.H.B., J. Zhang, M.H. Shao, K. Sasaki, M.B. Vukmirovic, E.A. Ticianelli, and R.R. Adzic, *Catalytic activity - d-band center correlation for the O2 reduction reaction on platinum in alkaline solutions.* Journal of Physical Chemistry C, 2007. **111**(1): p. 404-410.

96.   Enyo, M., T. Yamazaki, K. Kai, and K. Suzuki, *Amorphous Pdî—¸Zr alloys for water electrolysis cathode materials.* Electrochimica Acta, 1983. **28**(11): p. 1573-1579.

97.   Senthil Kumar, S.M., J. Soler Herrero, S. Irusta, and K. Scott, *The effect of*

pretreatment of Vulcan XC-72R carbon on morphology and electrochemical oxygen reduction kinetics of supported Pd nano-particle in acidic electrolyte. Journal of Electroanalytical Chemistry, 2010. **647**(2): p. 211-221.

98. Figueiredo, J.L., M.F.R. Pereira, M.M.A. Freitas, and J.J.M. Ã"rfÃ£o, *Modification of the surface chemistry of activated carbons.* Carbon, 1999. **37**(9): p. 1379-1389.

99. Lefevre, M., E. Proietti, F. Jaouen, and J.P. Dodelet, *Iron-Based catalysts with improved oxygen reduction activity in polymer electrolyte fuel cells.* Science, 2009. **324**(5923): p. 71-74.

100. Chang, Y.M., P.W. Wu, C.Y. Wu, and Y.C. Hsieh, *Synthesis of La0.6Ca0.4Co0.8Ir0.2O3 perovskite for bi-functional catalysis in an alkaline electrolyte.* Journal of Power Sources, 2009. **189**(2): p. 1003-1007.

101. Ananth, M.V., V.V. Giridhar, and K. Renuga, *Linear sweep voltametry studies on oxygen reduction of some oxides in alkaline electrolytes.* International Journal of Hydrogen Energy, 2009. **34**(2): p. 658-664.

102. Lima, F.H.B., M.L. Calegaro, and E.A. Ticianelli, *Investigations of the catalytic properties of manganese oxides for the oxygen reduction reaction in alkaline media.* Journal of Electroanalytical Chemistry, 2006. **590**(2): p. 152-160.

103. Li, N., X. Yan, Y. Jin, S. Li, and B. Lin, *Spinel-type oxides LiMn2-xMxO4 [M=Co, Fe, (CoFe)] as electrocatalyst for oxygen evolution/reduction in alkaline solution.* Journal of Applied Electrochemistry, 1999. **29**(11): p. 1351-1354.

104. Xie, X.Y., Z.F. Ma, X.X. Ma, Q. Ren, V.M. Schmidt, and L. Huang, *Preparation and electrochemical characteristics of MnOx-CoTMPP/BP composite catalyst for oxygen reduction reaction in alkaline solution.* Journal of The Electrochemical Society, 2007. **154**(8): p. B733-B738.

105. Sugawara, M., M. Ohno, and K. Matsuki, *Oxygen reduction catalysis of Mn-Co spinel oxides on a graphite electrode in alkaline solution.* Journal of Materials Chemistry, 1997. **7**(5): p. 833-836.

106. Jiang, L., A. Hsu, D. Chu, and R. Chen, *A highly active Pd coated Ag*

electrocatalyst for oxygen reduction reactions in alkaline media. Electrochimica Acta, 2010. **55**(15): p. 4506-4511.

107. Erikson, H., G. Jürmann, A. Sarapuu, R.J. Potter, and K. Tammeveski, *Electroreduction of oxygen on carbon-supported gold catalysts.* Electrochimica Acta, 2009. **54**(28): p. 7483-7489.

108. Guo, J., A. Hsu, D. Chu, and R. Chen, *Improving oxygen reduction reaction activities on carbon-supported Ag nanoparticles in alkaline solutions.* Journal of Physical Chemistry C. **114**(10): p. 4324-4330.

109. Bashyam, R. and P. Zelenay, *A class of non-precious metal composite catalysts for fuel cells.* Nature, 2006. **443**(7107): p. 63-66.

110. Jasinski, R., *A new fuel cell cathode catalyst [13].* Nature, 1964. **201**(4925): p. 1212-1213.

111. Gojkovic, S.L., S. Gupta, and R.F. Savinell, *Heat-treated iron(III) tetramethoxyphenyl porphyrin supported on high-area carbon as an electrocatalyst for oxygen: I. Characterization of the electrocatalyst.* Journal of the Electrochemical Society, 1998. **145**(10): p. 3493-3499.

112. Gojkovic, S.L., S. Gupta, and R.F. Savinell, *Heat-treated iron(III) tetramethoxyphenyl porphyrin chloride supported on high-area carbon as an electrocatalyst for oxygen reduction: Part II. Kinetics of oxygen reduction.* Journal of Electroanalytical Chemistry, 1999. **462**(1): p. 63-72.

113. Collman, J.P., P. Denisevich, Y. Konai, M. Marrocco, C. Koval, and F.C. Anson, *Electrode catalysis of the four-electron reduction of oxygen to water by dicobalt face-to-face porphyrins.* Journal of the American Chemical Society, 1980. **102**(19): p. 6027-6036.

114. Van den Brink, F., W. Visscher, and E. Barendrecht, *Electrocatalysis of cathodic oxygen reduction by metal phthalocyanines. Part IV. Iron phthalocyanine as electrocatalyst: Mechanism.* Journal of Electroanalytical Chemistry, 1984. **175**(1-2): p. 279-289.

115. Kobayashi, R. and J.I. Ozaki, *Novel N-doped carbon cathode catalyst for polymer electrolyte membrane fuel cells formed on carbon black.* Chemistry

Letters, 2009. **38**(5): p. 396-397.

116. Gong, K., Y. Yan, M. Zhang, L. Su, S. Xiong, and L. Mao, *Electrochemistry and electroanalytical applications of carbon nanotubes: A review.* Analytical Sciences, 2005. **21**(12): p. 1383-1393.

117. Ozaki, J.i., N. Kimura, T. Anahara, and A. Oya, *Preparation and oxygen reduction activity of BN-doped carbons.* Carbon, 2007. **45**(9): p. 1847-1853.

118. Ozaki, J.I., S.I. Tanifuji, N. Kimura, A. Furuichi, and A. Oya, *Enhancement of oxygen reduction activity by carbonization of furan resin in the presence of phthalocyanines.* Carbon, 2006. **44**(7): p. 1324-1326.

119. Ozaki, J.i., T. Anahara, N. Kimura, and A. Oya, *Simultaneous doping of boron and nitrogen into a carbon to enhance its oxygen reduction activity in proton exchange membrane fuel cells.* Carbon, 2006. **44**(15): p. 3358-3361.

120. Meng, H., F. Jaouen, E. Proietti, M. Lefèvre, and J.-P. Dodelet, *pH-effect on oxygen reduction activity of Fe-based electro-catalysts.* Electrochemistry Communications, 2009. **11**(10): p. 1986-1989.

121. HaoYu, E., S. Cheng, K. Scott, and B. Logan, *Microbial fuel cell performance with non-Pt cathode catalysts.* Journal of Power Sources, 2007. **171**(2): p. 275-281.

122. Zhao, F., F. Harnisch, U. Schröder, F. Scholz, P. Bogdanoff, and I. Herrmann, *Application of pyrolysed iron(II) phthalocyanine and CoTMPP based oxygen reduction catalysts as cathode materials in microbial fuel cells.* Electrochemistry Communications, 2005. **7**(12): p. 1405-1410.

123. Cheng, H. and K. Scott, *Investigation of non-platinum cathode catalysts for direct borohydride fuel cells.* Journal of Electroanalytical Chemistry, 2006. **596**(2): p. 117-123.

124. Bezerra, C.W.B., L. Zhang, K. Lee, H. Liu, A.L.B. Marques, E.P. Marques, H. Wang, and J. Zhang, *A review of Fe-N/C and Co-N/C catalysts for the oxygen reduction reaction.* Electrochimica Acta, 2008. **53**(15): p. 4937-4951.

125. Baranton, S., C. Coutanceau, C. Roux, F. Hahn, and J.M. Léger, *Oxygen reduction reaction in acid medium at iron phthalocyanine dispersed on high*

surface area carbon substrate: tolerance to methanol, stability and kinetics. Journal of Electroanalytical Chemistry, 2005. **577**(2): p. 223-234.

126. Behret, H., H. Binder, G. Sandstede, and G.G. Scherer, *On the mechanism of electrocatalytic oxygen reduction at metal chelates: Part III. Metal phthalocyanines.* Journal of Electroanalytical Chemistry, 1981. **117**(1): p. 29-42.

127. Zagal, J., M. PÃ¡ez, A.A. Tanaka, J.R. dos Santos Jr, and C.A. Linkous, *Electrocatalytic activity of metal phthalocyanines for oxygen reduction.* Journal of Electroanalytical Chemistry, 1992. **339**(1-2): p. 13-30.

128. Lalande, G., G. Faubert, R. Côté, D. Guay, J.P. Dodelet, L.T. Weng, and P. Bertrand, *Catalytic activity and stability of heat-treated iron phthalocyanines for the electroreduction of oxygen in polymer electrolyte fuel cells.* Journal of Power Sources, 1996. **61**(1-2): p. 227-237.

129. Lalande, G., R. Côté, G. Tamizhmani, D. Guay, J.P. Dodelet, L. Dignard-Bailey, L.T. Weng, and P. Bertrand, *Physical, chemical and electrochemical characterization of heat-treated tetracarboxylic cobalt phthalocyanine adsorbed on carbon black as electrocatalyst for oxygen reduction in polymer electrolyte fuel cells.* Electrochimica Acta, 1995. **40**(16): p. 2635-2646.

130. Lalande, G., R. CÃ´tÃ©, D. Guay, J.P. Dodelet, L.T. Weng, and P. Bertrand, *Is nitrogen important in the formulation of Fe-based catalysts for oxygen reduction in solid polymer fuel cells?* Electrochimica Acta, 1997. **42**(9): p. 1379-1388.

131. Jaouen, F., M. LefeÌ€vre, J.P. Dodelet, and M. Cai, *Heat-treated Fe/N/C catalysts for O2 electroreduction: Are active sites hosted in micropores?* Journal of Physical Chemistry B, 2006. **110**(11): p. 5553-5558.

132. Yuasa, M., A. Yamaguchi, H. Itsuki, K. Tanaka, M. Yamamoto, and K. Oyaizu, *Modifying Carbon Particles with Polypyrrole for Adsorption of Cobalt Ions as Electrocatatytic Site for Oxygen Reduction.* Chemistry of Materials, 2005. **17**(17): p. 4278-4281.

133. Nagaiah, T.C., S. Kundu, M. Bron, M. Muhler, and W. Schuhmann, *Nitrogen-doped carbon nanotubes as a cathode catalyst for the oxygen reduction reaction in alkaline medium.* Electrochemistry Communications, 2010. **12**(3): p.

338-341.

134. Shen, P.K., C. Xu, R. Zeng, and Y. Liu, *Electro-oxidation of Methanol on NiO-Promoted Pt/C and Pd/C Catalysts.* Electrochemical and Solid-State Letters, 2006. **9**(2): p. A39-A42.

135. Hu, F., C. Chen, Z. Wang, G. Wei, and P.K. Shen, *Mechanistic study of ethanol oxidation on Pd-NiO/C electrocatalyst.* Electrochimica Acta, 2006. **52**(3): p. 1087-1091.

136. Hu, F., F. Ding, S. Song, and P.K. Shen, *Pd electrocatalyst supported on carbonized TiO2 nanotube for ethanol oxidation.* Journal of Power Sources, 2006. **163**(1 SPEC. ISS.): p. 415-419.

137. Shen, P.K. and C. Xu, *Alcohol oxidation on nanocrystalline oxide Pd/C promoted electrocatalysts.* Electrochemistry Communications, 2006. **8**(1): p. 184-188.

138. Xu, C., P.k. Shen, and Y. Liu, *Ethanol electrooxidation on Pt/C and Pd/C catalysts promoted with oxide.* Journal of Power Sources, 2007. **164**(2): p. 527-531.

139. Zheng, H.T., Y. Li, S. Chen, and P.K. Shen, *Effect of support on the activity of Pd electrocatalyst for ethanol oxidation.* Journal of Power Sources, 2006. **163**(1 SPEC. ISS.): p. 371-375.

140. Shen, S.Y., T.S. Zhao, J.B. Xu, and Y.S. Li, *Synthesis of PdNi catalysts for the oxidation of ethanol in alkaline direct ethanol fuel cells.* Journal of Power Sources, 2010. **195**(4): p. 1001-1006.

141. Hu, F.P. and P.K. Shen, *Ethanol oxidation on hexagonal tungsten carbide single nanocrystal-supported Pd electrocatalyst.* Journal of Power Sources, 2007. **173**(2 SPEC. ISS.): p. 877-881.

142. Zeng, R., S.D. Poynton, J.P. Kizewski, R.C.T. Slade, and J.R. Varcoe, *A novel reference electrode for application in alkaline polymer electrolyte membrane fuel cells.* Electrochemistry Communications, 2010. **12**(6): p. 823-825.

143. Sheng, W., H.A. Gasteiger, and Y. Shao-Horn, *Hydrogen Oxidation and Evolution Reaction Kinetics on Platinum: Acid vs Alkaline Electrolytes.* Journal

of the Electrochemical Society, 2010. **157**(11): p. B1529-B1536.

144. Varcoe, J.R., R.C.T. Slade, E. LamHowYee, S.D. Poynton, D.J. Driscoll, and D.C. Apperley, *Poly(ethylene-co-tetrafluoroethylene)-Derived Radiation-Grafted Anion-Exchange Membrane with Properties Specifically Tailored for Application in Metal-Cation-Free Alkaline Polymer Electrolyte Fuel Cells.* Chem. Mater., 2007. **19**(10): p. 2686-2693.

145. Sawyer, D.T. and J. Julian L. Roberts, *Experimental Electrochemistry for Chemists*1974: John Wiley & Sons, Inc.

146. Avram, E., E. Butuc, C. Luca, and I. Druta, *Polymers with pendant functional group. III. Polysulfones containing viologen group.* Journal of Macromolecular Science - Pure and Applied Chemistry, 1997. **34**(9): p. 1701-1714.

147. Chen, R., H. Li, D. Chu, and G. Wang, *Unraveling oxygen reduction reaction mechanisms on carbon-supported fe-phthalocyanine and co-phthalocyanine catalysts in alkaline solutions.* Journal of Physical Chemistry C, 2009. **113**(48): p. 20689-20697.

148. Mamlouk, M., X. Wang, K. Scott, J.A. Horsfall, and C. Williams, *Characterization and application of anion exchange polymer membranes with non-platinum group metals for fuel cells.* Proceedings of the Institution of Mechanical Engineers, Part A: Journal of Power and Energy, 2011. **225**(2): p. 152-160.

149. *N4-Macrocyclic Metal Complexes*, ed. J.H. Zagal, F. Bedioui, and J.P. Dodelet2006.

150. Sousa, T., M. Mamlouk, and K. Scott, *A dynamic non-isothermal model of a laboratory intermediate temperature fuel cell using PBI doped phosphoric acid membranes.* International Journal of Hydrogen Energy, 2010. **35**(21): p. 12065-12080.

151. Tanaka, M., M. Koike, K. Miyatake, and M. Watanabe, *Synthesis and properties of anion conductive ionomers containing fluorenyl groups for alkaline fuel cell applications.* Polymer Chemistry, 2011. **2**(1): p. 99-106.

152. Tanaka, M., K. Fukasawa, E. Nishino, S. Yamaguchi, K. Yamada, H. Tanaka, B.

Bae, K. Miyatake, and M. Watanabe, *Anion Conductive Block Poly(arylene ether)s: Synthesis, Properties, and Application in Alkaline Fuel Cells.* Journal of the American Chemical Society, 2011. **133**(27): p. 10646-10654.

153.   Karlsson, L.E. and P. Jannasch, *Polysulfone ionomers for proton-conducting fuel cell membranes: 2. Sulfophenylated polysulfones and polyphenylsulfones.* Electrochimica Acta, 2005. **50**(9): p. 1939-1946.

154.   Pandey, A.K., A. Goswami, D. Sen, S. Mazumder, and R.F. Childs, *Formation and characterization of highly crosslinked anion-exchange membranes.* Journal of Membrane Science, 2003. **217**(1-2): p. 117-130.

155.   Rodríguez-Reinoso, F., *The role of carbon materials in heterogeneous catalysis.* Carbon, 1998. **36**(3): p. 159-175.

156.   Imbihl, R., *Catalysis and Electrocatalysis at Nanoparticle Surfaces. Edited by Andrzej Wieckowski, Elena R. Savinova and Constantinos G. Vayenas.* Angewandte Chemie International Edition, 2005. **44**(3): p. 359-359.

157.   Breiter, M.W., *Dissolution and adsorption of hydrogen at smooth Pd wires at potentials of the alpha phase in sulfuric acid solution.* Journal of Electroanalytical Chemistry, 1977. **81**(2): p. 275-284.

158.   Van Den Brink, F., W. Visscher, and E. Barendrecht, *Electrocatalysis of cathodic oxygen reduction by metal phthalocyanines. Part III. Iron phthalocyanine as electrocatalyst: experimental part.* Journal of Electroanalytical Chemistry, 1984. **172**(1-2): p. 301-325.

159.   Mamlouk, M., S.M.S. Kumar, P. Gouerec, and K. Scott, *Electrochemical and fuel cell evaluation of Co based catalyst for oxygen reduction in anion exchange polymer membrane fuel cells.* Journal of Power Sources, 2011. **196**(18): p. 7594-7600.

160.   Ma, J., J. Wang, and Y. Liu, *Iron phthalocyanine as a cathode catalyst for a direct borohydride fuel cell.* Journal of Power Sources, 2007. **172**(1): p. 220-224.

161.   Lefevre, M. and J.P. Dodelet, *Fe-based electrocatalysts made with microporous pristine carbon black supports for the reduction of oxygen in PEM fuel cells.* Electrochimica Acta, 2008. **53**(28): p. 8269-8276.

162. Perez, J., E.R. Gonzalez, and E.A. Ticianelli, *Oxygen electrocatalysis on thin porous coating rotating platinum electrodes.* Electrochimica Acta, 1998. **44**(8-9): p. 1329-1339.

163. Varcoe, J.R., R.C.T. Slade, and E. Lam How Yee, *An alkaline polymer electrochemical interface: A breakthrough in application of alkaline anion-exchange membranes in fuel cells.* Chemical Communications, 2006(13): p. 1428-1429.

164. Scott, K., E. Yu, G. Vlachogiannopoulos, M. Shivare, and N. Duteanu, *Performance of a direct methanol alkaline membrane fuel cell.* Journal of Power Sources, 2008. **175**(1): p. 452-457.

165. Uchida, H., Y. Ueno, H. Hagihara, and M. Watanabe, *Self-Humidifying Electrolyte Membranes for Fuel Cells.* Journal of The Electrochemical Society, 2003. **150**(1): p. A57-A62.

APPENDIX: LIST OF PUBLICATIONS

Journal publications

1.   Yu, E.H., X. Wang, U. Krewer, L. Li, and K. Scott, *Direct oxidation alkaline fuel cells: from materials to systems.* Energy & Environmental Science, 2012. **5**(2).

2.   Wang, X., C. Xu, B.T. Golding, M. Sadeghi, Y. Cao, and K. Scott, *A novel phosphoric acid loaded quaternary 1,4-diazabicyclo-[2.2.2]-octane polysulfone membrane for intermediate temperature fuel cells.* International Journal of Hydrogen Energy, 2011. **36**(14): p. 8550-8556.

3.   Wang, X., M. Li, B.T. Golding, M. Sadeghi, Y. Cao, E.H. Yu, and K. Scott, *A polytetrafluoroethylene-quaternary 1,4-diazabicyclo-[2.2.2]-octane polysulfone composite membrane for alkaline anion exchange membrane fuel cells.* International Journal of Hydrogen Energy, 2011. **36**(16): p. 10022-10026.

4.   Mamlouk, M., X. Wang, K. Scott, J.A. Horsfall, and C. Williams, *Characterization and application of anion exchange polymer membranes with non-platinum group metals for fuel cells.* Proceedings of the Institution of Mechanical Engineers, Part A: Journal of Power and Energy, 2011. **225**(2): p. 152-160.

5.   Cao, Y.-C., X. Wang, M. Mamlouk, and K. Scott, *Preparation of alkaline anion exchange polymer membrane from methylated melamine grafted poly(vinylbenzyl chloride) and its fuel cell performance.* Journal of Materials Chemistry, 2011. **21**(34).

6.   Xu, C., X. Wu, X. Wang, M. Mamlouk, and K. Scott, *Composite membranes of polybenzimidazole and caesium-salts-of-heteropolyacids for intermediate temperature fuel cells.* Journal of Materials Chemistry, 2011. **21**(16).

7.   Cao, Y.-C., X. Wang, and K. Scott, *The synthesis and characteristic of an anion conductive polymer membrane for alkaline anion exchange fuel cells.* Journal of Power Sources, 2012. **201**(0): p. 226-230.

8.   Cao, Y.-C., C. Xu, X. Wu, X. Wang, L. Xing, and K. Scott, *A poly (ethylene*

oxide)/graphene oxide electrolyte membrane for low temperature polymer fuel cells. Journal of Power Sources, 2011. **196**(20): p. 8377-8382.

9.   Xu, C., Y. Cao, R. Kumar, X. Wu, X. Wang, and K. Scott, *A polybenzimidazole/sulfonated graphite oxide composite membrane for high temperature polymer electrolyte membrane fuel cells.* Journal of Materials Chemistry, 2011. **21**(30).

Presentations

05/2008   ***IRD, Denmark***
Title of presentation: Solid state electrolyte cell for oxygen reduction reaction at high temperature

06/2008 and 05/2009   ***Imperial College London***
EPSRC project meeting

06/2011   ***SZENT ISTVÁN UNIVERSITY, Hungary***
Title of presentation: A novel PTFE-quaternary DABCO polysulfone composite membrane for alkaline anion exchange membrane fuel cells